Naval Research Laboratory
Washington, DC 20375-5320

NRL/FR/7140--97-9822

Bottom Scattering Strengths Measured Using Explosive Sources in the Critical Sea Test Program

PETER M. OGDEN
FRED T. ERSKINE

Acoustic Systems Branch
Acoustics Division

February 5, 1997

DTIC QUALITY INSPECTED 4

19970307 036

Approved for public release; distribution unlimited.

REPORT DOCUMENTATION PAGE

Form Approved
OMB No. 0704-0188

Public reporting burden for this collection of information is estimated to average 1 hour per response, including the time for reviewing instructions, searching existing data sources, gathering and maintaining the data needed, and completing and reviewing the collection of information. Send comments regarding this burden estimate or any other aspect of this collection of information, including suggestions for reducing this burden, to Washington Headquarters Services, Directorate for Information Operations and Reports, 1215 Jefferson Davis Highway, Suite 1204, Arlington, VA 22202-4302, and to the Office of Management and Budget. Paperwork Reduction Project (0704-0188), Washington, DC 20503.

1. AGENCY USE ONLY (*Leave Blank*)	2. REPORT DATE	3. REPORT TYPE AND DATES COVERED
	February 5, 1997	Interim

4. TITLE AND SUBTITLE

Bottom Scattering Strengths Measured Using Explosive Sources in the Critical Sea Test Program

5. FUNDING NUMBERS

PU - 63747N

6. AUTHOR(S)

Peter M. Ogden and Fred T. Erskine

7. PERFORMING ORGANIZATION NAME(S) AND ADDRESS(ES)

Naval Research Laboratory
Washington, DC 20375-5320

8. PERFORMING ORGANIZATION REPORT NUMBER

NRL/FR/7140--97-9822

9. SPONSORING/MONITORING AGENCY NAME(S) AND ADDRESS(ES)

Space and Naval Warfare Systems Command
2451 Crystal Drive
Arlington, VA 22217

10. SPONSORING/MONITORING AGENCY REPORT NUMBER

11. SUPPLEMENTARY NOTES

12a. DISTRIBUTION/AVAILABILITY STATEMENT

Approved for public release; distribution unlimited.

12b. DISTRIBUTION CODE

13. ABSTRACT (*Maximum 200 words*)

Bottom backscattering strengths were measured in the Critical Sea Test (CST) program at many sites using explosive charges as sources and a horizontal line array as a receiver. This report is a catalog, with minimal analysis, of the values measured at each site. Scattering strengths were obtained for frequencies from 70 to 1500 Hz and at grazing angles from 25 to 50 deg (intermediate angles). For each site where a data set was collected, two plots are given showing representative bottom scattering strengths: a plot showing broadside scattering strengths, and another showing scattering strengths at 40 deg either forward or aft of broadside. The data for each test are summarized in plots showing the frequency dependence of the results at a 30 deg grazing angle.

14. SUBJECT TERMS

Reverberation
Bottom scattering
Scattering strength
Active sonar
Antisubmarine Warfare

15. NUMBER OF PAGES

71

16. PRICE CODE

17. SECURITY CLASSIFICATION OF REPORT	18. SECURITY CLASSIFICATION OF THIS PAGE	19. SECURITY CLASSIFICATION OF ABSTRACT	20. LIMITATION OF ABSTRACT
UNCLASSIFIED	UNCLASSIFIED	UNCLASSIFIED	UL

NSN 7540-01-280-5500

Standard Form 298 (Rev. 2-89)
Prescribed by ANSI Std 239-18
298-102

CONTENTS

TABLES

Table **Page**

FIGURES

Fig. Page

Bottom Scattering Strengths for CST-3

Bottom Scattering Strengths for CST-4

Bottom Scattering Strengths for CST-5

Fig. Page

Bottom Scattering Strengths for CST-5 (Continued)

Bottom Scattering Strengths for CST-7

Fig. Page

Bottom Scattering Strengths for CST-8

BOTTOM SCATTERING STRENGTHS MEASURED USING EXPLOSIVE SOURCES IN THE CRITICAL SEA TEST PROGRAM

INTRODUCTION

The Critical Sea Test (CST) program was an at-sea testing program sponsored by the Space and Naval Warfare Systems Command (SPAWAR PMW-182) that explored issues related to the development and testing of low-frequency active acoustic systems. CST-sponsored and -supported exercises took place at various locations around the world between 1987 and 1995. During these at-sea tests, a variety of problems related to the areas of science and technology of low-frequency active acoustics, acoustic warfare, and systems support were addressed.

One objective of the CST program was the measurement of environmental acoustic (EVA) reverberation parameters of importance to existing and emerging low-frequency active systems. These parameters are necessary to allow models to make accurate predictions of the effects of all types of reverberation on system performance. In particular, the recent emphasis on littoral warfare has made the understanding of bottom reverberation a high priority. Bottom backscattering is probably the least well understood of the three reverberation mechanisms, at least in part because of a scarcity of scattering strength databases.

During the CST at-sea tests, a substantial number of measurements of bottom backscattering strength were made using several different techniques. One of these techniques involved the use of omnidirectional SUS (Signals, Underwater Sound) explosive charges as sources and a horizontal line array (HLA) as a receiver. Measurements of this type were conducted during the majority of the CST tests, all using the same basic geometry and techniques. The use of explosive charges as sources has the advantage over controlled waveforms of giving results at many frequencies simultaneously. The principal disadvantage of the technique is that the omnidirectional nature of the source causes many unwanted raypaths to be populated, which in turn limits the grazing angles for which useful results can be acquired.

The purpose of this report is to summarize, with little analysis, the bottom scattering strength database that was acquired using SUS charges in the CST program. For each site at which a SUS test was conducted, we present scattering strength results for three different beams at a range of frequencies. In addition, we present summary plots that show the frequency dependence of the scattering for each sea test.

DATA ANALYSIS

A complete description of the experiment technique and the analysis process may be found in Ogden and Erskine (1994a, b). During each of the CST tests listed in Table 1, between 5 and 20 SUS runs were conducted. A typical run consisted of the deployment of either 10 SUS charges in a half-hour period or 20 charges in a one-hour period. These individual events were analyzed to produce a single set of scattering strength vs grazing angle curves for each run. Because the deploying ship normally moved at about 1.5 m/s (3 kt), the scattering strength results were averaged over linear distances as large as 4.5 km, though distances of less than 2 km were much more typical. In an average data set, differences in descent rate and detonation depth led most shots to be excluded from the averaging process. As a result, the typical analysis result is

Manuscript approved September 13, 1996.

based on averaging three to five shots. The uncertainties in the scattering strengths caused by shot-to-shot variability are generally about ± 2 to 3 dB, making the overall uncertainties about ± 4 to 5 dB.

The bottom scattering strengths presented in this report were obtained using direct-path measurements, i.e., the raypaths intersected the bottom only once between source and receiver. For direct-path measurements, four multipaths can contribute to the measured reverberation. For this reason, a multipath correction is normally made in reporting bottom scattering strengths. While this correction can be anywhere between 0 dB (if one path is dominant) and 6 dB (if all paths contribute equally), we applied a 3 dB correction to all scattering strength results. This was an arbitrary choice, but it represents a reasonable compromise in a situation where the proper correction is generally unknown. We assumed that the bottom is flat in the analyses. The grazing angles assigned to the scattering strengths were calculated based on the assumption that the scattering was occurring at the water-sediment interface. While this assumption is almost surely not true for the frequencies and most of the locations reported herein (CST-7 Phase 2 is the principal likely exception), the assumption is almost universally made in extracting scattering strengths from measured data.

The analysis was done using Hamming-weighted 16-hydrophone subapertures of the HLA. Seventeen beams were formed with beam 0 as forward endfire, beam 16 as aft endfire, and beam 8 as the broadside beam. For each run, results are presented in this report for two beams or sets of beams: an average of the three beams that include broadside (i.e., beams 7, 8, and 9), and either beam 3 (40 deg forward of broadside) or beam 13 (40 deg aft of broadside). For most runs, we arbitrarily chose to show the results for beam 13 and show those of beam 3 only for the cases where beam 13 showed some kind of artifact or was pointed toward a pronounced bathymetric feature.

For the SUS charges used in the CST tests, the fundamental bubble frequency was normally around 70 Hz, so this represents the lowest frequency for which measurements were made. The analyses were carried out at the harmonics of the fundamental bubble pulse frequency, which changed somewhat from run to run as the average detonation depth and charge weight changed. The HLA used in the measurements had a design frequency of about 1000 Hz; most of the analyses were carried out at frequencies below the design frequency. However, the lowpass filter through which the data were acquired had a rolloff frequency of 1500 Hz, and as the data were sampled at 4096 samples/s, it was possible to analyze broadside beams up to 1500 Hz. For off-broadside beams, the presence of spatial aliasing prevented analysis above 1000 Hz. In the figures, therefore, beginning with CST-3 (Fig. 35), the broadside results are given for frequencies between 70 and 1500 Hz, while the off-broadside results are given for frequencies between 70 and 1000 Hz.

While the directions of the beam centers do not depend on frequency, the width of each beam does. In order to try to keep beamwidths from getting too large, different 16-phone subapertures were used for different frequencies. In CST-1, CST-2, and CST-3, results are for 16 contiguous phones, and since this would result in huge beams at the lowest frequencies, no results are given for frequencies below 190 Hz. In CST-4, 16 phones were used but with two different spacings: contiguous phones for frequencies of 200 Hz and up and every fifth phone for frequencies below 200 Hz. In CST-5, CST-7 Phase 2, and CST-8, two different subapertures were used: contiguous phones for frequencies of 250 Hz and up and every fourth phone for frequencies below 250 Hz.

CST SUS BOTTOM SCATTERING STRENGTHS

Tables 2 through 8 list the locations of the various CST SUS runs. These tables give the names of the runs and the beginning (COMEX) and ending (FINEX) latitudes and longitudes for each run. As previously noted, the exercise ship was on constant course and speed during each run, with an average ship's speed of about 1.5 m/s through the water. The tracks of the SUS runs are overlaid on DBDB5 bathymetry contour plots in Figs. 1 through 7. Note that in Fig. 6, only a subset of the CST-7 Phase 2 tracks is shown due to the similarity of many of the track positions.

Figures 8 to 14 present summaries of the bottom scatter data that show the frequency dependence of the various sites at 30 deg grazing angle. These plots were prepared by taking the scattering strengths on the broadside beams and averaging them over grazing angles of 30 ± 2 deg. Also included as a reference on each of the plots is the Mackenzie scattering level (Mackenzie 1961), which is Lambert's law with a constant of –27 dB. In spite of the strong influence of normal-incidence fathometer returns on the broadside beams, the validity of looking at frequency dependence in this way is strengthened by the observation that, at virtually every site surveyed, the broadside and off-broadside results are in excellent agreement at grazing angles around 30 deg. This strongly suggests that the influence of the fathometer returns is minimal at these grazing angles and that some type of true backscatter is being measured. Note that at higher grazing angles, most of the scattering strength curves for the off-broadside beams maintain a shape close to Lambert's law, while the broadside beam results show the influence of the fathometer returns by rising much faster than Lambert's law as grazing angle increases.

The bottom scattering strengths measured in each of the SUS tests are shown in Figs. 15 to 152. Each of these figures has the same format: bottom scattering strength plotted against mean grazing angle for a range of frequencies. As a standard of reference, each figure shows the Mackenzie scattering curve.

The following paragraphs present brief comments on each of the areas and data sets.

CST-1

The first three runs (A6, A6 Mod 1, and A6 Mod 2) were conducted in the Norwegian Basin in an area of flat bathymetry and thick sediment cover. Run A16 was carried out in the basin close alongside the Aegir Ridge. The presence of the ridge is clearly seen in Fig. 7 (broadside), but the results in Fig. 8 for beam 13 do not appear to be influenced by the ridge. Runs B9 and B29 were made directly over the Aegir Ridge. For these two runs, no off-broadside beam results are available. During this initial test of the CST test series, the navigation of the experiment ship was poorer than for any of the other tests due to a lack of GPS. As a consequence, the uncertainties in the ship positions during the CST-1 SUS runs were considerably higher than for the other tests.

CST-2

One run of the CST-2 SUS tests, Run 43 Mod 1, was conducted at the base of the Hatton Bank. All the other tests were done out in the Icelandic Basin in areas with generally flat bathymetry. All areas were thickly sedimented.

CST-3

The CST-3 tests were conducted in areas of two different bottom types, though all were thickly sedimented and showed almost no bathymetry features. The first five tests were carried out over the Bermuda Rise, while the last three (33A, 37A, and 51B) occurred over the Hatteras Abyssal Plain. Runs 33A and 37A, by coincidence, were carried out in almost the same position, though the ship tracks were in roughly opposite directions. The Bermuda Rise results were all similar, but the Hatteras Abyssal Plain results showed some interesting differences, even though the sites were reasonably close together. In particular, Run 51B in the Hatteras Abyssal Plain is the only case in the entire series of CST SUS runs in which scattering strengths increase nearly monotonically with increasing frequency. The results for Runs 33A and 37A also show unusual frequency behavior, but they are somewhat more U-shaped as a function of frequency. It is interesting to note that although the site for 33A and 37A and the site for 51B were close, they correspond to two different 3.5-kHz Damuth echo provinces (Laine, Damuth, and Jacobi 1986).

CST-4

The runs all took place in the Aleutian Abyssal Plain, a thickly sedimented area that has a number of seamounts and other substantial bathymetric features. Though none of the SUS runs were conducted over any significant bathymetric features, a number of them, such as Runs 43B, 50E, 51E, and 59, were close enough to seamounts that the results may have been affected by changes in basement topography. In addition, Runs 12B, 28B, and 32 were carried out very close to one another, though with the ship going in different directions.

CST-5

The first five CST-5 SUS runs were carried out over the Messina Rise on the northern edge of the Ionian Abyssal Plain. This area is fairly flat with a gentle slope and a thick sediment cover. Runs 14A and 26 were conducted in nearly identical locations. Run T1-3 took place at a location on top of the Malta Ridge in an area of complicated bathymetry. Both Runs T2-6 and 46 were carried out south of the Malta Ridge; Run 46, however, took place directly adjacent to the ridge and the results are undoubtedly affected by the presence of the ridge. Finally, Run 48 occurred directly over another part of the Malta Ridge in an area of complicated bathymetry.

CST-7 Phase 2

The CST-7 Phase 2 test was primarily intended as a surface scatter experiment. As a result, the experiment ship crossed the same patch of ocean floor over and over again, with a goal of keeping the ship parallel to the wind direction. Thus the only CST-7 Phase 2 run that is in even a slightly different place is Run 1A. All the other runs were nearly coincident, though the ship direction varied considerably from run to run. Run 34 was three hours long and was divided up into three parts for analysis, with each part being roughly an hour long. Little appears to be known about this portion of the Gulf of Alaska, which is on the southern part of the Sila Fracture Zone. Our interpretation of the scattering strength results suggests that this is a typical North Pacific thinly sedimented area dominated by basement scattering. Because most of the sites were so close together and the scattering strength results were so similar, the frequency-dependence plot in Fig. 13 only includes a subset of the runs.

CST-8

All of the CST-8 SUS runs were conducted over very thickly sedimented areas. The sites fell into two general categories. The first run (B1) was on the Nile Cone, while the second (B3) was at one of the deepest parts of the Herodotus Abyssal Plain. The remainder of the SUS runs were made along a single line running from the approximate location of Deep Sea Drilling Project site 131A in the middle of the Herodotus Abyssal Plain up to a point on the Nile Cone just outside the Alexandria Canyon. The depths along this line went from 3100 m for Run B7 to 1640 m for Run B18.

SUMMARY

Seventy SUS runs that were carried out during the CST program have been analyzed to yield bottom scattering strengths. These scattering strengths were measured for grazing angles between about 27 and 55 deg and frequencies from roughly 70 to 1500 Hz. The sites at which measurements were made are scattered all around the world, but, with the probable exception of the CST-7 Phase 2 sites, they all have certain elements in common: the sites are all in relatively deep water, with thick sediment covers composed primarily of clays, silts, or muds, rather than sand. Additional information on some of the bottom scatter results can be found in Ogden and Erskine (1993a, b).

This report summarizes the scattering strength results by reporting the scattering strengths derived for two beams or sets of beams: the average of three broadside beams, and the beam either 40 deg forward or 40 deg aft of broadside. While the broadside results do not discriminate against returns at any grazing angle, the off-broadside beams mostly suppress the normal-incidence fathometer returns that are largely responsible for the sharp increase in scattering strengths as grazing angle increases on the broadside beams. Thus the off-broadside beams are closer to being able to measure "true" backscatter than the broadside beams. It is interesting to note, however, that in virtually all cases, the broadside and off-broadside results are similar at a 30 deg grazing angle, suggesting that the influence of fathometer returns is minimal by that time.

Since the original processing that led to the scattering strength results reported here, we have done additional work on the bottom scattering data sets to extend the grazing angle range of the results. By using an adaptive beamformer and looking at results for beams closer to endfire, we have been able to derive scattering strengths for grazing angles as low as 5 deg in some cases (Ogden and Erskine 1995). Results from the adaptive beamforming processing will be published in the future.

ACKNOWLEDGMENTS

This work was funded by the Space and Naval Warfare Systems Command, PMW-182, and by the Office of Naval Research. We thank Jerome Richardson, Elisabeth Kim, and Brenda Vest of Planning Systems, Inc. and Michael Jackson and Joseph Jeffery of NRL for their assistance with the processing and Terrell Dossey of Planning Systems, Inc. for the preparation of the maps.

REFERENCES

E.P. Laine, J.E. Damuth, and R. Jacobi, 1986. "Surficial Sedimentary Processes Revealed by Echo-Character Mapping in the Western North Atlantic Ocean," in *The Geology of North America, Volume M: The Western North Atlantic Region,* P.R. Vogt and B.E. Tucholke, eds. (Geological Society of America, Washington, DC).

K.V. Mackenzie, 1961. "Bottom Reverberation for 530-and 1030-cps Sound in Deep Water," *J. Acoust. Soc. Am.* **33**, 1498–1504.

P.M. Ogden and F.T. Erskine, 1993a. "Low-Frequency Bottom Backscattering Strengths Measured Using SUS Charges," in *Acoustic Classification and Mapping of the Seabed*, Proceedings of the Institute of Acoustics, Vol. 15, Pt. 2, N.G. Pace and D.N. Langhorne, eds., April 14-16, 1993, University of Bath, UK, pp. 271-278.

P.M. Ogden and F.T. Erskine, 1993b. "Low-Frequency Surface and Bottom Scattering Strengths Measured Using SUS Charges," in *Ocean Reverberation,* D. Ellis, J. Preston, and H. Urban, eds., Kluwer Academic Publishers, Dordrecht.

P.M. Ogden and F.T. Erskine, 1994a. "Surface Scattering Measurements Using Broadband Explosive Charges in the Critical Sea Test Experiments," *J. Acoust. Soc. Am.* **95**, 746–761.

P.M. Ogden and F.T. Erskine, 1994b. "Surface and Volume Scattering Measurements Using Broadband Explosive Charges in the Critical Sea Test 7 Experiment," *J. Acoust. Soc. Am.* **96**, 2908–2920.

P.M. Ogden and F.T. Erskine, 1995. "Bottom Backscattering Strengths at Low Grazing Angles Using Adaptive Beamforming," *J. Acoust. Soc. Am.* **97**(2), 3385.

Table 1— Summary of CST SUS Tests

Test	Date	Location	No. of SUS Runs	Range of Depths (m)
CST-1	August 1988	Norwegian Basin and Aegir Ridge	6	3100–3660
CST-2	April 1989	Icelandic Basin and Hatton Bank	5	2500–2580
CST-3	August 1989	Bermuda Rise and Hatteras Abyssal Plain	8	5130–5400
CST-4	April 1990	Gulf of Alaska/Aleutian Abyssal Plain	11	4750–4890
CST-5	June 1991	Central Mediterranean/Ionian Abyssal Plain and Malta Ridge	9	1670–3650
CST-7 Phase 2	February 1992	Gulf of Alaska/Sila Fracture Zone	20	4660
CST-8	May 1993	Eastern Mediterranean/Herodotus Abyssal Plain and Nile Cone	11	1640–3100

Table 2 — Locations of CST-1 SUS Runs

Run	Type	Latitude (deg, min)	Longitude (deg, min)
A6	COMEX	67 50.66 N	3 39.74 W
	FINEX	67 52.96 N	3 37.64 W
A6 Mod 1	COMEX	68 21.64 N	4 40.80 W
	FINEX	68 23.46 N	4 51.64 W
A6 Mod 2	COMEX	68 00.83 N	4 20.22 W
	FINEX	67 57.42 N	4 15.22 W
A16	COMEX	67 37.94 N	4 08.19 W
	FINEX	67 34.42 N	4 09.79 W
B9	COMEX	67 35.64 N	4 02.42 W
	FINEX	67 36.60 N	4 09.94 W
B29	COMEX	67 30.60 N	3 01.80 W
	FINEX	67 31.20 N	3 25.20 W

Table 3 — Locations of CST-2 SUS Runs

Run	Type	Latitude (deg, min)	Longitude (deg, min)
29	COMEX	60 25.34 N	18 10.94 W
	FINEX	60 28.64 N	18 08.94 W
33 Mod	COMEX	60 16.84 N	18 39.50 W
	FINEX	60 15.10 N	18 29.66 W
43 Mod 1	COMEX	59 47.22 N	17 53.45 W
	FINEX	59 45.75 N	17 49.03 W
43 Mod 2	COMEX	60 04.75 N	18 22.09 W
	FINEX	60 07.13 N	18 25.95 W
43 Mod 3	COMEX	59 57.41 N	18 11.07 W
	FINEX	59 51.58 N	18 00.49 W

Table 4 — Locations of CST-3 SUS Runs

Run	Type	Latitude (deg, min)	Longitude (deg, min)
2B	COMEX	30 03.08 N	69 40.41 W
	FINEX	30 02.29 N	69 37.76 W
3B	COMEX	29 51.95 N	69 07.56 W
	FINEX	29 51.10 N	69 05.00 W
5D	COMEX	29 27.90 N	68 25.50 W
	FINEX	29 25.00 N	68 26.00 W
5H	COMEX	29 09.80 N	68 28.64 W
	FINEX	29 06.65 N	68 28.93 W
5J	COMEX	29 05.18 N	68 29.87 W
	FINEX	29 02.54 N	68 31.50 W
33A	COMEX	27 50.47 N	70 26.18 W
	FINEX	27 52.28 N	70 32.92 W
37A	COMEX	27 51.25 N	70 32.38 W
	FINEX	27 50.33 N	70 28.95 W
51B	COMEX	28 21.48 N	70 04.54 W
	FINEX	28 20.40 N	70 01.00 W

Table 5 — Locations of CST-4 SUS Runs

Run	Type	Latitude (deg, min)	Longitude (deg, min)
7	COMEX	51 00.3 N	159 09.0 W
	FINEX	50 59.7 N	159 14.4 W
12B	COMEX	50 29.23 N	159 20.89 W
	FINEX	50 31.57 N	159 23.40 W
28B	COMEX	50 27.34 N	159 20.84 W
	FINEX	50 29.56 N	159 20.89 W
32	COMEX	50 25.50 N	159 19.39 W
	FINEX	50 29.43 N	159 21.35 W
43B	COMEX	50 25.90 N	160 11.10 W
	FINEX	50 23.85 N	160 11.71 W
46B	COMEX	50 09.38 N	160 02.06 W
	FINEX	50 06.83 N	160 04.66 W
49A	COMEX	50 04.02 N	159 24.10 W
	FINEX	50 05.04 N	159 20.09 W
50E	COMEX	50 14.59 N	158 35.19 W
	FINEX	50 15.18 N	158 31.76 W
51E	COMEX	50 13.48 N	158 38.79 W
	FINEX	50 13.56 N	158 42.75 W
52B	COMEX	50 05.70 N	159 33.38 W
	FINEX	50 05.05 N	159 35.39 W
59	COMEX	50 11.25 N	159 28.19 W
	FINEX	50 15.16 N	159 24.64 W

Table 6 — Locations of CST-5 SUS Runs

Run	Type	Latitude (deg, min)	Longitude (deg, min)
2	COMEX	36 13.0 N	17 18.4 E
	FINEX	36 14.2 N	17 15.4 E
14A	COMEX	36 35.9 N	18 50.0 E
	FINEX	36 35.4 N	18 46.4 E
20	COMEX	36 28.2 N	18 06.9 E
	FINEX	36 28.7 N	18 10.2 E
26	COMEX	36 35.8 N	18 47.9 E
	FINEX	36 35.7 N	18 46.2 E
33	COMEX	35 50.3 N	16 45.3 E
	FINEX	35 51.5 N	16 41.4 E
T1-3	COMEX	35 15.0 N	16 34.9 E
	FINEX	35 14.1 N	16 34.2 E
T2-6	COMEX	34 53.9 N	16 50.4 E
	FINEX	34 55.7 N	16 53.0 E
46	COMEX	34 52.0 N	17 03.3 E
	FINEX	34 52.5 N	17 07.0 E
48	COMEX	35 07.5 N	17 32.6 E
	FINEX	35 09.2 N	17 30.4 E

Table 7 — Locations of CST-7 Phase 2 SUS Runs

Run	Type	Latitude (deg, min)	Longitude (deg, min)
1A	COMEX	48 54.2 N	149 21.7 W
	FINEX	48 54.2 N	149 23.2 W
3C	COMEX	48 44.4 N	150 02.5 W
	FINEX	48 43.7 N	150 05.3 W
5B	COMEX	48 46.0 N	150 08.8 W
	FINEX	48 45.9 N	150 06.0 W
11C	COMEX	48 45.3 N	149 58.7 W
	FINEX	48 44.5 N	150 01.3 W
12D	COMEX	48 43.0 N	150 00.0 W
	FINEX	48 44.2 N	149 59.0 W
13C	COMEX	48 42.0 N	150 01.0 W
	FINEX	48 40.6 N	150 01.1 W
16B	COMEX	48 39.5 N	149 58.7 W
	FINEX	48 40.6 N	149 59.5 W
16G	COMEX	48 46.0 N	150 06.8 W
	FINEX	48 46.8 N	150 08.9 W
18B	COMEX	48 44.3 N	149 57.4 W
	FINEX	48 43.8 N	149 55.4 W
19C	COMEX	48 44.3 N	149 54.6 W
	FINEX	48 45.0 N	149 57.1 W
20B	COMEX	48 45.2 N	149 56.5 W
	FINEX	48 44.4 N	149 54.2 W
21C	COMEX	48 43.6 N	149 55.6 W
	FINEX	48 44.5 N	149 58.0 W
23C	COMEX	48 46.4 N	150 00.6 W
	FINEX	48 47.3 N	150 02.9 W
24B	COMEX	48 46.0 N	149 59.0 W
	FINEX	48 45.4 N	149 56.3 W
25D	COMEX	48 45.8 N	150 01.2 W
	FINEX	48 46.2 N	150 04.2 W
26B	COMEX	48 47.0 N	149 59.9 W
	FINEX	48 46.6 N	149 57.4 W
29E	COMEX	48 45.9 N	149 58.8 W
	FINEX	48 45.6 N	149 56.5 W
34A	COMEX	48 47.3 N	149 59.8 W
	FINEX	48 47.1 N	149 35.4 W

Table 8 — Locations of CST-8 SUS Runs

Run	Type	Latitude (deg, min)	Longitude (deg, min)
B1A	COMEX	32 59.3 N	29 19.5 E
	FINEX	32 57.8 N	29 16.5 E
B3	COMEX	32 56.2 N	28 16.2 E
	FINEX	33 06.1 N	28 16.6 E
B7	COMEX	33 05.7 N	28 31.2 E
	FINEX	33 02.9 N	28 34.2 E
B9	COMEX	32 57.1 N	28 40.6 E
	FINEX	32 55.1 N	28 42.7 E
B11	COMEX	32 48.2 N	28 50.1 E
	FINEX	32 45.7 N	28 52.8 E
B13	COMEX	32 40.7 N	28 58.1 E
	FINEX	32 38.8 N	29 00.2 E
B14	COMEX	32 33.3 N	29 06.0 E
	FINEX	32 31.4 N	29 08.0 E
B15	COMEX	32 25.9 N	29 13.9 E
	FINEX	32 23.8 N	29 16.2 E
B16	COMEX	32 18.5 N	29 21.4 E
	FINEX	32 16.2 N	29 23.7 E
B17	COMEX	32 11.8 N	29 28.2 E
	FINEX	32 09.6 N	29 30.3 E
B18	COMEX	32 05.5 N	29 34.6 E
	FINEX	32 03.3 N	29 36.8 E

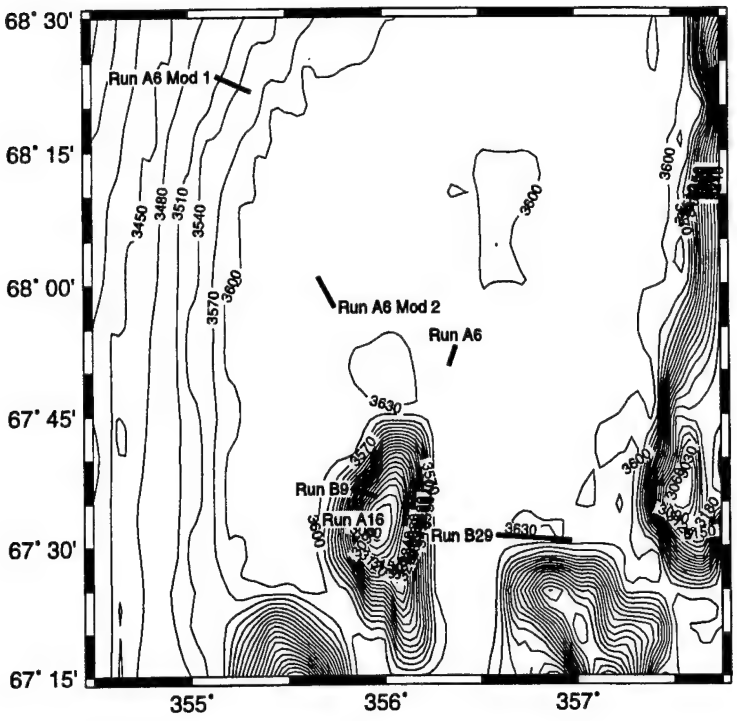

Fig. 1 — DBDB5 bathymetry contour plot: Tracks of the CST-1 SUS runs

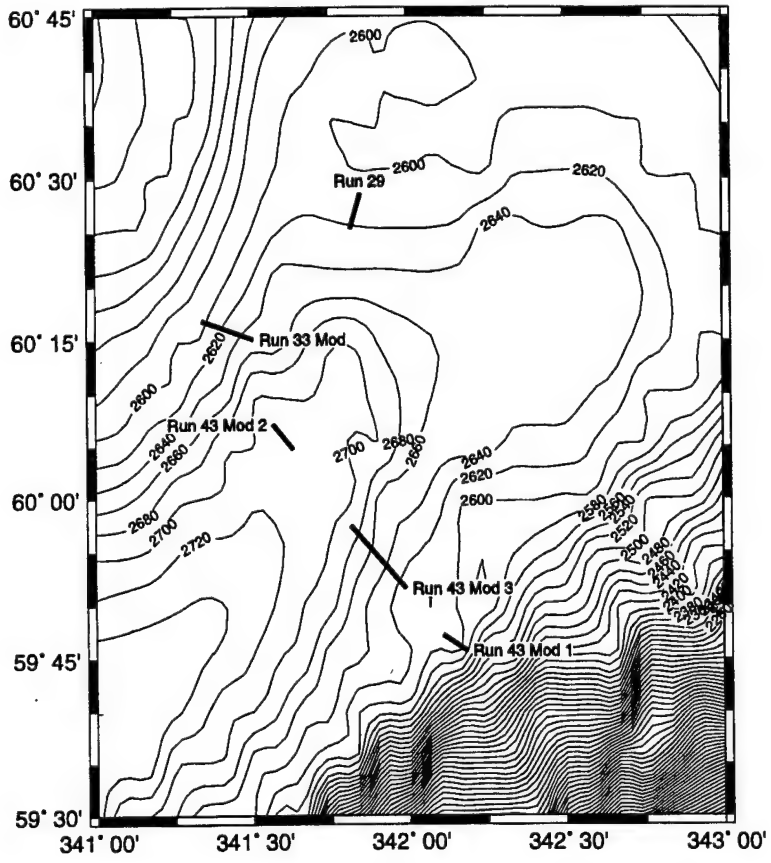

Fig. 2 — DBDB5 bathymetry contour plot: Tracks of the CST-2 SUS runs

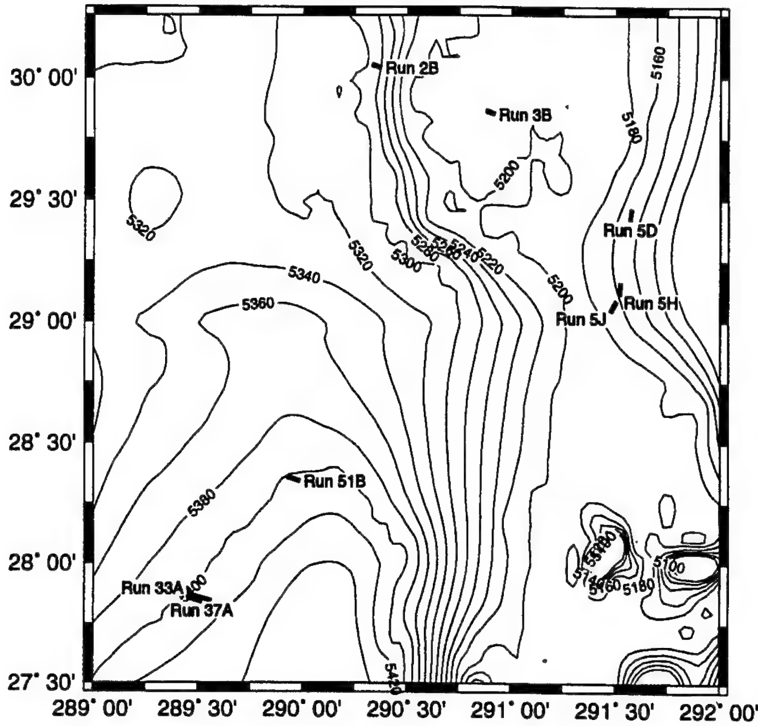

Fig. 3 — DBDB5 bathymetry contour plot: Tracks of the CST-3 SUS runs

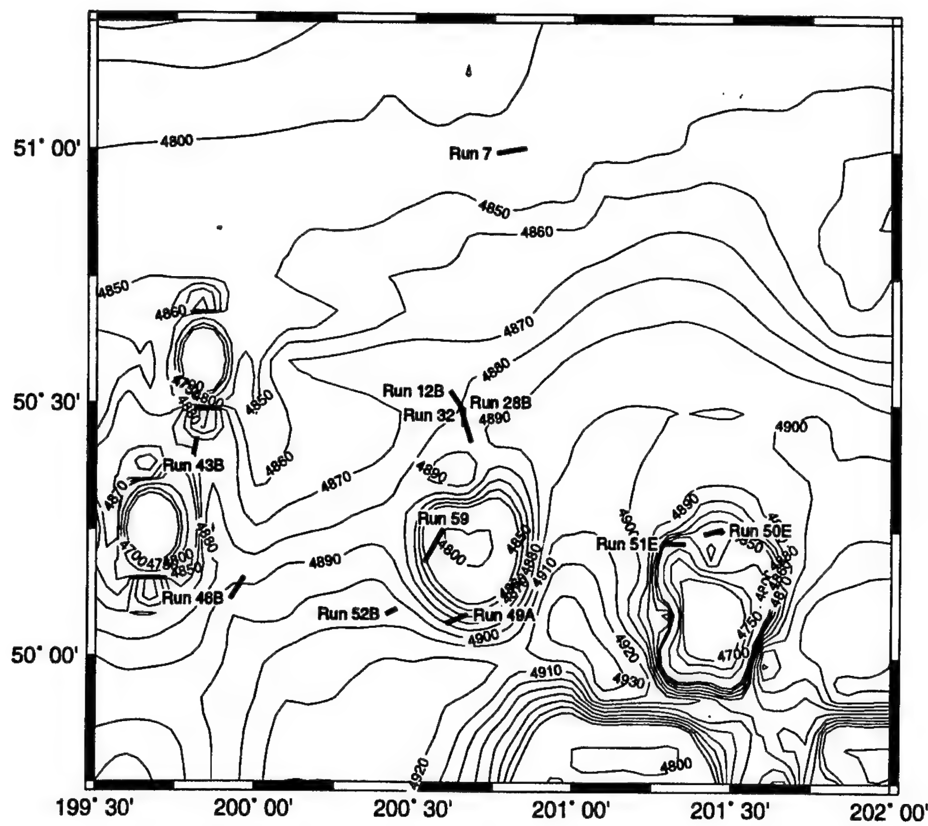

Fig. 4 — DBDB5 bathymetry contour plot: Tracks of the CST-4 SUS runs

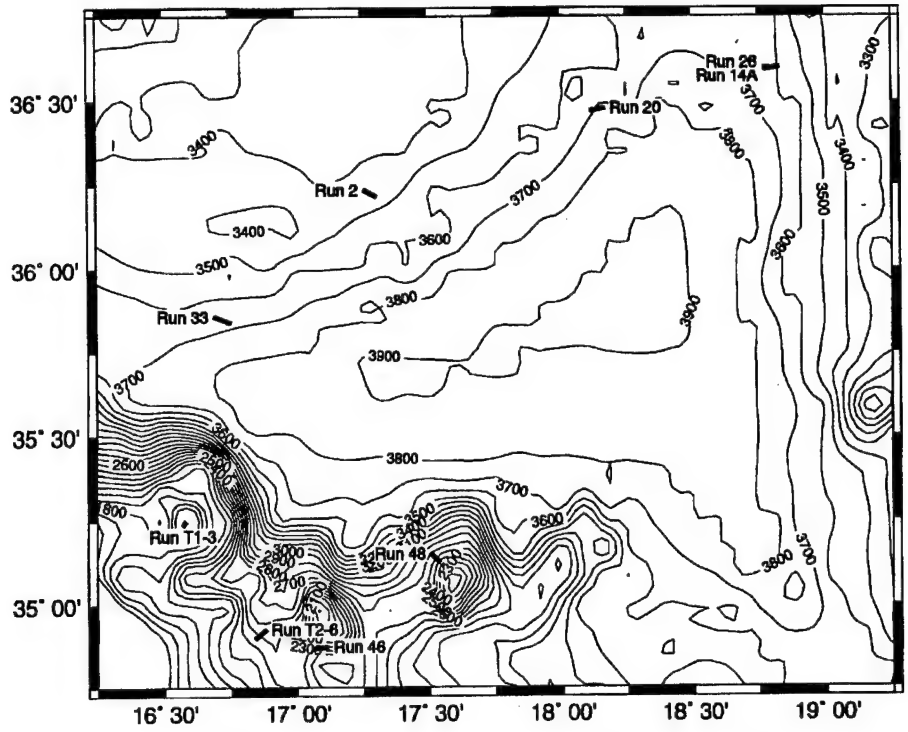

Fig. 5 — DBDB5 bathymetry contour plot: Tracks of the CST-5 SUS runs

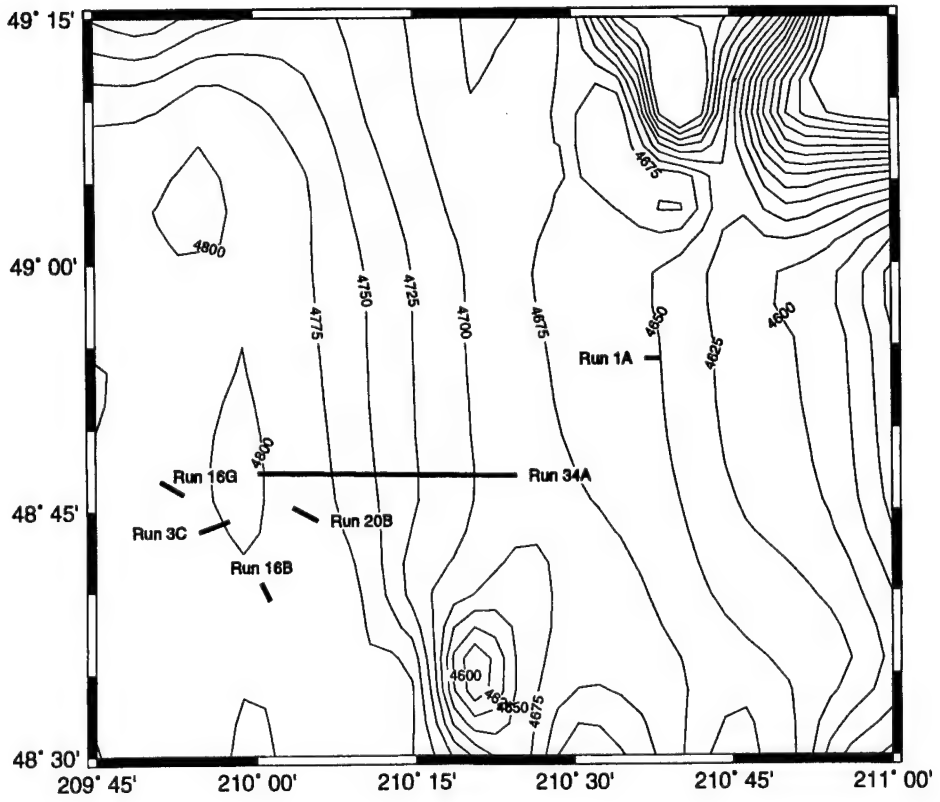

Fig. 6 — DBDB5 bathymetry contour plot: Tracks of a subset of the CST-7 Phase 2 SUS runs

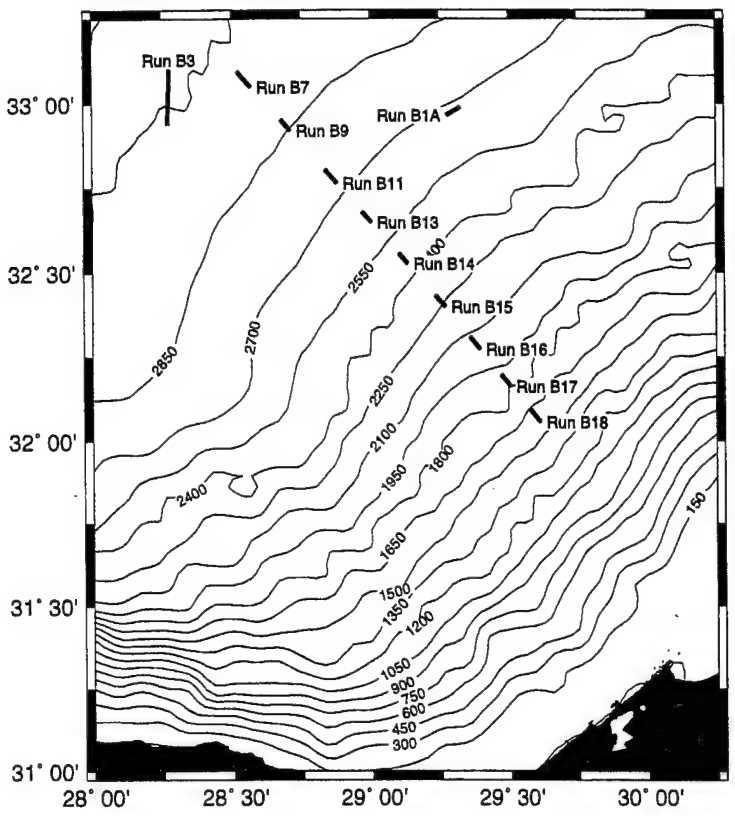

Fig. 7 — DBDB5 bathymetry contour plot: Tracks of the CST-8 SUS runs

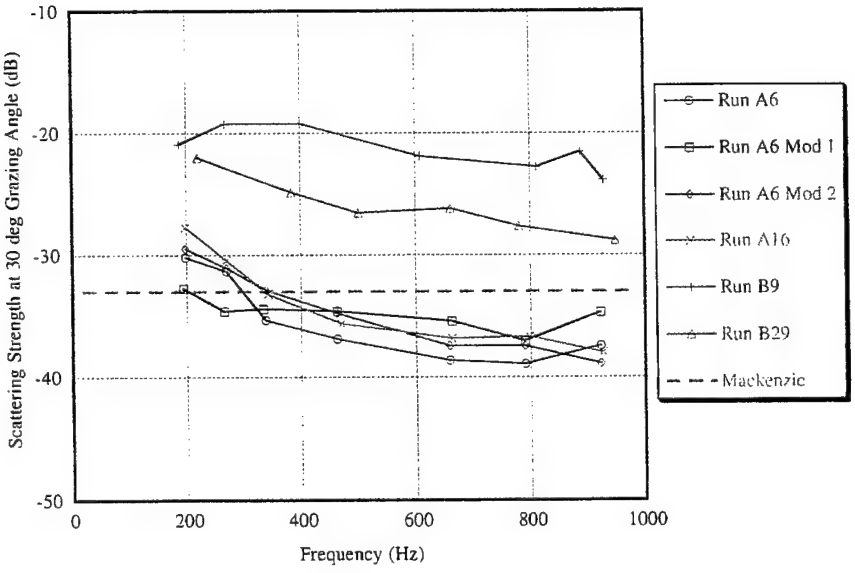

Fig. 8 — Bottom scattering strengths at 30 deg grazing angle for CST-1 sites

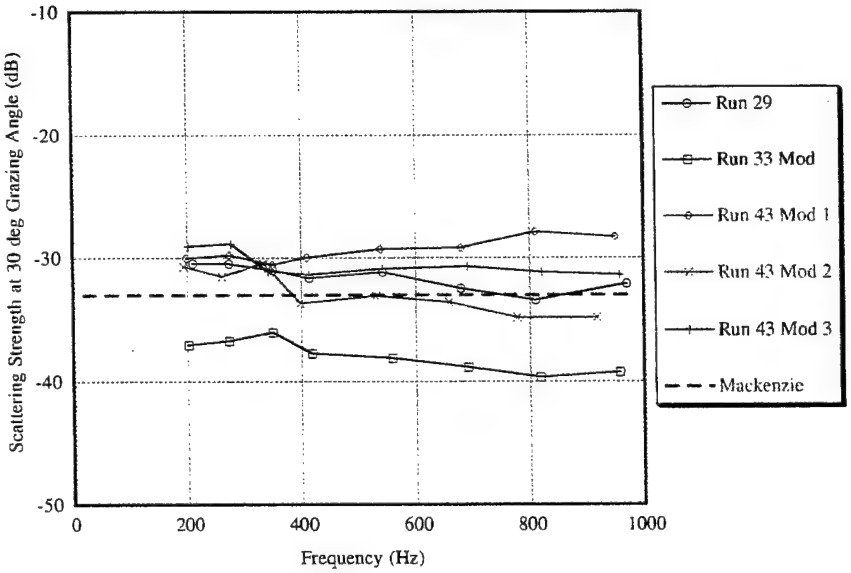

Fig. 9 — Bottom scattering strengths at 30 deg grazing angle for CST-2 sites

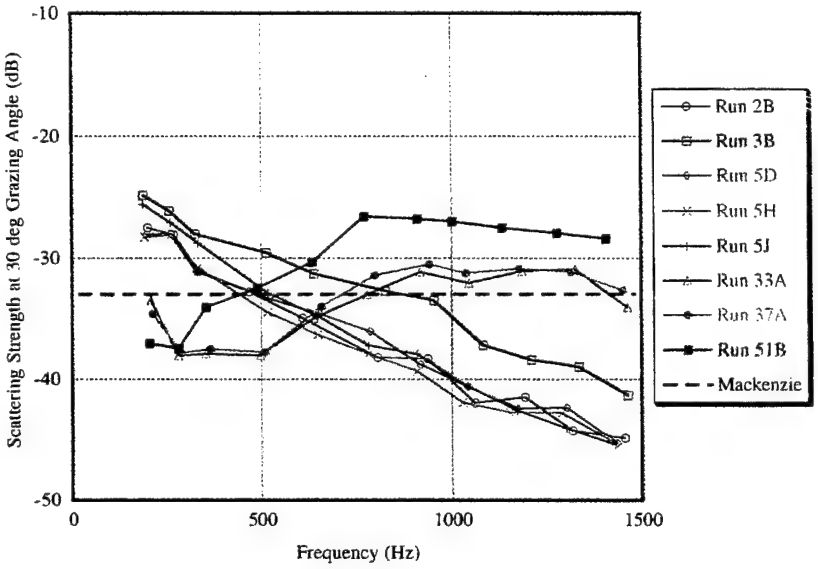

Fig. 10 — Bottom scattering strengths at 30 deg grazing angle for CST-3 sites

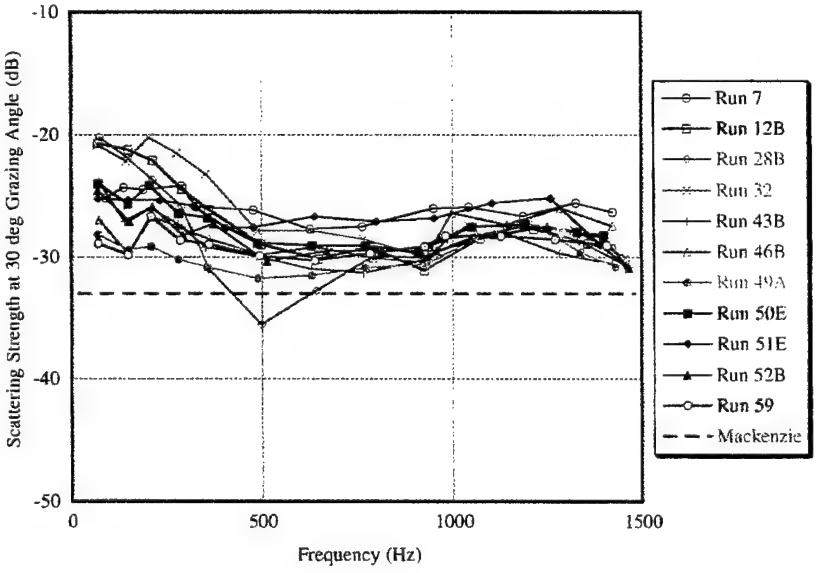

Fig. 11 — Bottom scattering strengths at 30 deg grazing angle for CST-4 sites

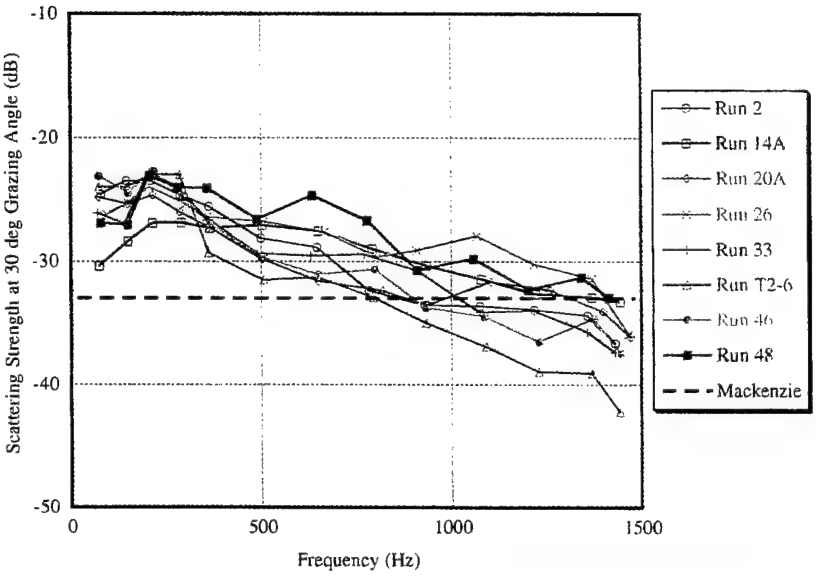

Fig. 12 — Bottom scattering strengths at 30 deg grazing angle for CST-5 sites

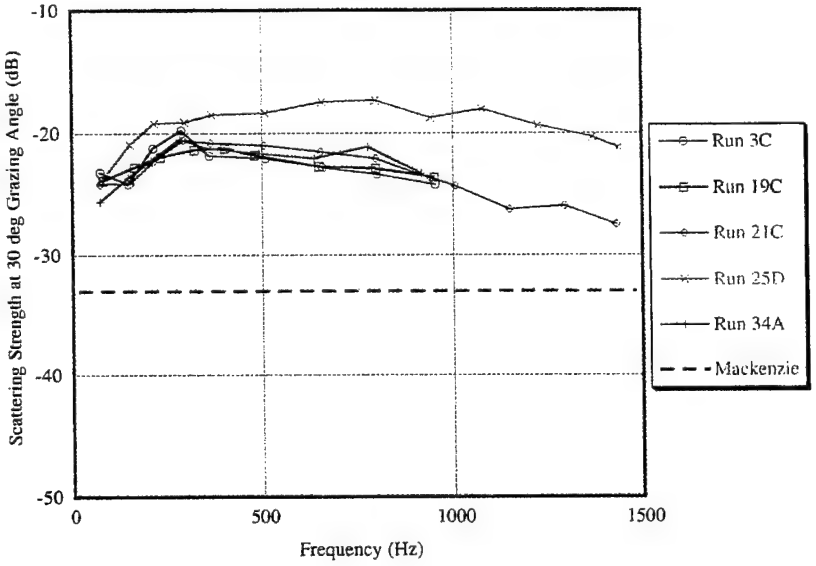

Fig. 13 — Bottom scattering strengths at 30 deg grazing angle for CST-7 Phase 2 sites

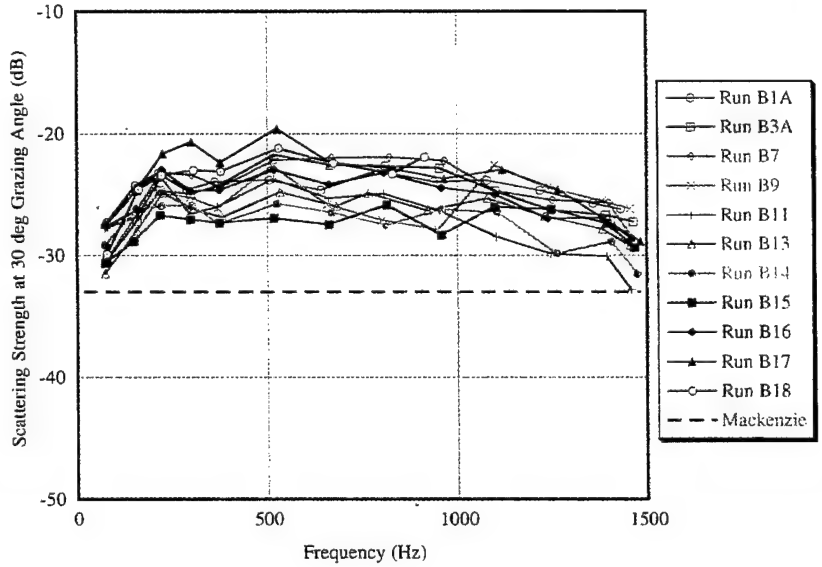

Fig. 14 — Bottom scattering strengths at 30 deg grazing angle for CST-8 sites

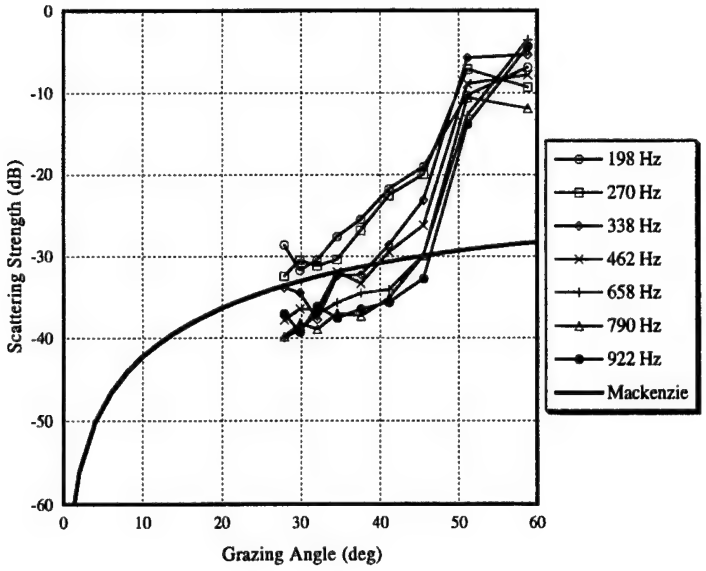

Fig. 15 — Bottom scattering strengths for CST-1 Run A6 beams 7-9

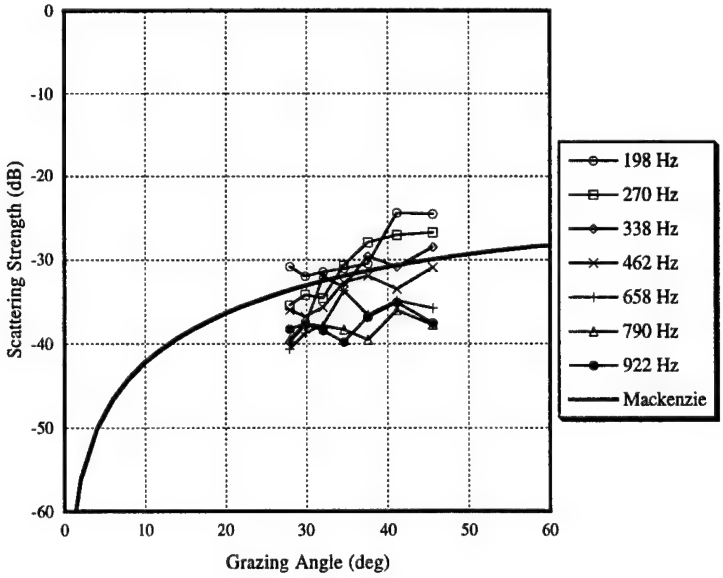

Fig. 16 — Bottom scattering strengths for CST-1 Run A6 beam 13

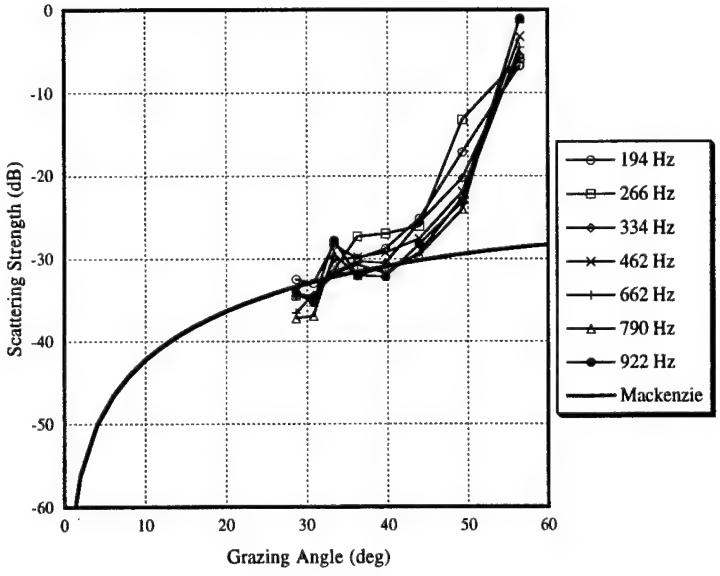

Fig. 17 — Bottom scattering strengths for CST-1 Run A6 Mod 1 beams 7-9

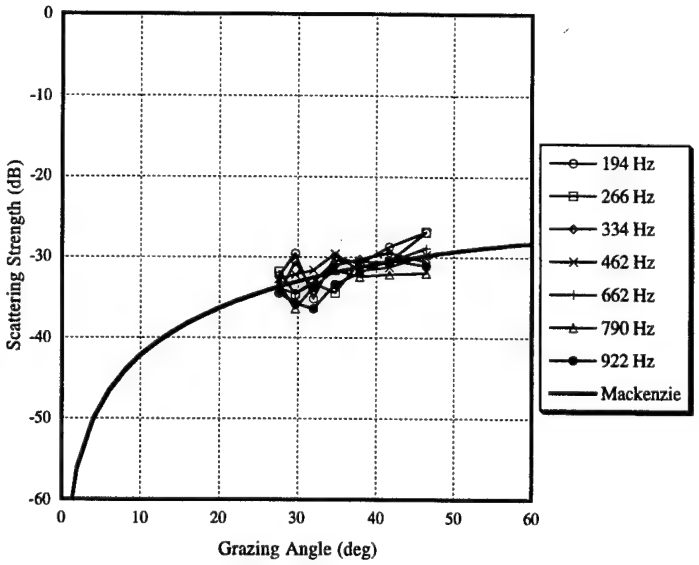

Fig. 18 — Bottom scattering strengths for CST-1 Run A6 Mod 1 beam 13

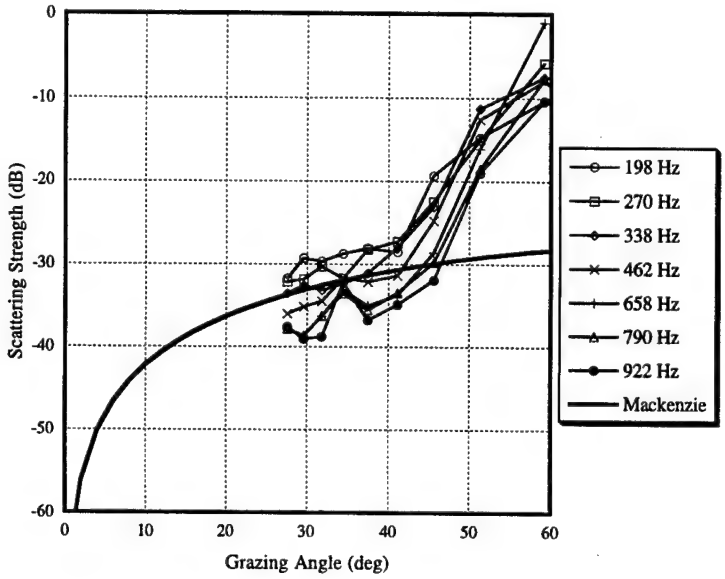

Fig. 19 — Bottom scattering strengths for CST-1 Run A6 Mod 2 beams 7-9

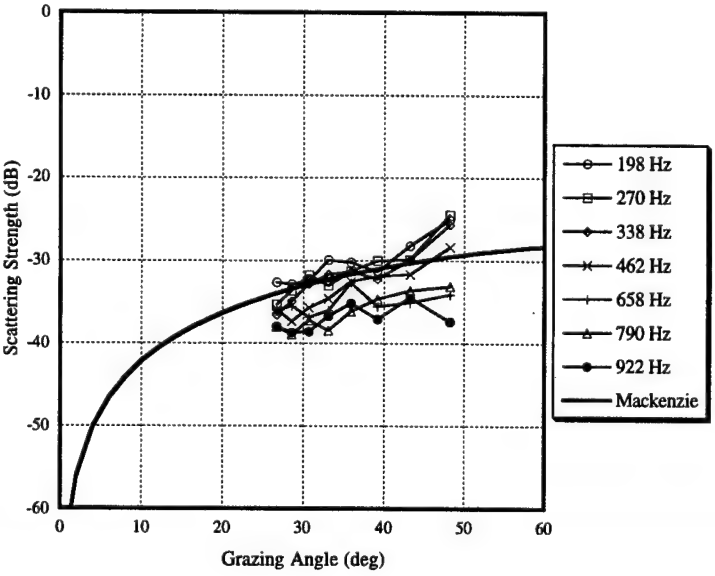

Fig. 20 — Bottom scattering strengths for CST-1 Run A6 Mod 2 beam 13

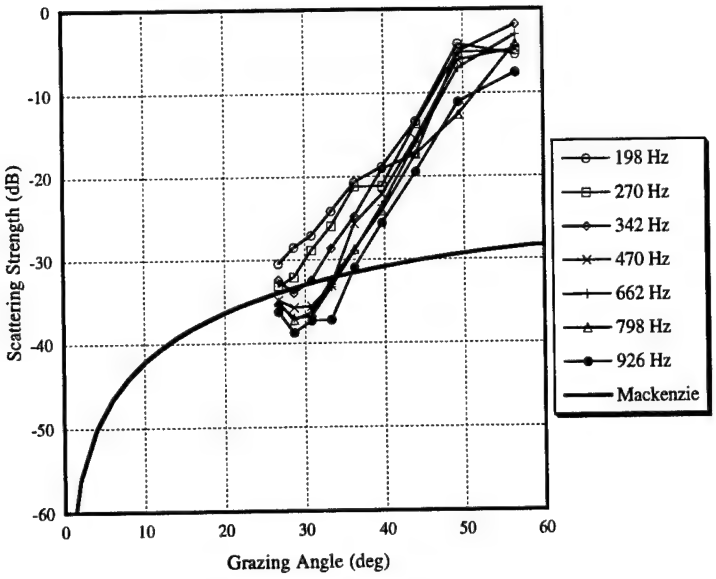

Fig. 21 — Bottom scattering strengths for CST-1 Run A16 beams 7-9

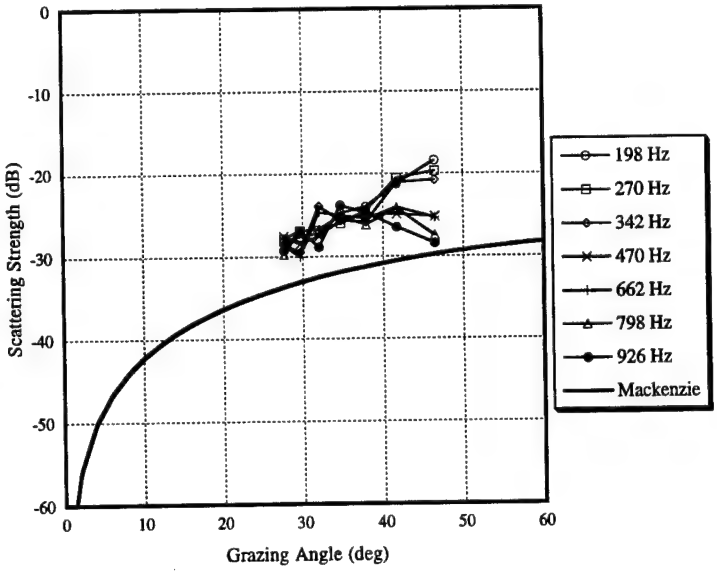

Fig. 22 — Bottom scattering strengths for CST-1 Run A16 beam 13

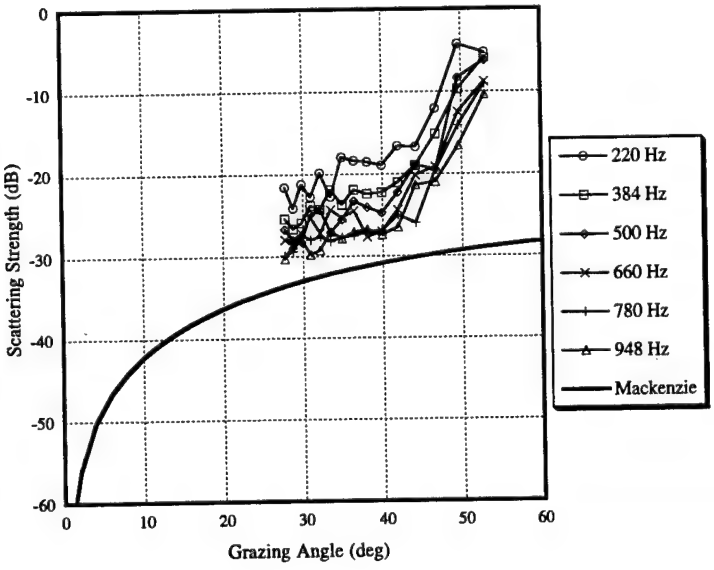

Fig. 23 — Bottom scattering strengths for CST-1 Run B9 beams 7-9

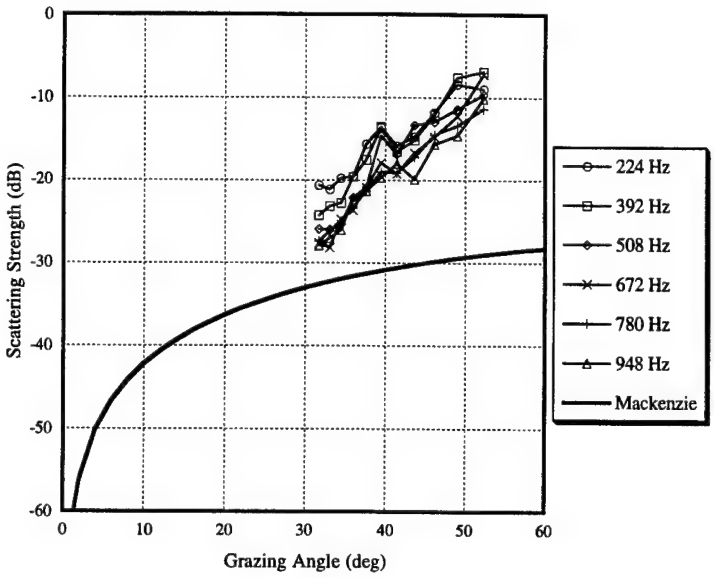

Fig. 24 — Bottom scattering strengths for CST-1 Run B29 beams 7-9

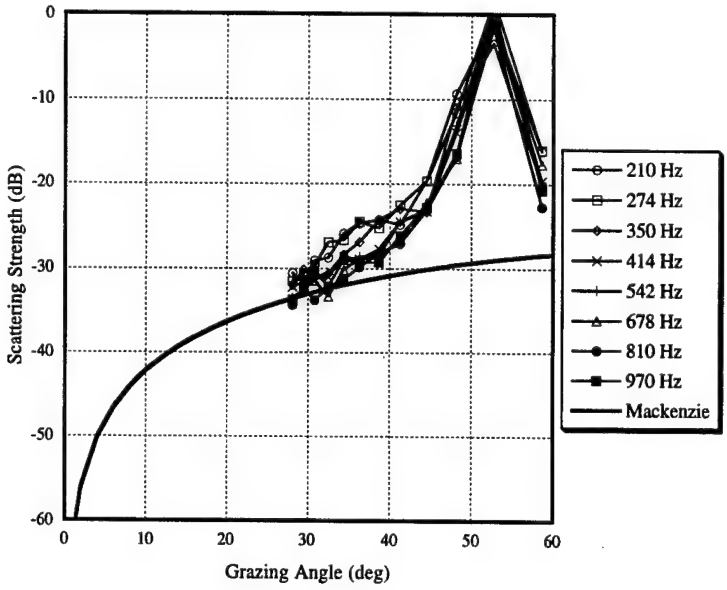

Fig. 25 — Bottom scattering strengths for CST-2 Run 29 beams 7-9

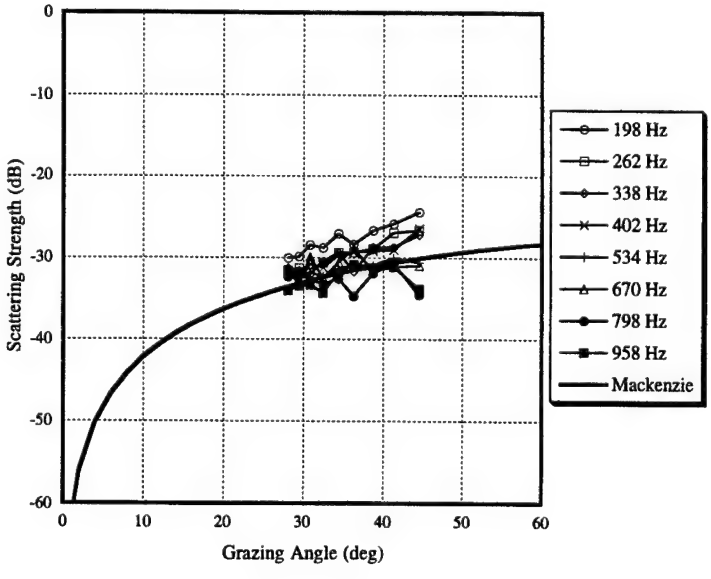

Fig. 26 — Bottom scattering strengths for CST-2 Run 29 beam 13

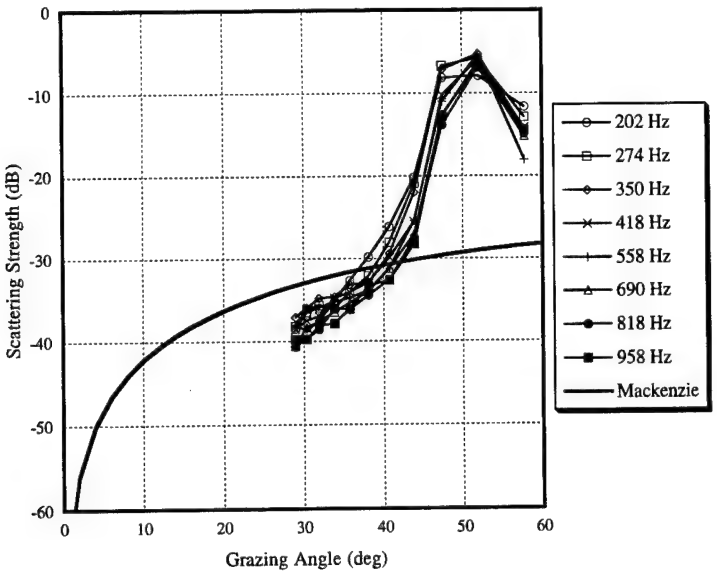

Fig. 27 — Bottom scattering strengths for CST-2 Run 33 Mod beams 7-9

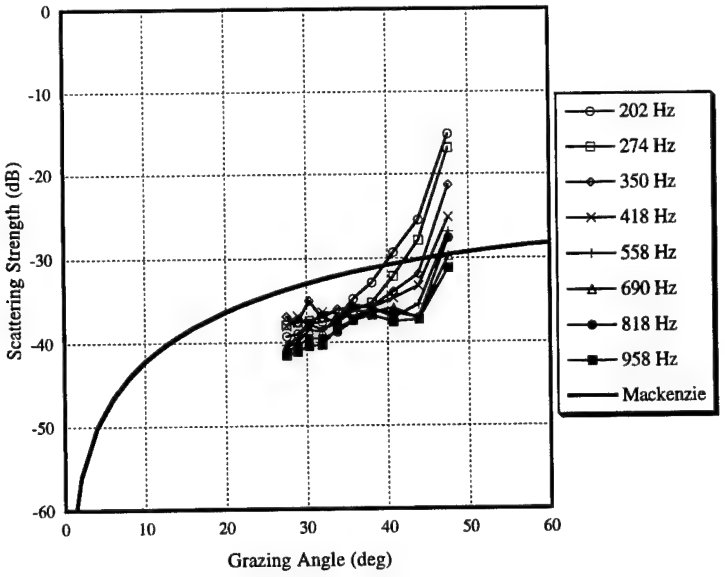

Fig. 28 — Bottom scattering strengths for CST-2 Run 33 Mod beam 3

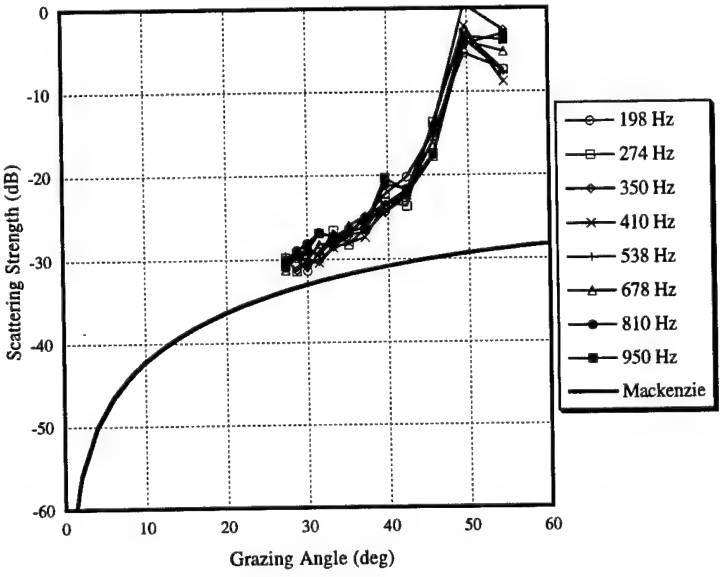

Fig. 29 — Bottom scattering strengths for CST-2 Run 43 Mod 1 beams 7-9

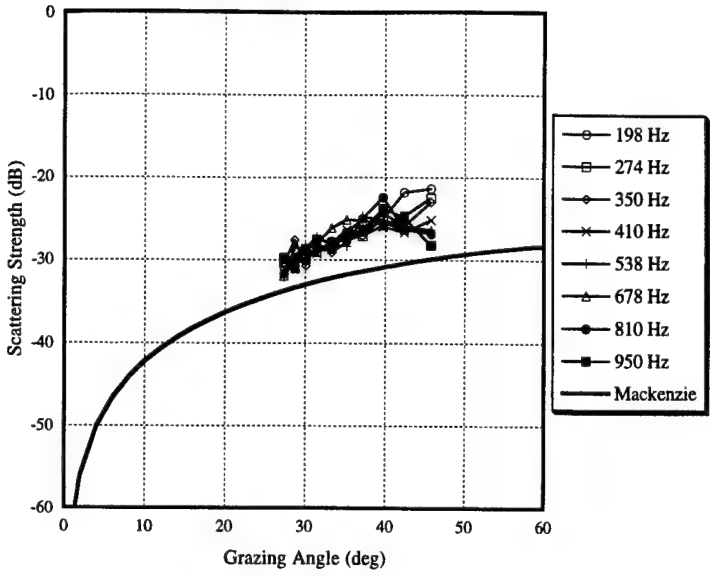

Fig. 30 — Bottom scattering strengths for CST-2 Run 43 Mod 1 beam 13

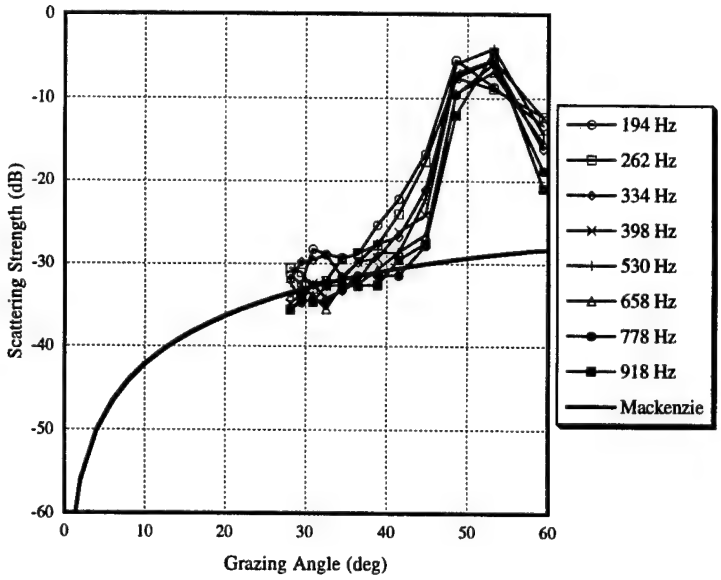

Fig. 31 — Bottom scattering strengths for CST-2 Run 43 Mod 2 beams 7-9

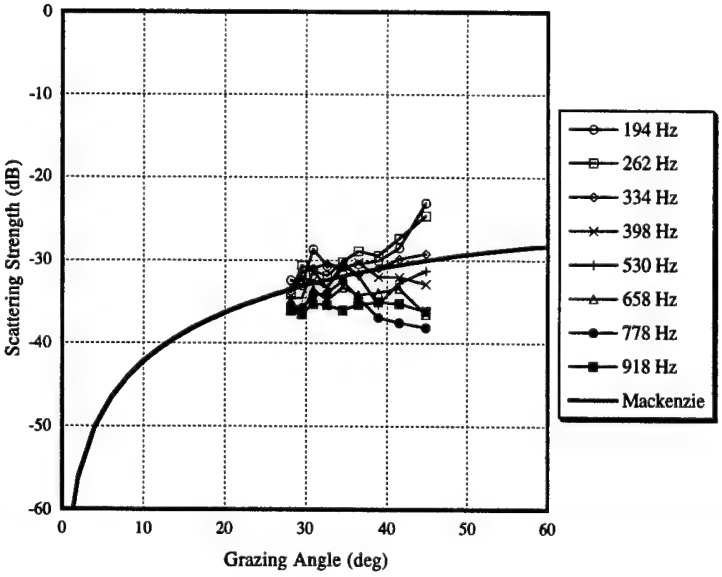

Fig. 32 — Bottom scattering strengths for CST-2 Run 43 Mod 2 beam 13

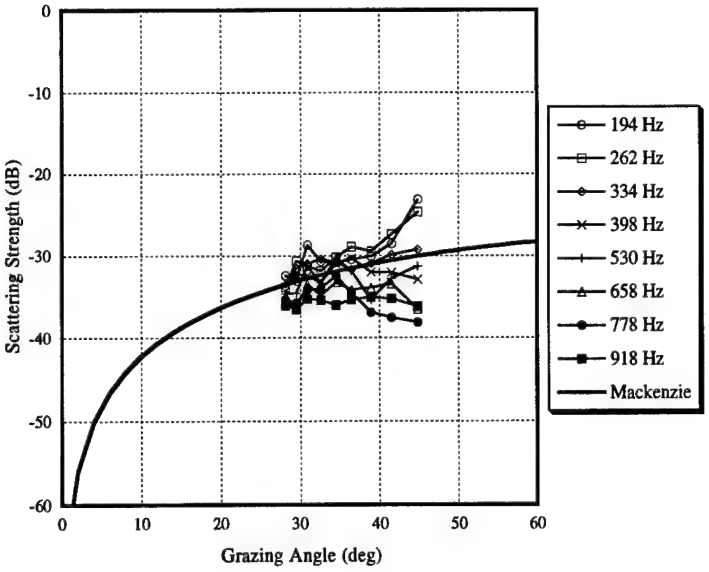

Fig. 33 — Bottom scattering strengths for CST-2 Run 43 Mod 3 beams 7-9

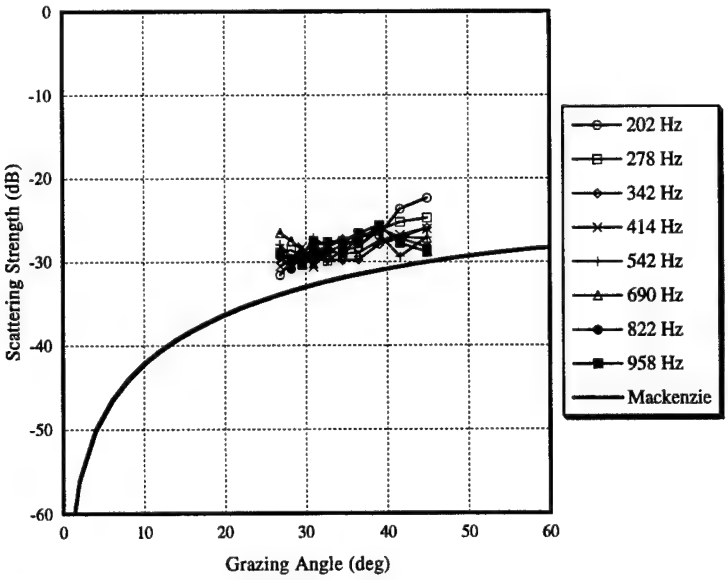

Fig. 34 — Bottom scattering strengths for CST-2 Run 43 Mod 3 beam 13

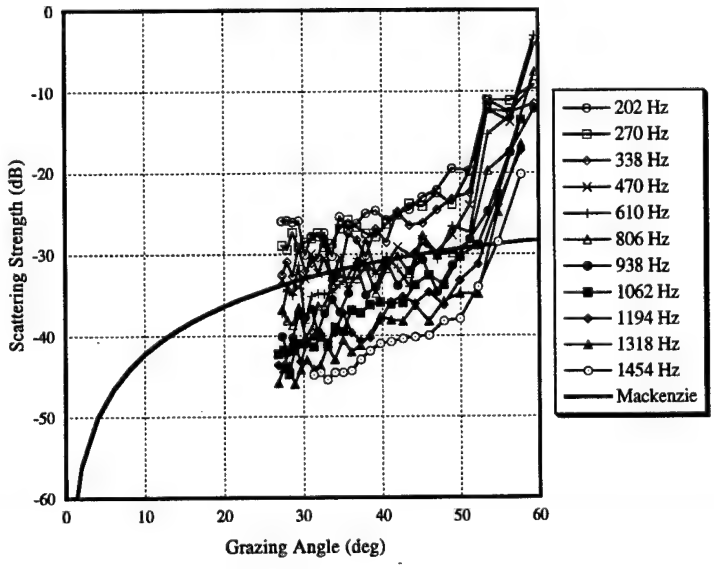

Fig. 35 — Bottom scattering strengths for CST-3 Run 2B beams 7-9

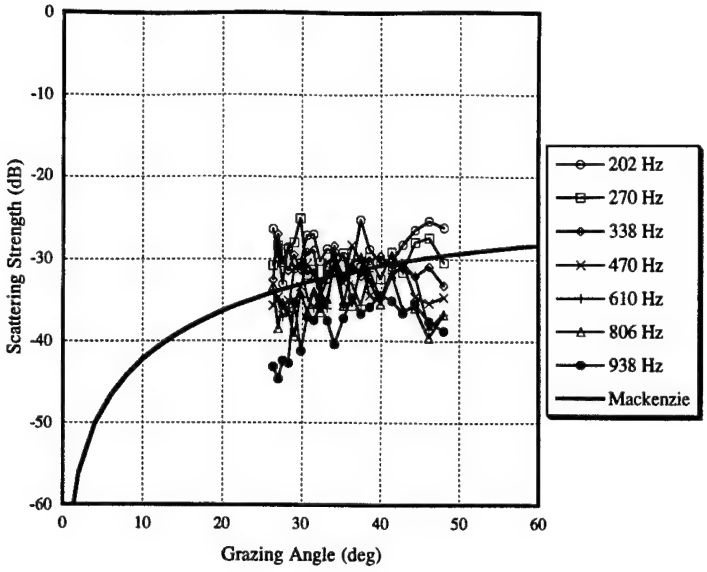

Fig. 36 — Bottom scattering strengths for CST-3 Run 2B beam 13

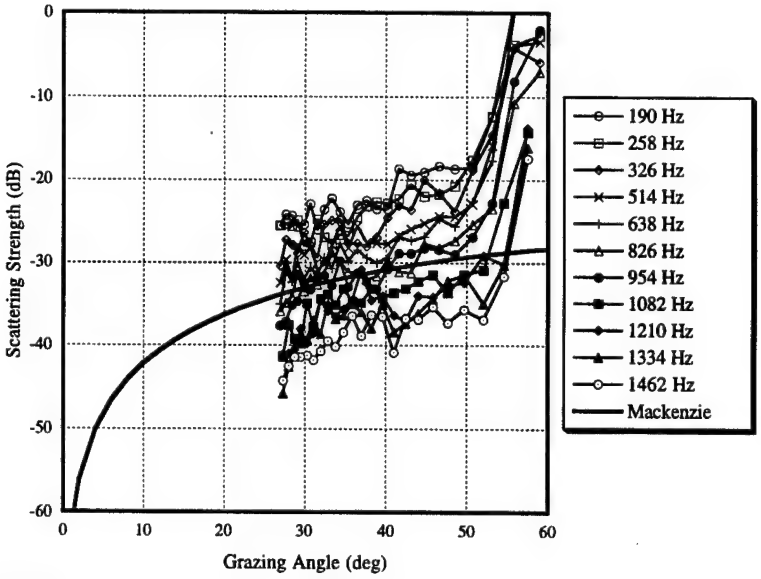

Fig. 37 — Bottom scattering strengths for CST-3 Run 3B beams 7-9

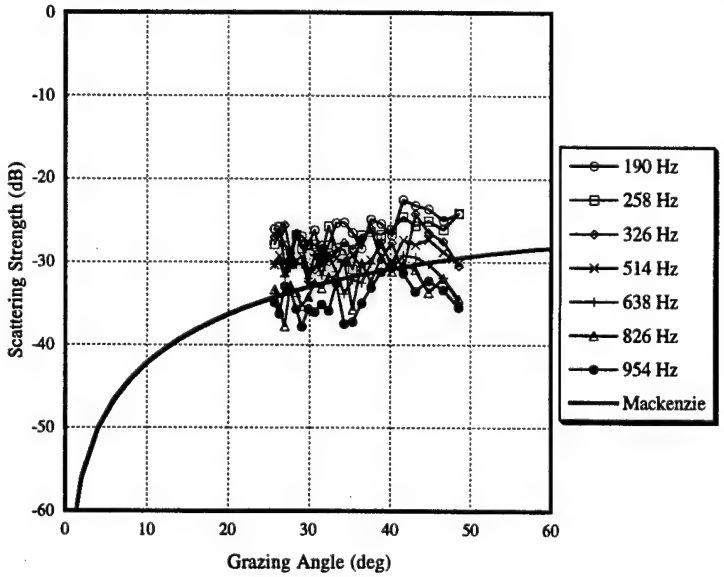

Fig. 38 — Bottom scattering strengths for CST-3 Run 3B beam 13

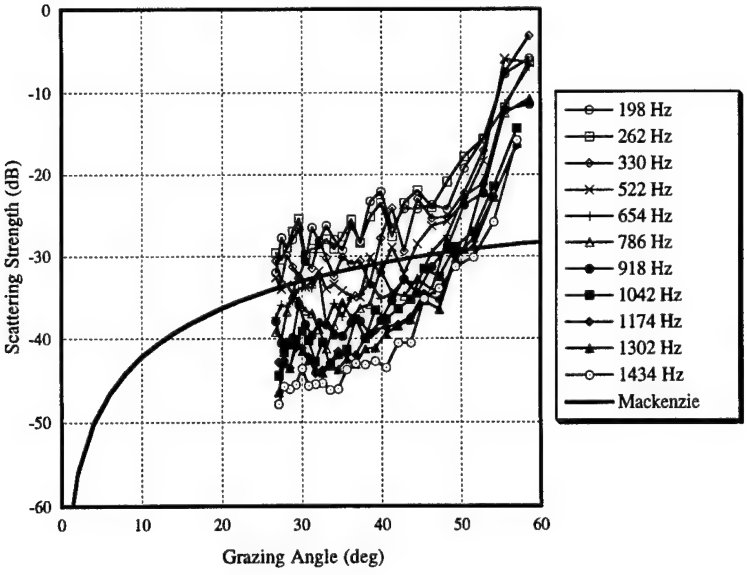

Fig. 39 — Bottom scattering strengths for CST-3 Run 5D beams 7-9

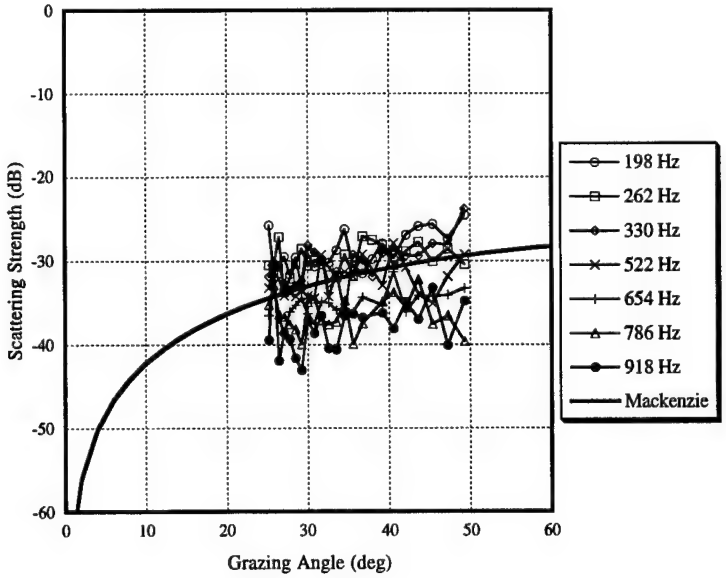

Fig. 40 — Bottom scattering strengths for CST-3 Run 5D beam 13

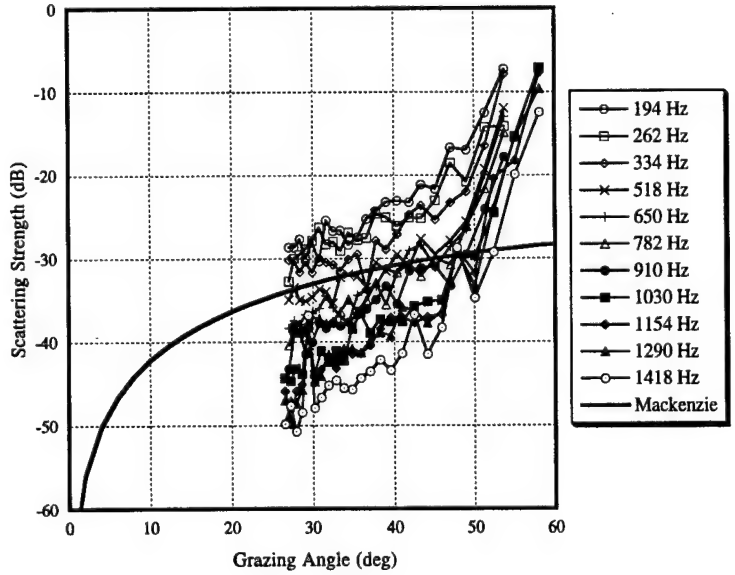

Fig. 41 — Bottom scattering strengths for CST-3 Run 5H beams 7-9

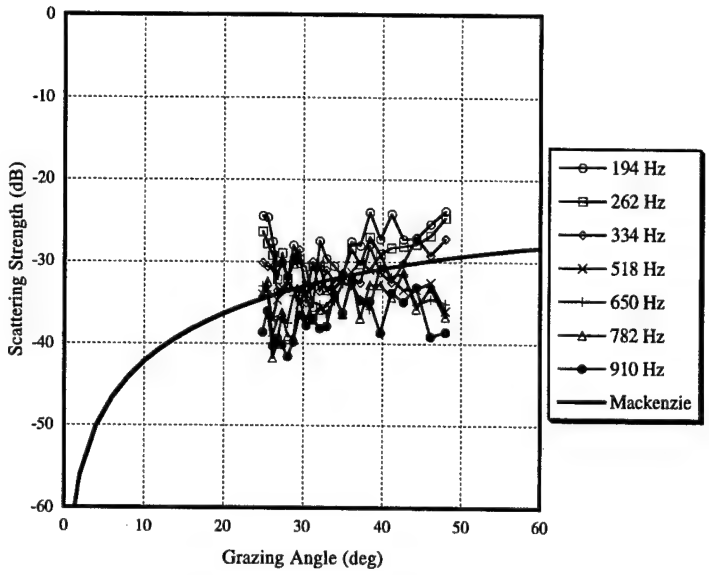

Fig. 42 — Bottom scattering strengths for CST-3 Run 5H beam 3

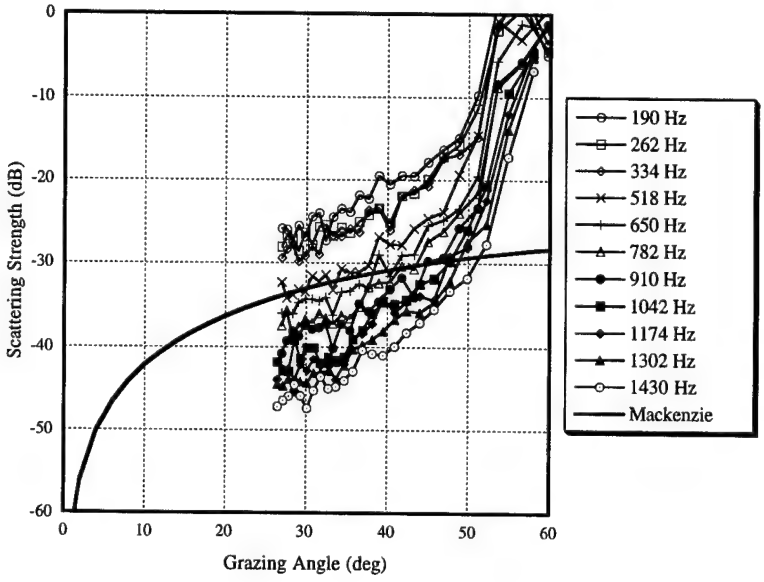

Fig. 43 — Bottom scattering strengths for CST-3 Run 5J beams 7-9

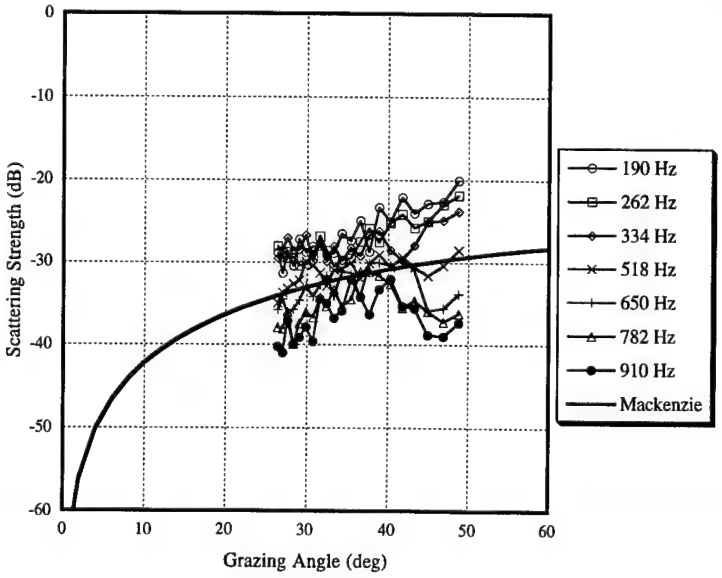

Fig. 44 — Bottom scattering strengths for CST-3 Run 5J beam 13

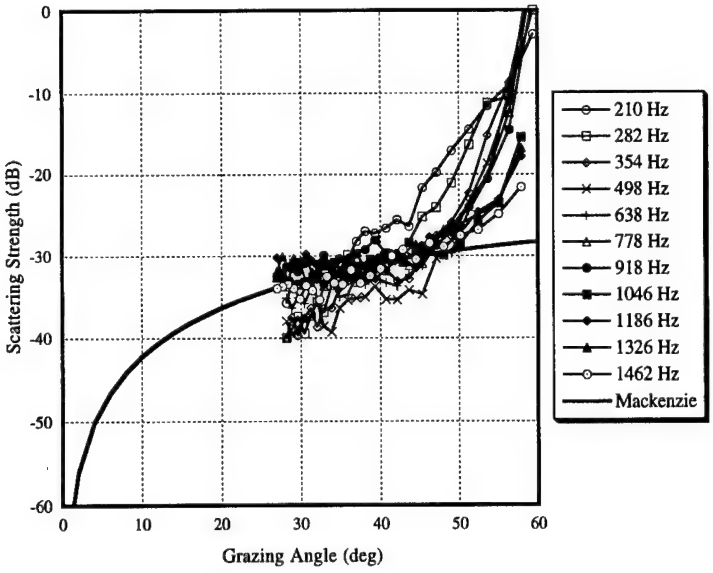

Fig. 45 — Bottom scattering strengths for CST-3 Run 33A beams 7-9

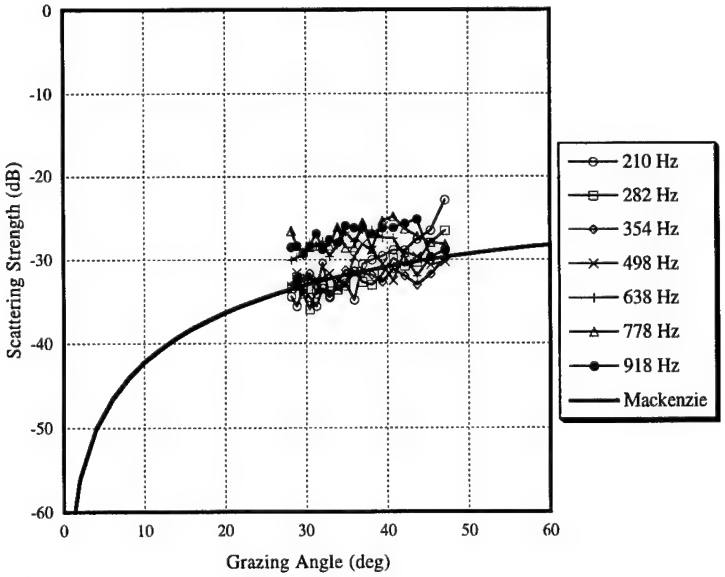

Fig. 46 — Bottom scattering strengths for CST-3 Run 33A beam 13

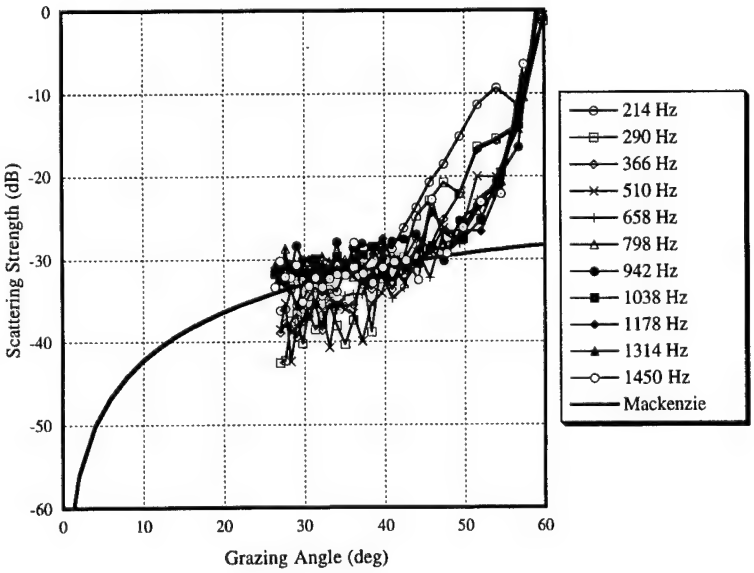

Fig. 47 — Bottom scattering strengths for CST-3 Run 37A beams 7-9

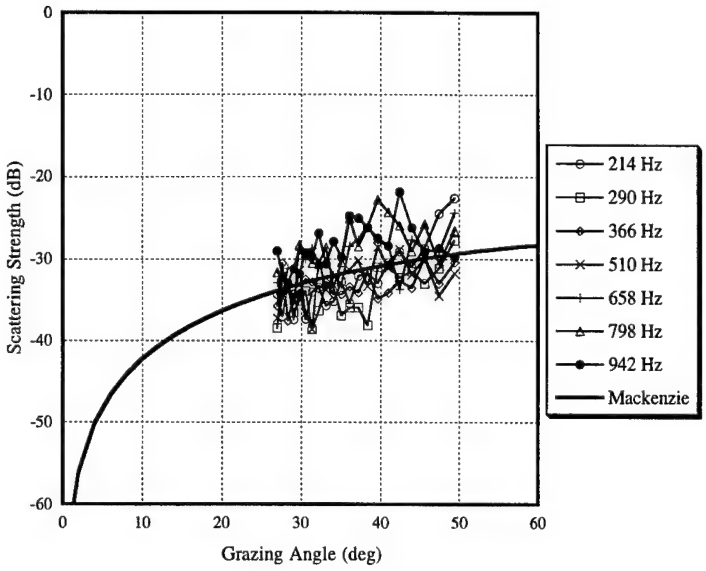

Fig. 48 — Bottom scattering strengths for CST-3 Run 37A beam 13

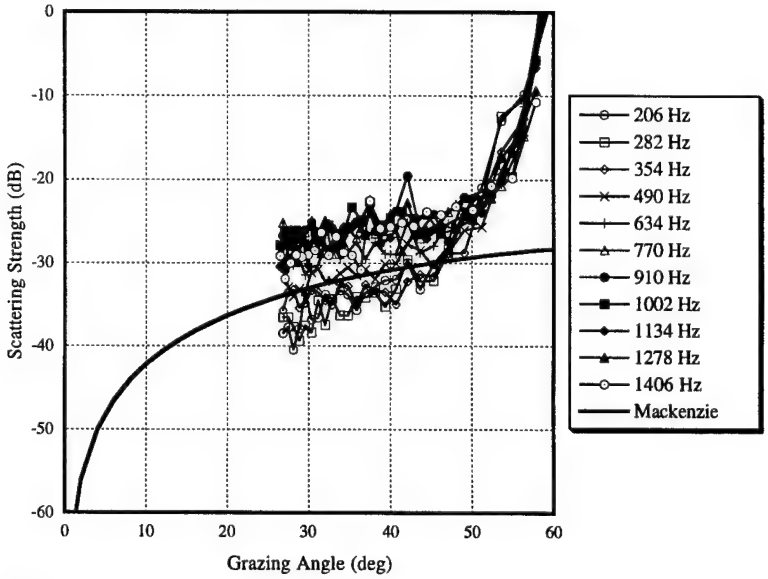

Fig. 49 — Bottom scattering strengths for CST-3 Run 51B beams 7-9

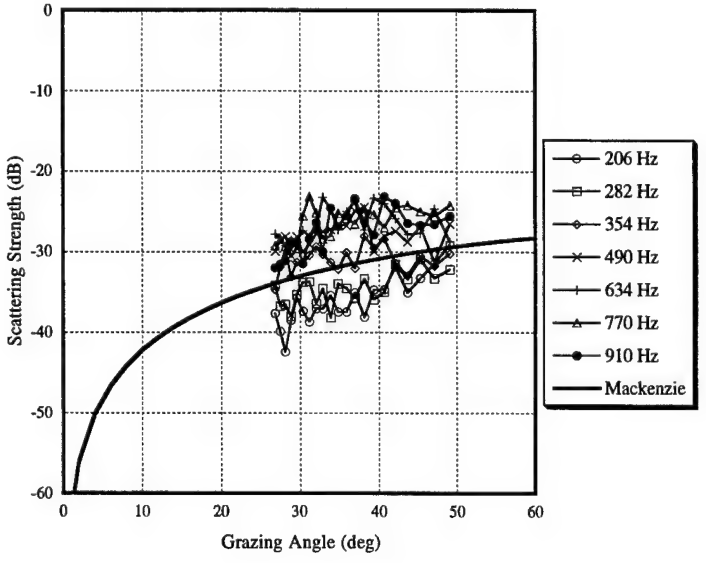

Fig. 50 — Bottom scattering strengths for CST-3 Run 51B beam 13

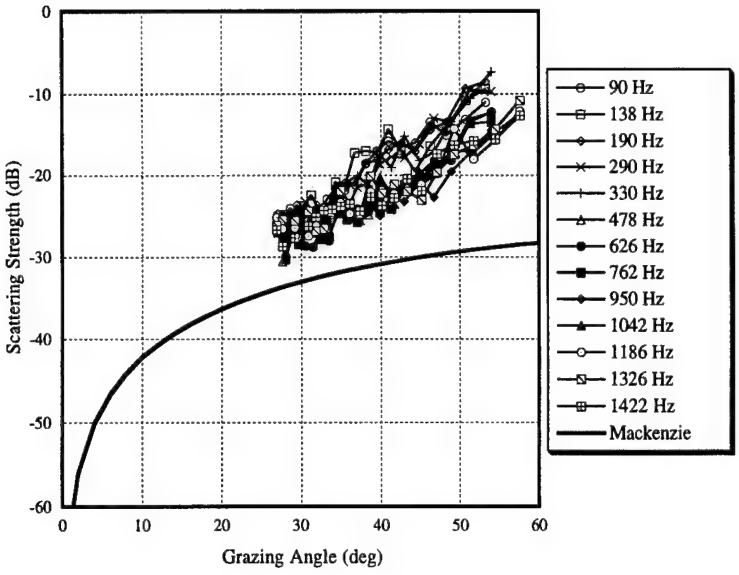

Fig. 51 — Bottom scattering strengths for CST-4 Run 7 beams 7-9

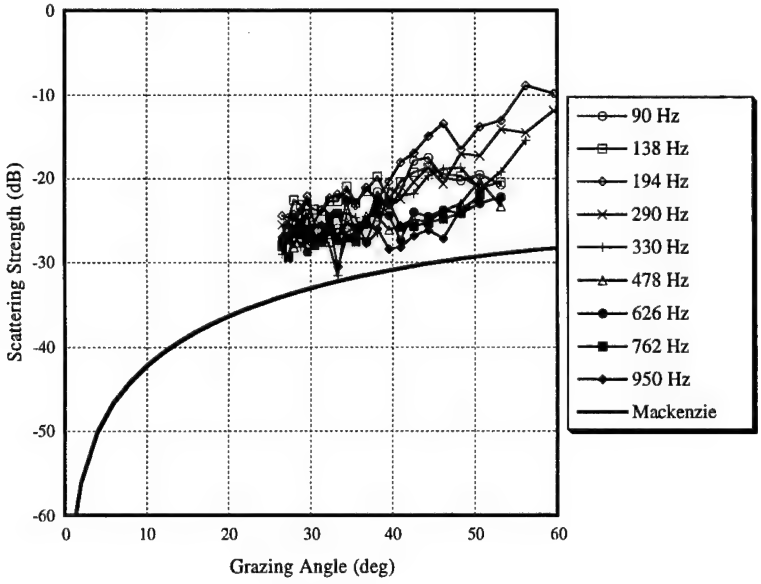

Fig. 52 — Bottom scattering strengths for CST-4 Run 7 beam 13

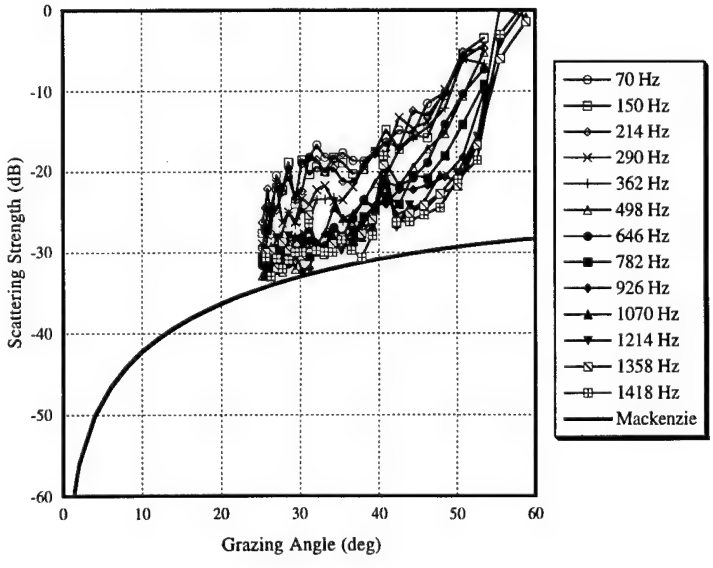

Fig. 53 — Bottom scattering strengths for CST-4 Run 12B beams 7-9

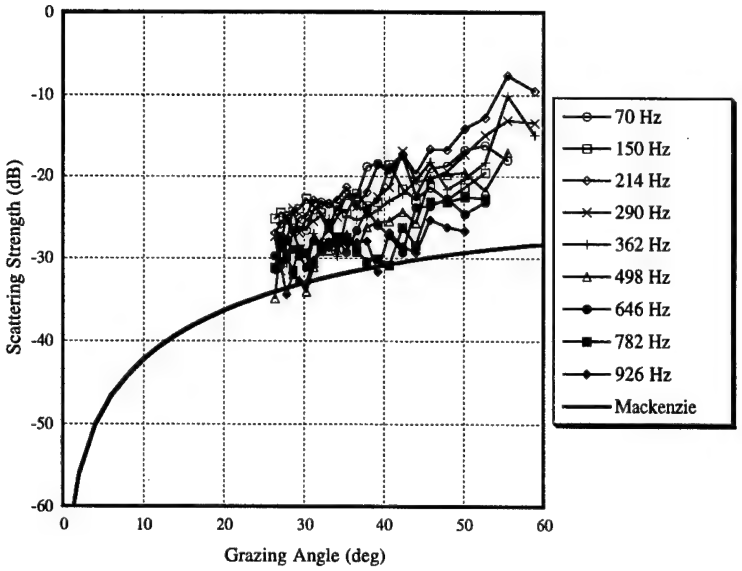

Fig. 54 — Bottom scattering strengths for CST-4 Run 12B beam 13

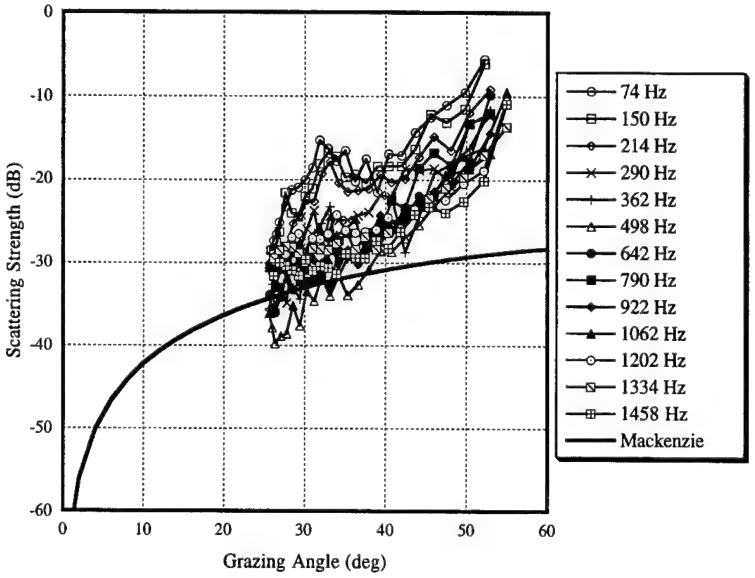

Fig. 55 — Bottom scattering strengths for CST-4 Run 28B beams 7-9

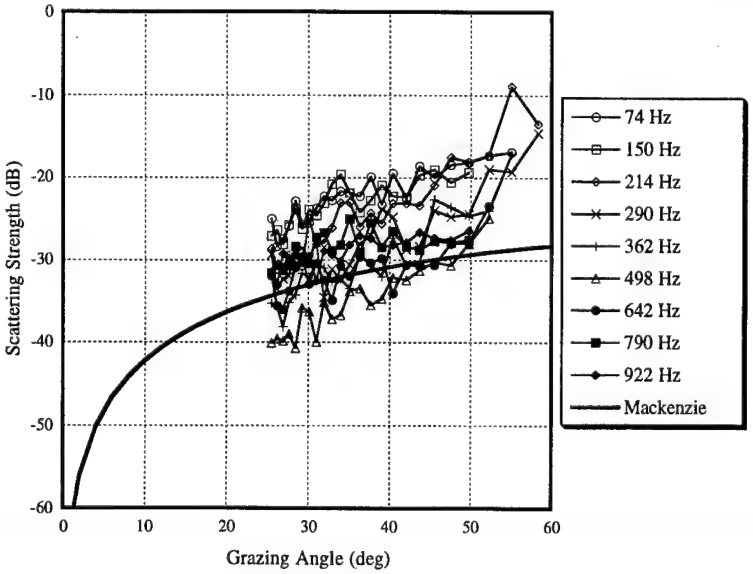

Fig. 56 — Bottom scattering strengths for CST-4 Run 28B beam 13

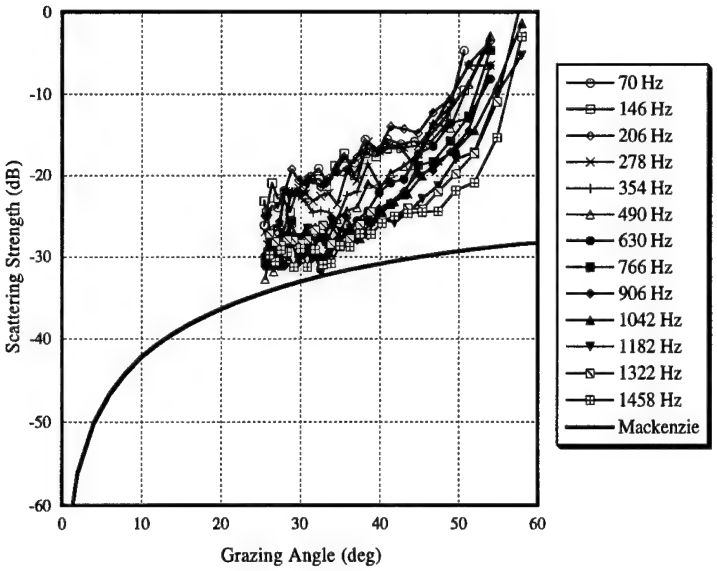

Fig. 57 — Bottom scattering strengths for CST-4 Run 32 beams 7-9

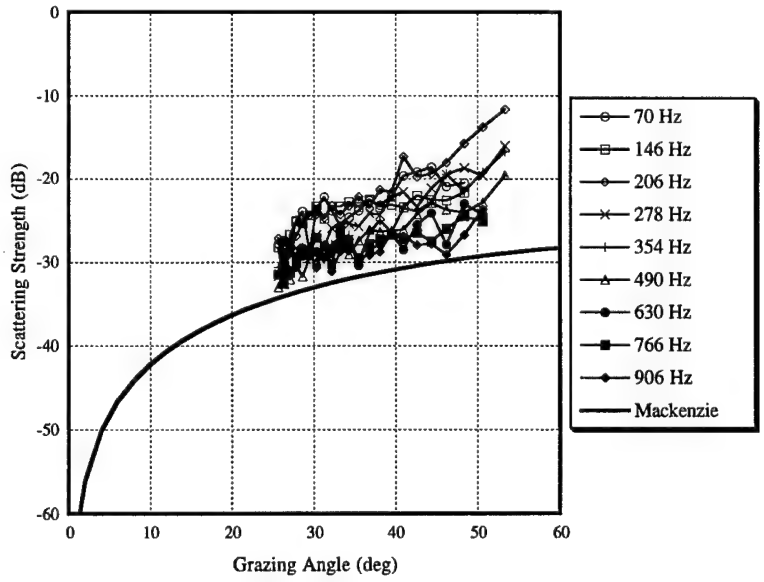

Fig. 58 — Bottom scattering strengths for CST-4 Run 32 beam 13

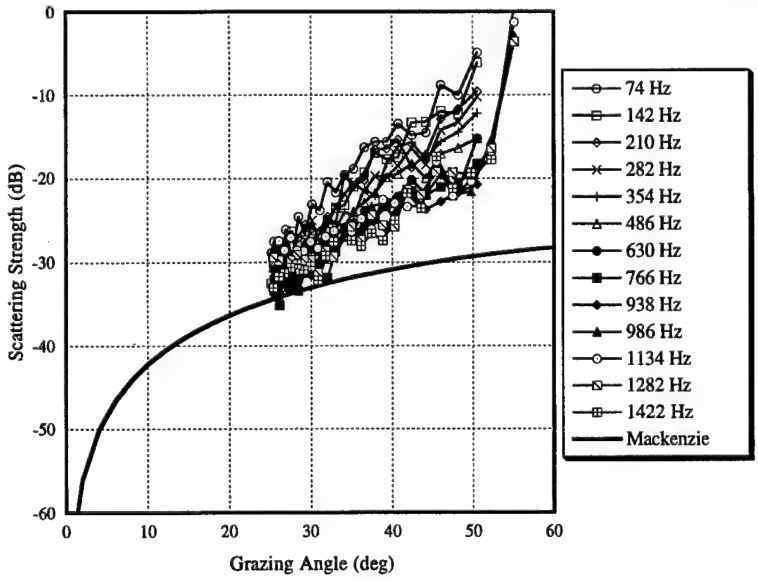

Fig. 59 — Bottom scattering strengths for CST-4 Run 43B beams 7-9

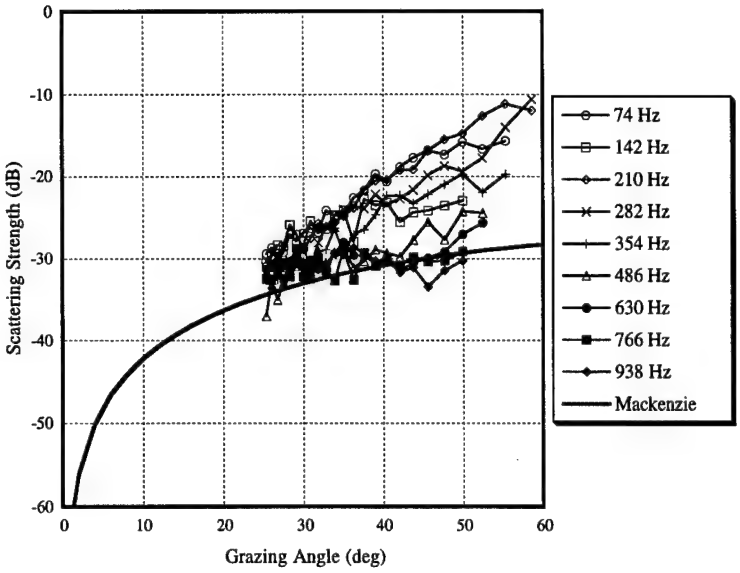

Fig. 60 — Bottom scattering strengths for CST-4 Run 43B beam 13

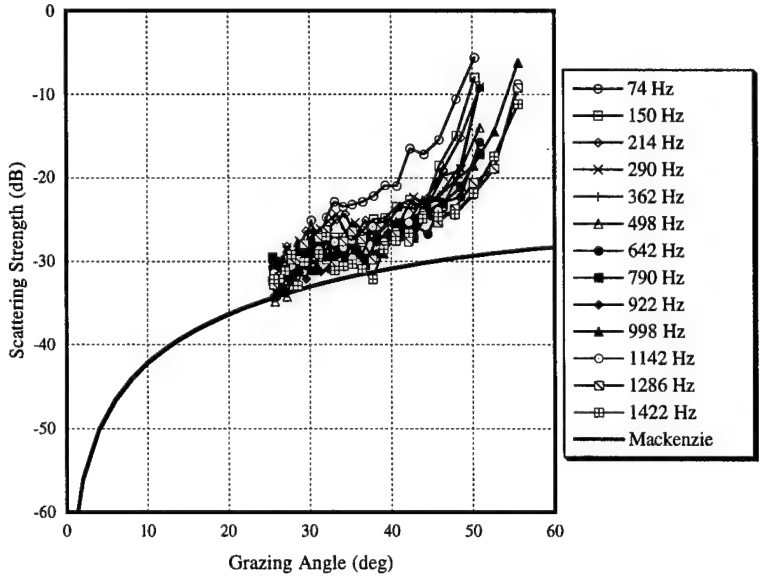

Fig. 61 — Bottom scattering strengths for CST-4 Run 46B beams 7-9

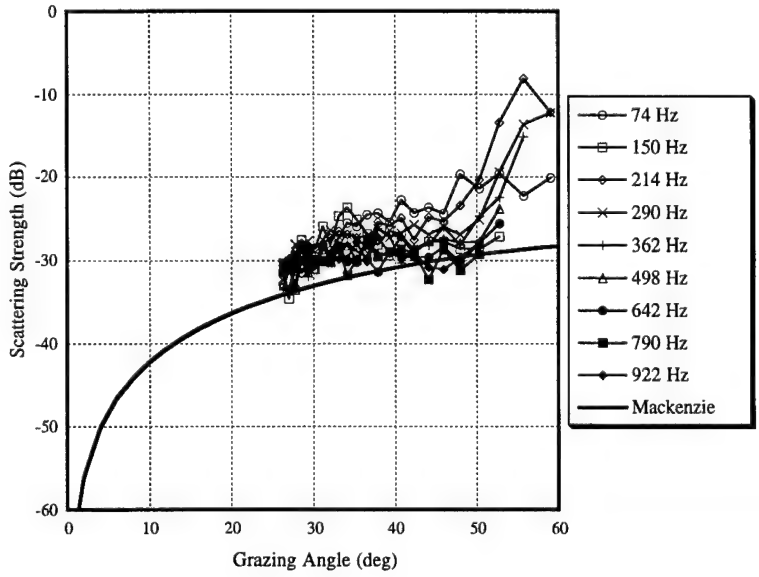

Fig. 62 — Bottom scattering strengths for CST-4 Run 46B beam 13

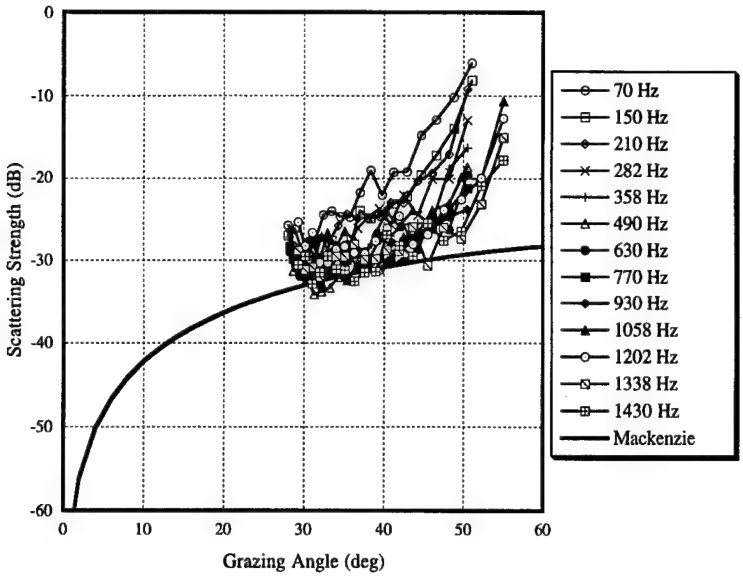

Fig. 63 — Bottom scattering strengths for CST-4 Run 49A beams 7-9

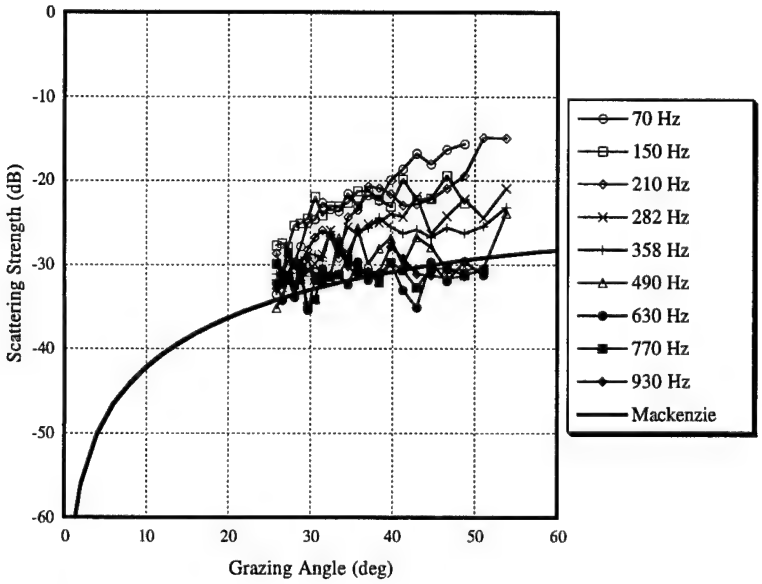

Fig. 64 — Bottom scattering strengths for CST-4 Run 49A beam 13

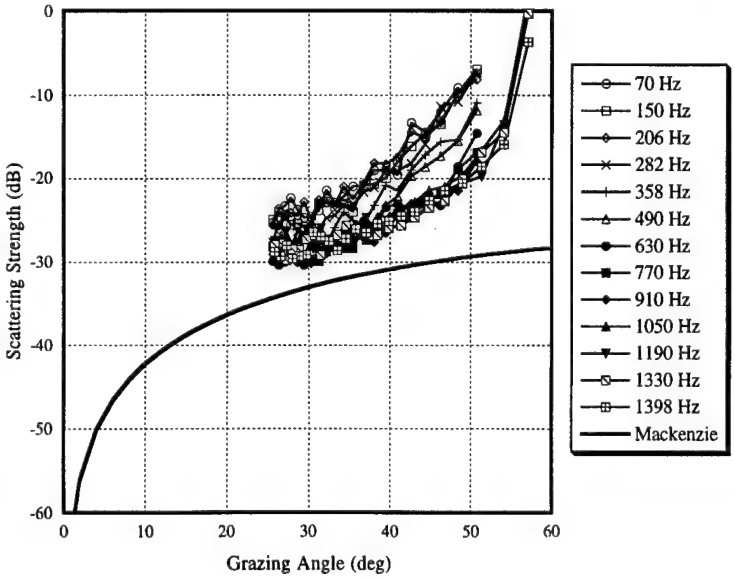

Fig. 65 — Bottom scattering strengths for CST-4 Run 50E beams 7-9

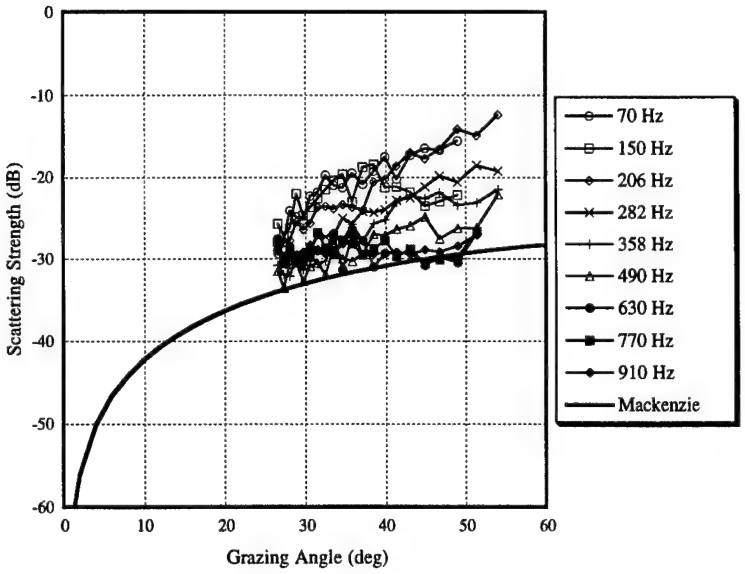

Fig. 66 — Bottom scattering strengths for CST-4 Run 50E beam 13

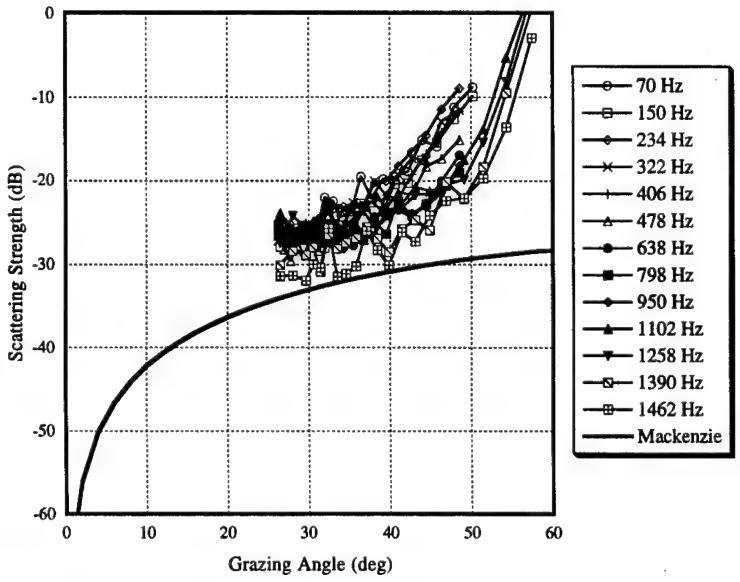

Fig. 67 — Bottom scattering strengths for CST-4 Run 51E beams 7-9

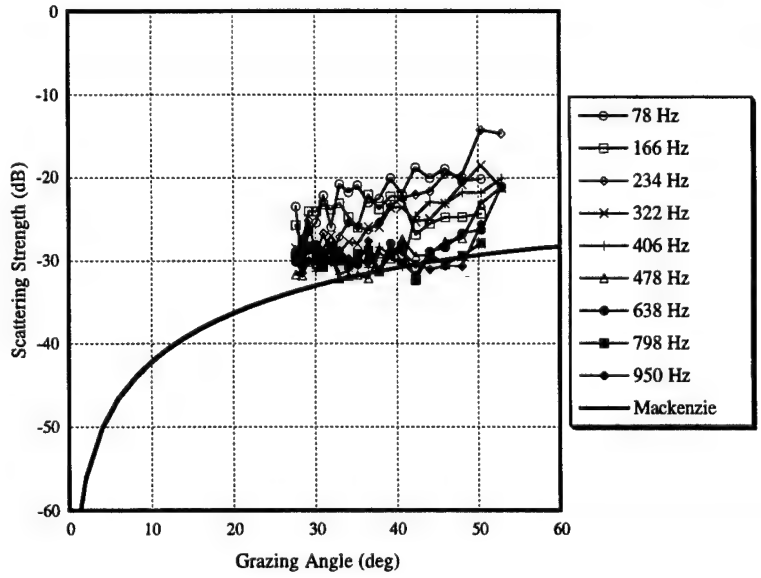

Fig. 68 — Bottom scattering strengths for CST-4 Run 51E beam 13

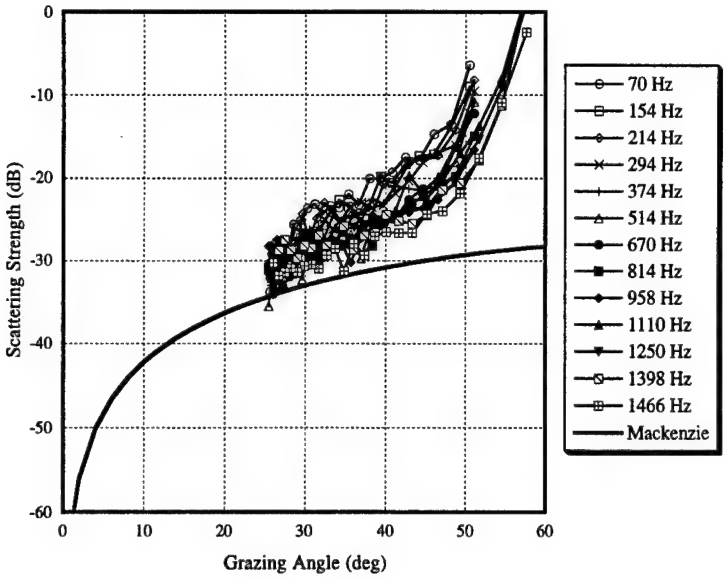

Fig. 69 — Bottom scattering strengths for CST-4 Run 52B beams 7-9

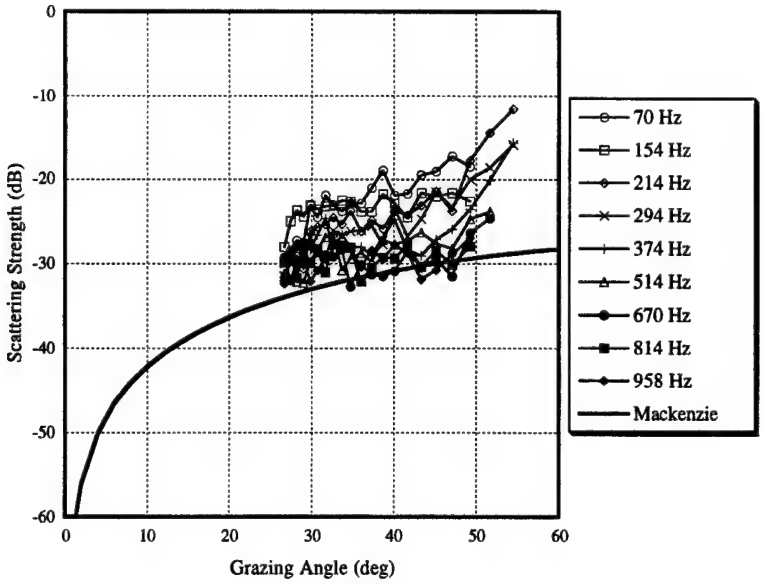

Fig. 70 — Bottom scattering strengths for CST-4 Run 52B beam 13

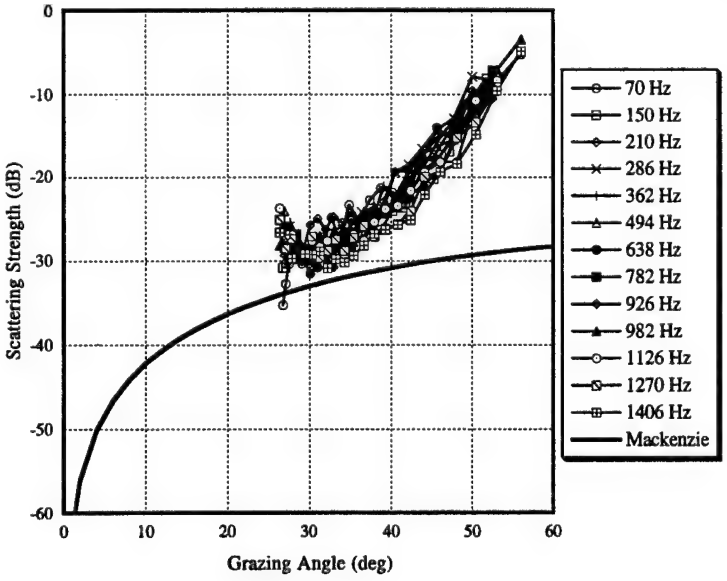

Fig. 71 — Bottom scattering strengths for CST-4 Run 59 beams 7-9

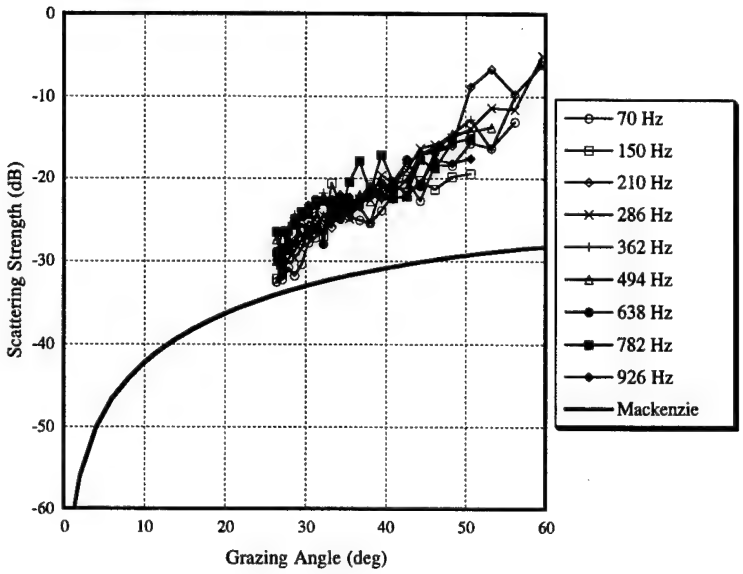

Fig. 72 — Bottom scattering strengths for CST-4 Run 59 beam 13

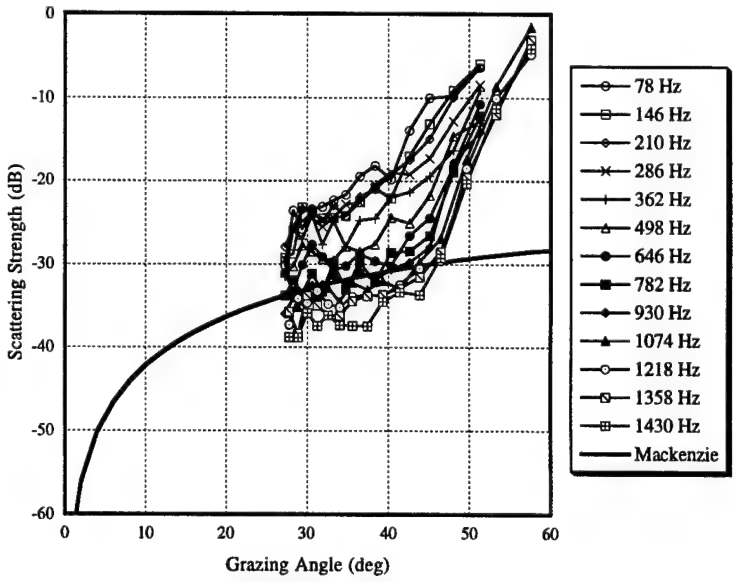

Fig. 73 — Bottom scattering strengths for CST-5 Run 2 beams 7-9

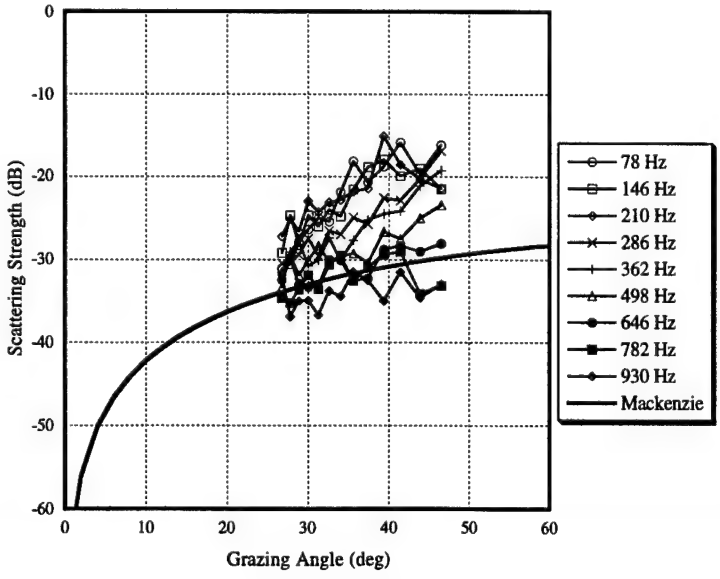

Fig. 74 — Bottom scattering strengths for CST-5 Run 2 beam 13

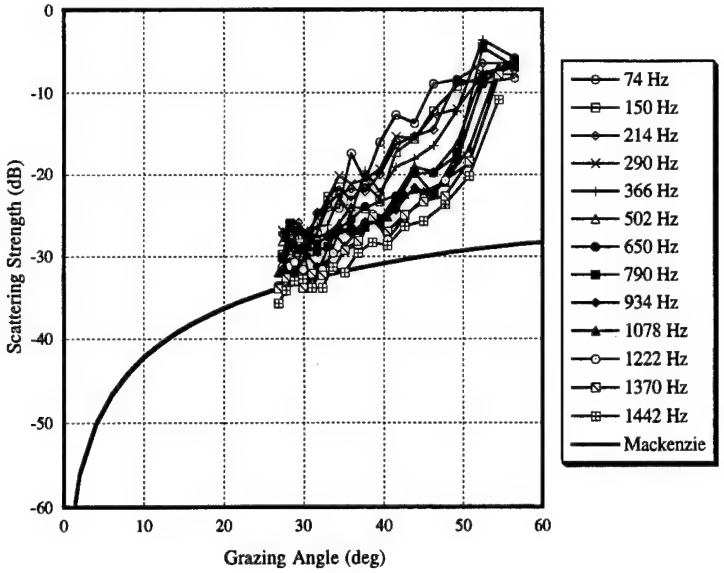

Fig. 75 — Bottom scattering strengths for CST-5 Run 14A beams 7-9

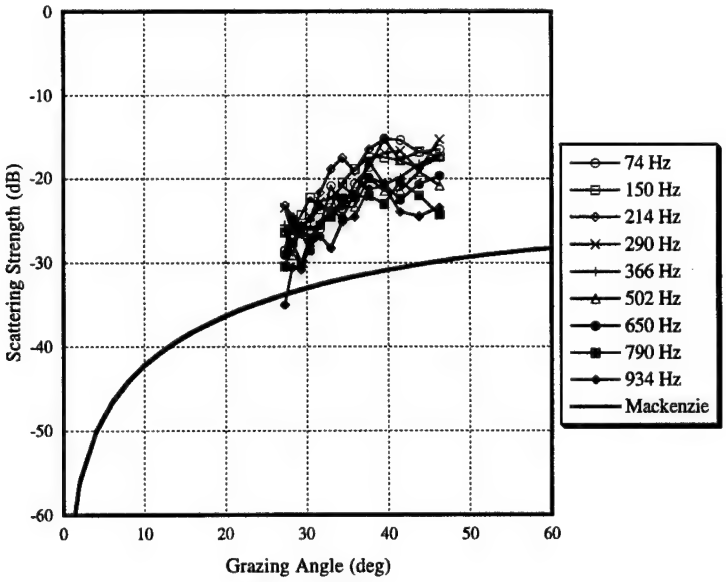

Fig. 76 — Bottom scattering strengths for CST-5 Run 14A beam 13

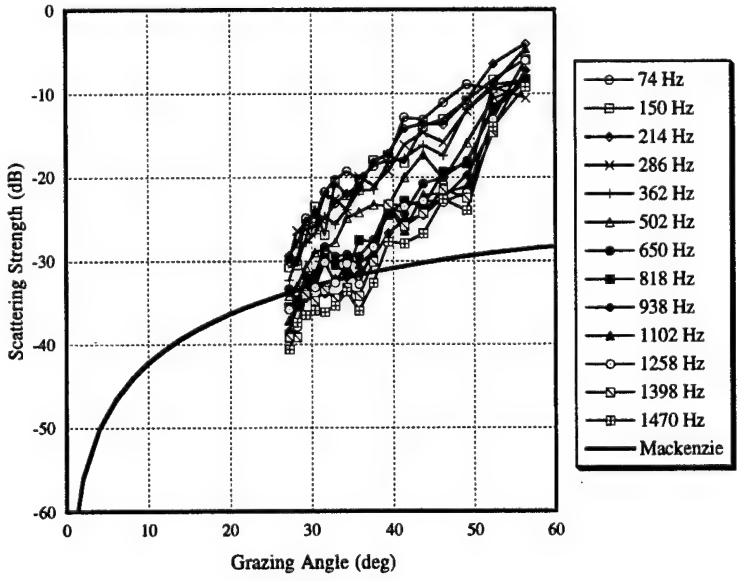

Fig. 77 — Bottom scattering strengths for CST-5 Run 20 beams 7-9

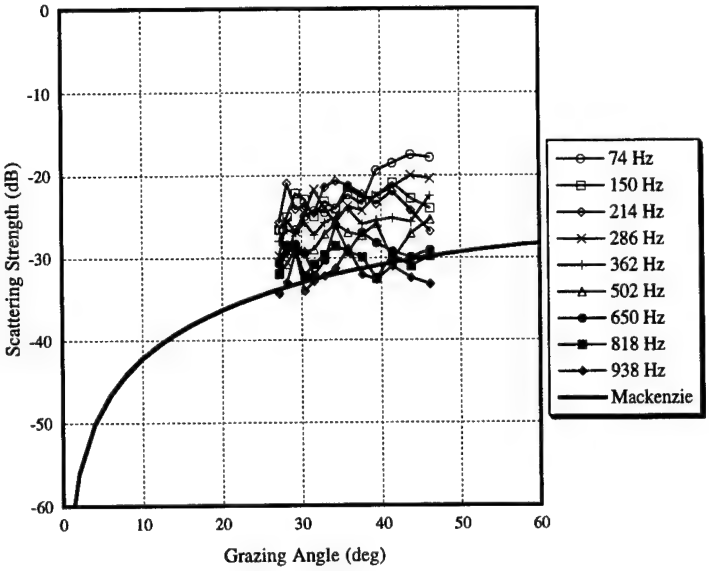

Fig. 78 — Bottom scattering strengths for CST-5 Run 20 beam 13

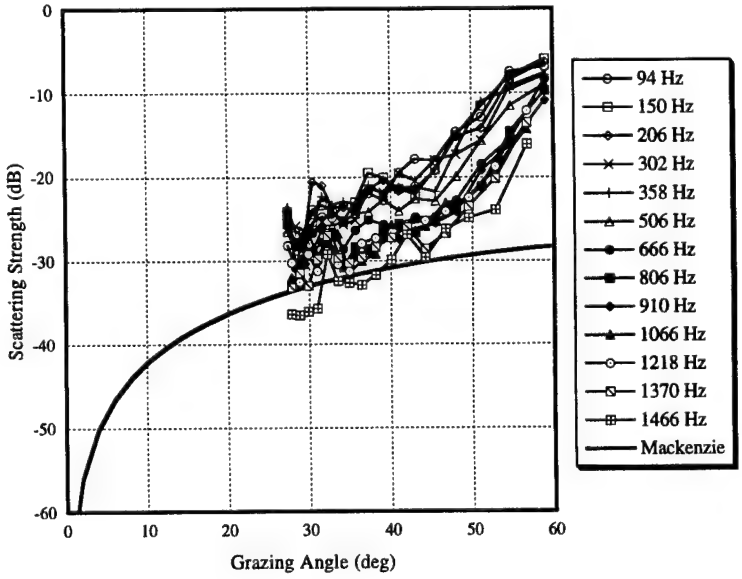

Fig. 79 — Bottom scattering strengths for CST-5 Run 26 beams 7-9

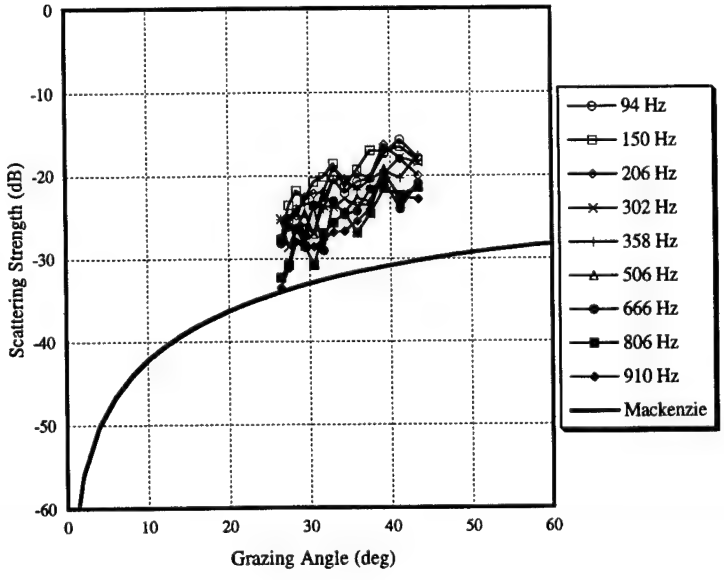

Fig. 80 — Bottom scattering strengths for CST-5 Run 26 beam 13

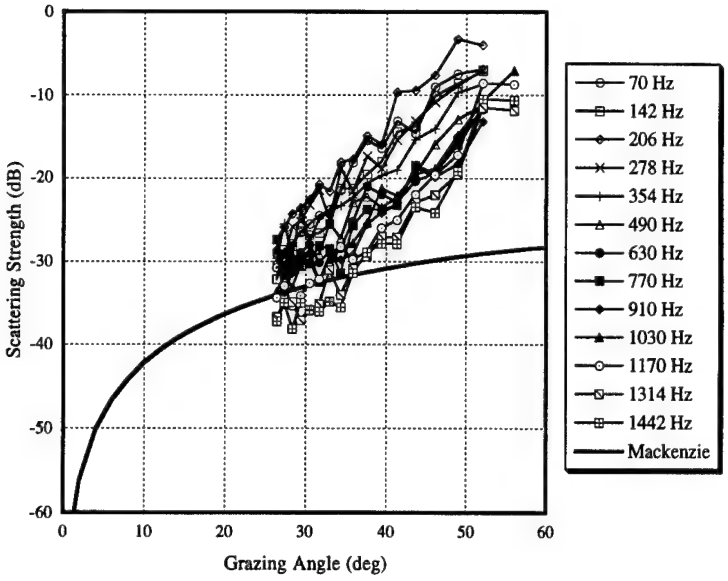

Fig. 81 — Bottom scattering strengths for CST-5 Run 33 beams 7-9

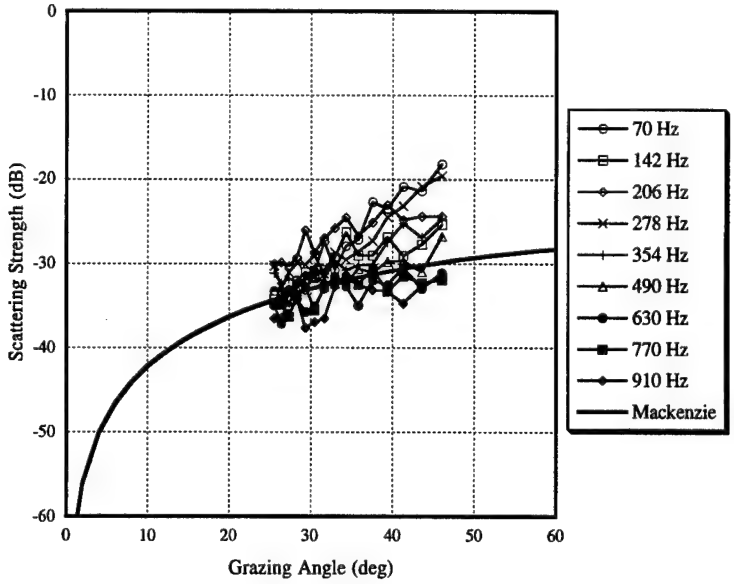

Fig. 82 — Bottom scattering strengths for CST-5 Run 33 beam 13

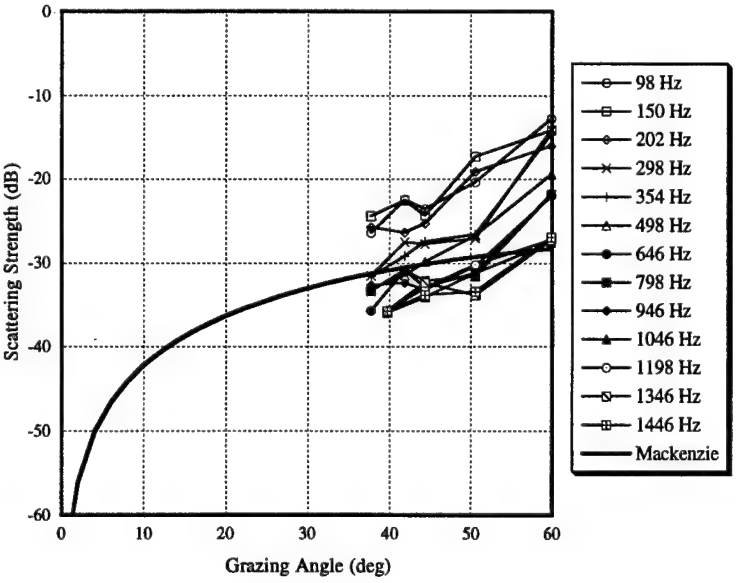

Fig. 83 — Bottom scattering strengths for CST-5 Run T1-3 beams 7-9

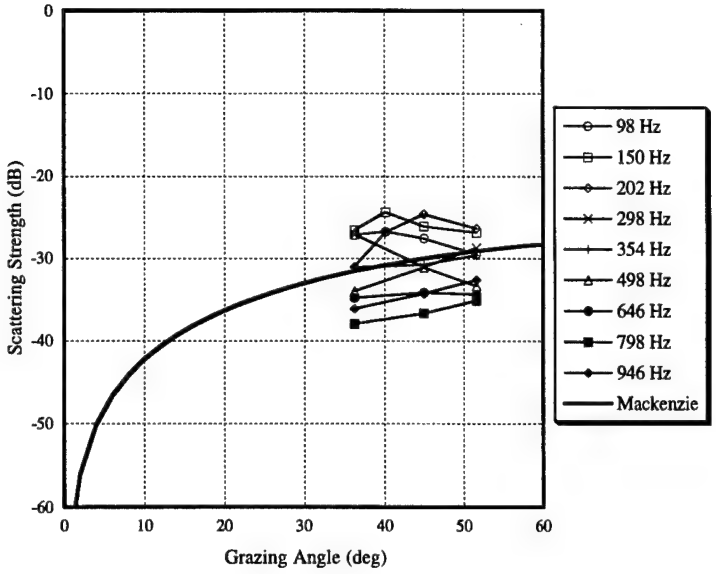

Fig. 84 — Bottom scattering strengths for CST-5 Run T1-3 beam 3

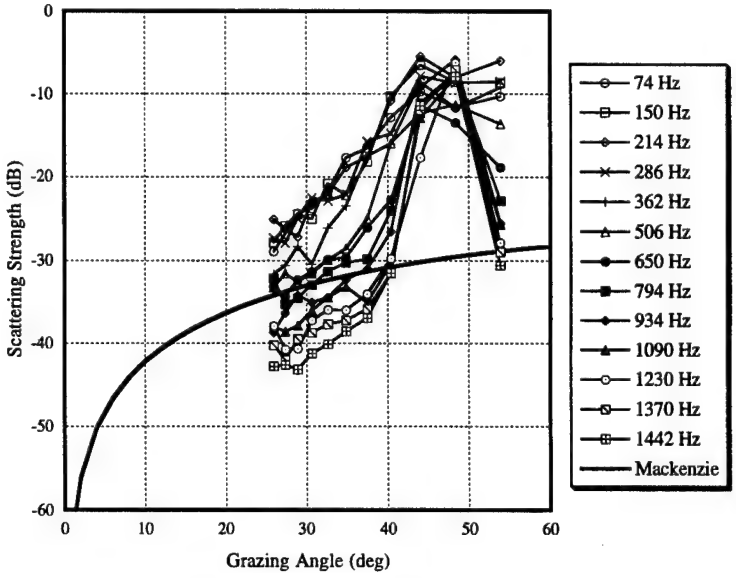

Fig. 85 — Bottom scattering strengths for CST-5 Run T2-6 beams 7-9

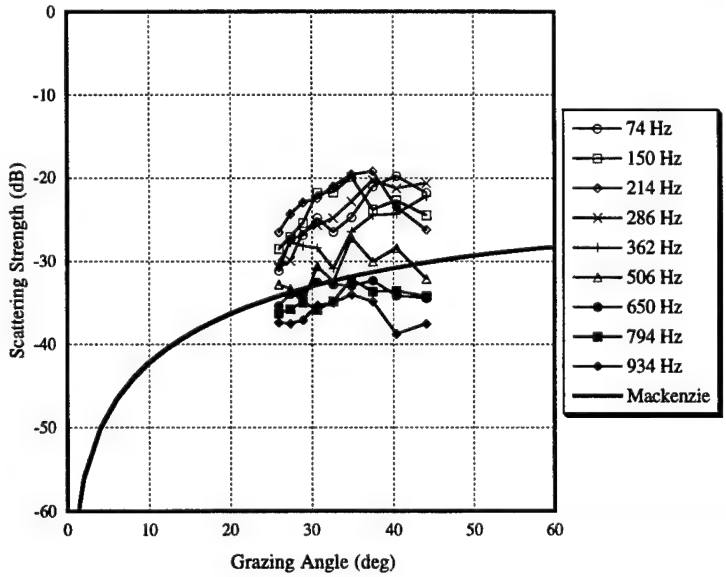

Fig. 86 — Bottom scattering strengths for CST-5 Run T2-6 beam 13

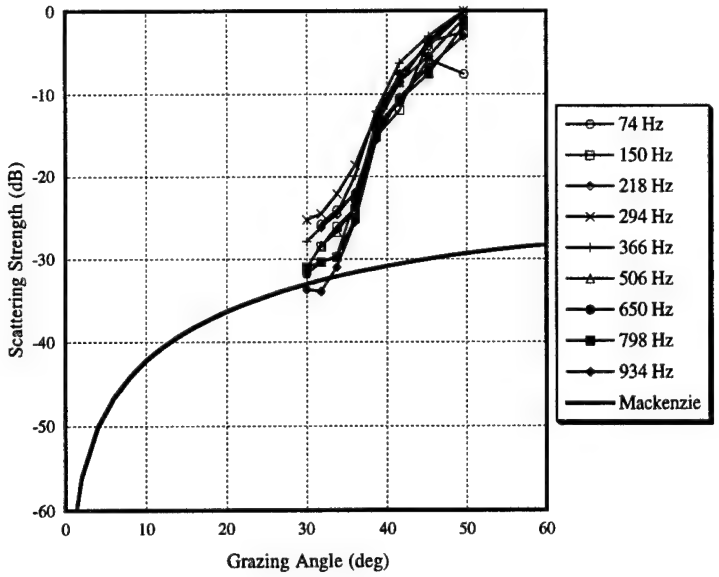

Fig. 87 — Bottom scattering strengths for CST-5 Run 46 beams 7-9

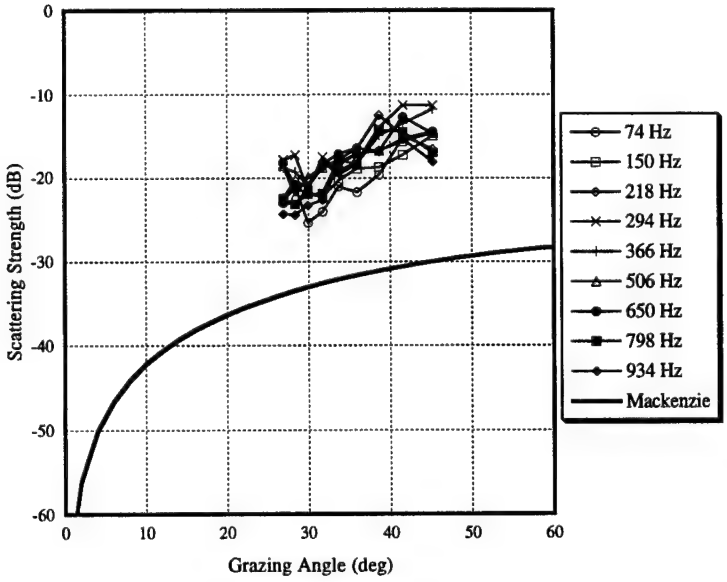

Fig. 88 — Bottom scattering strengths for CST-5 Run 46 beam 13

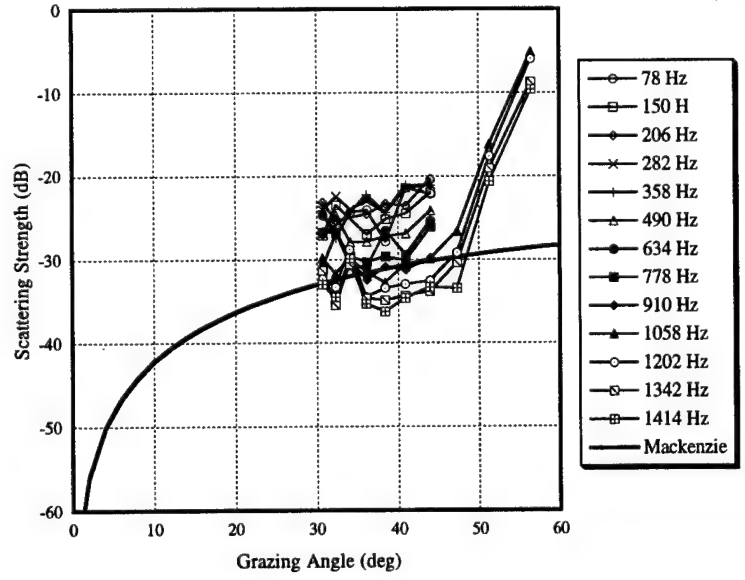

Fig. 89 — Bottom scattering strengths for CST-5 Run 48 beams 7-9

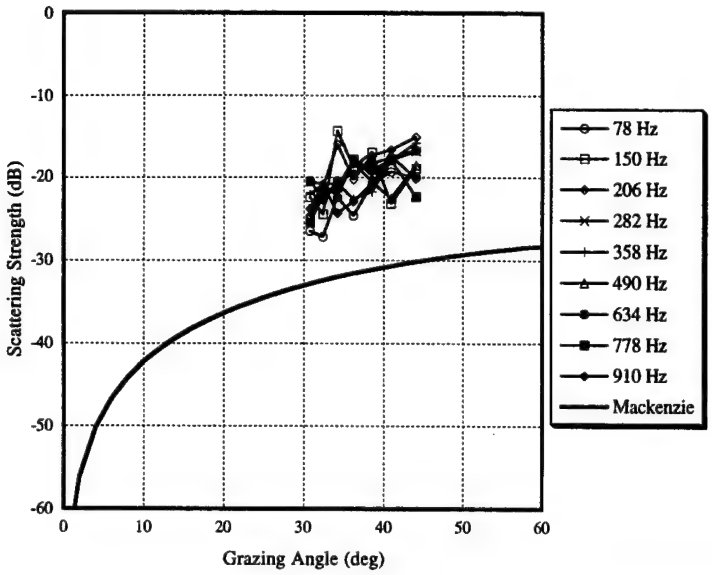

Fig. 90 — Bottom scattering strengths for CST-5 Run 48 beam 13

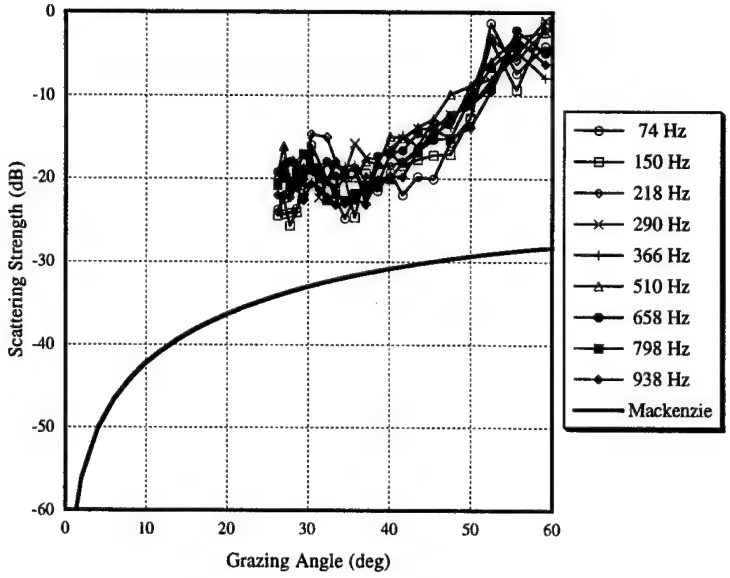

Fig. 91 — Bottom scattering strengths for CST-7 Run 1A beams 7-9

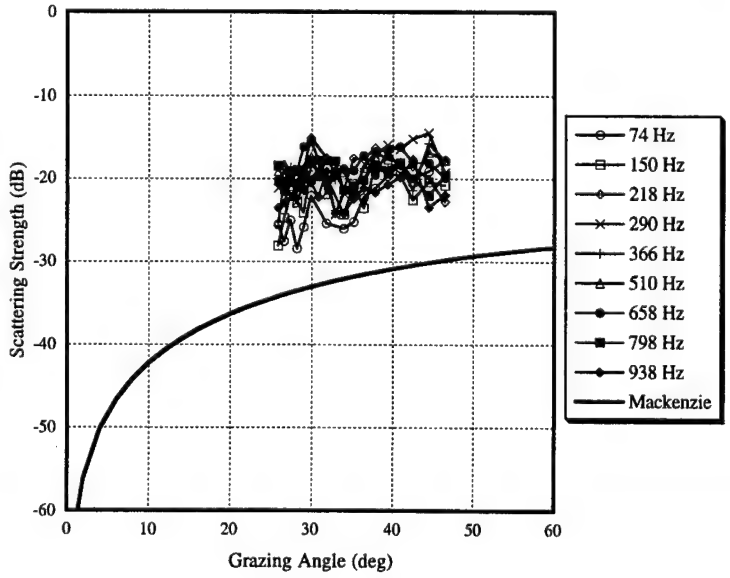

Fig. 92 — Bottom scattering strengths for CST-7 Run 1A beam 3

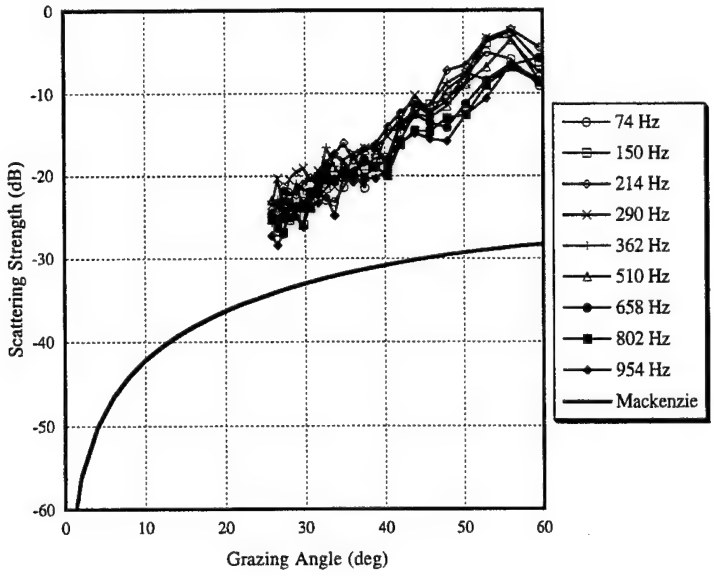

Fig. 93 — Bottom scattering strengths for CST-7 Run 3C beams 7-9

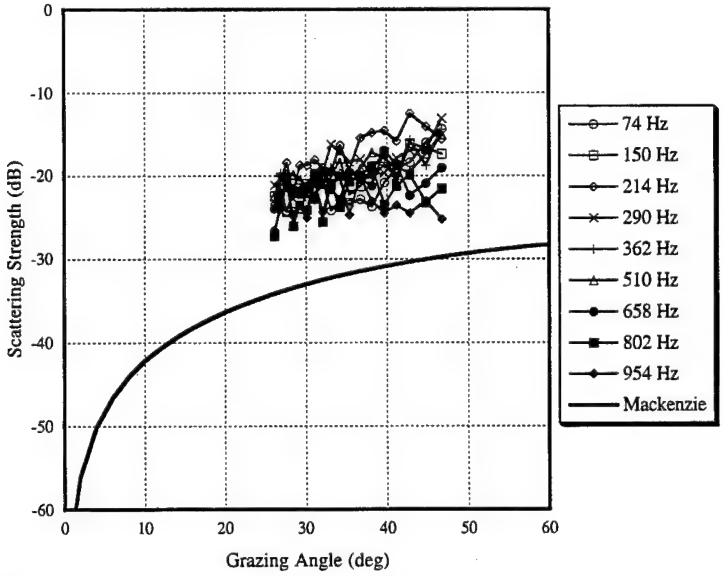

Fig. 94 — Bottom scattering strengths for CST-7 Run 3C beam 13

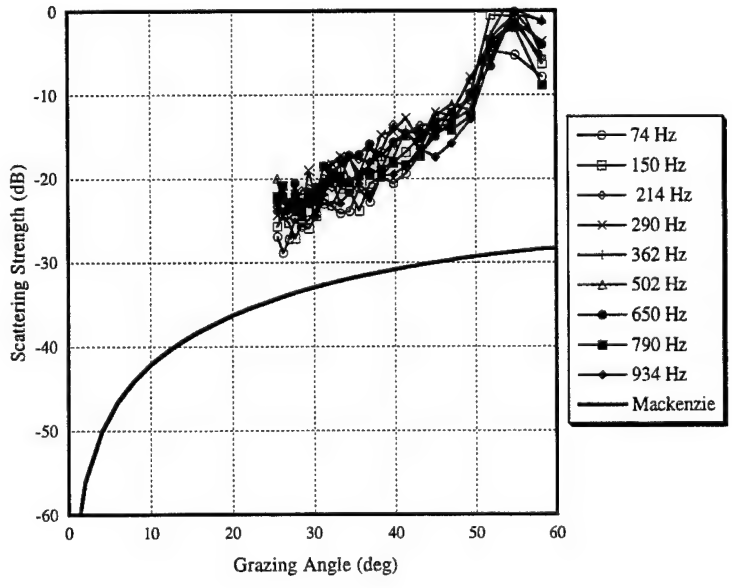

Fig. 95 — Bottom scattering strengths for CST-7 Run 5B beams 7-9

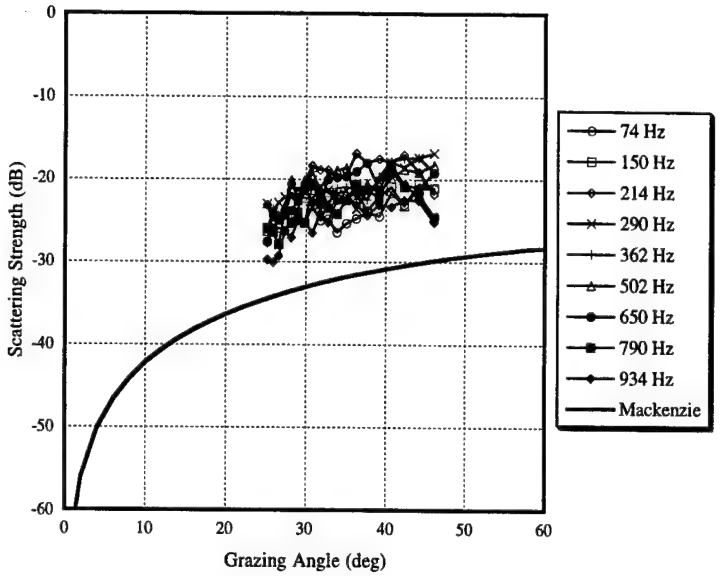

Fig. 96 — Bottom scattering strengths for CST-7 Run 5B beam 13

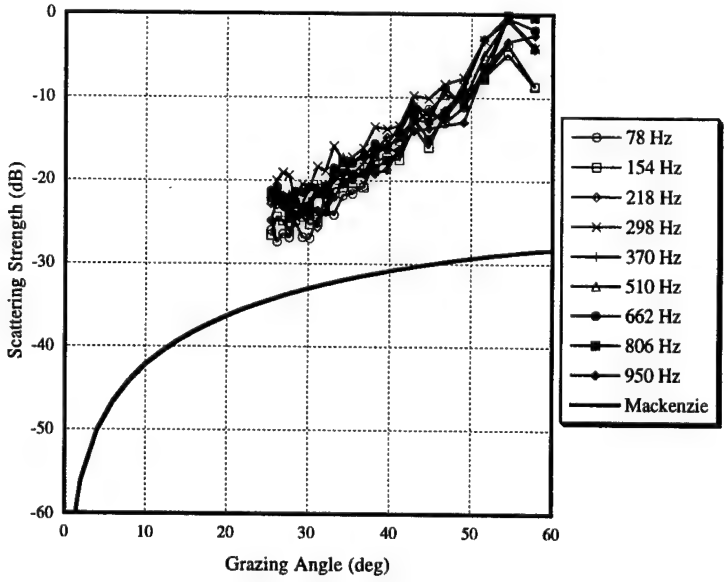

Fig. 97 — Bottom scattering strengths for CST-7 Run 11C beams 7-9

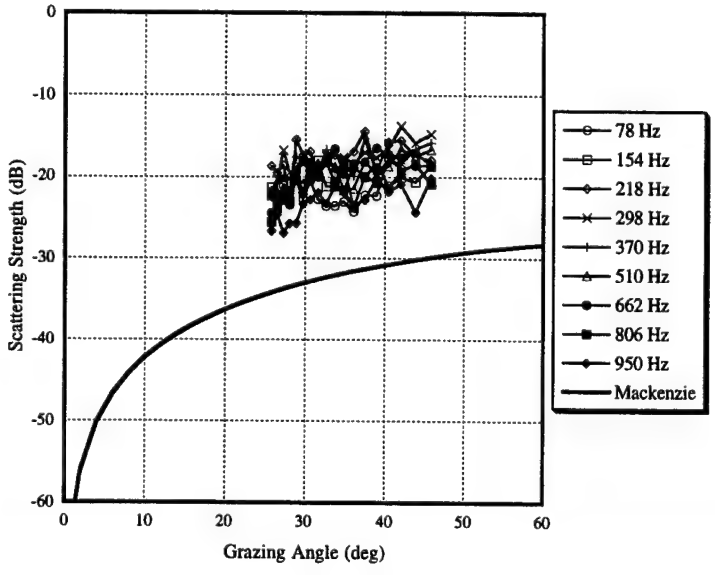

Fig. 98 — Bottom scattering strengths for CST-7 Run 11C beam 13

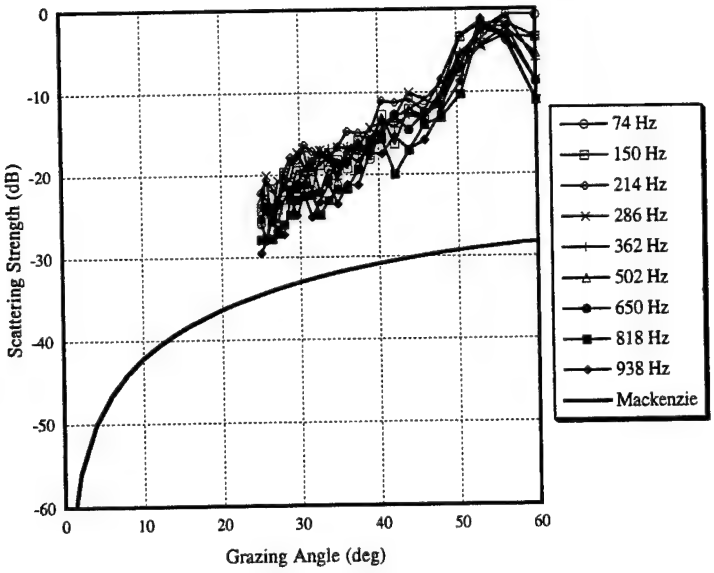

Fig. 99 — Bottom scattering strengths for CST-7 Run 12D beams 7-9

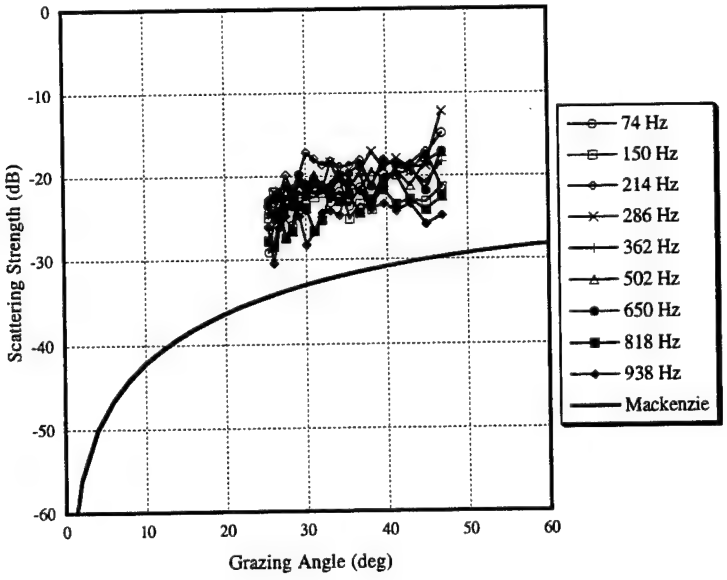

Fig. 100 — Bottom scattering strengths for CST-7 Run 12D beam 3

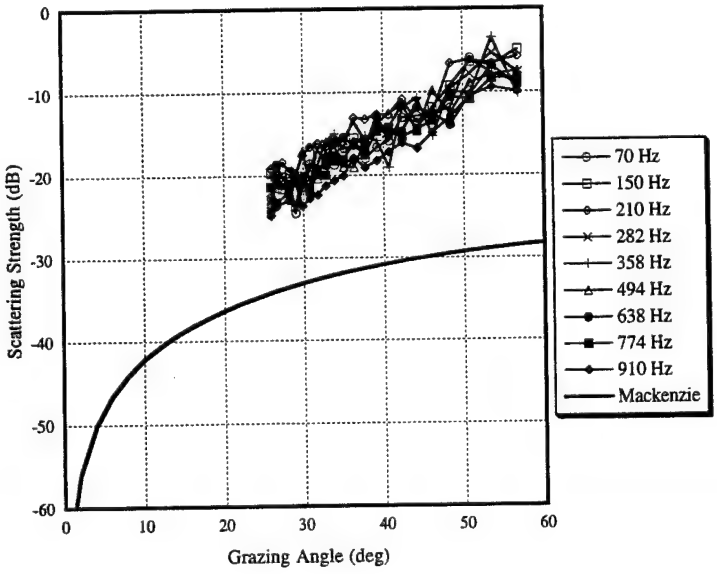

Fig. 101 — Bottom scattering strengths for CST-7 Run 13C beams 7-9

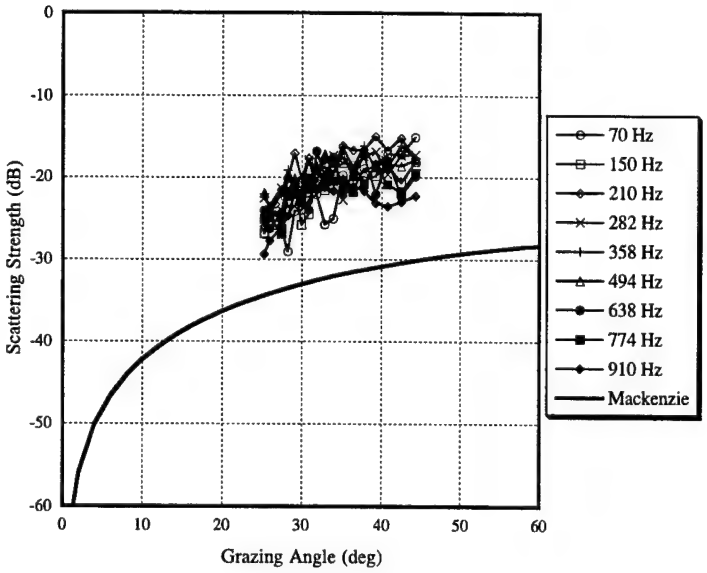

Fig. 102 — Bottom scattering strengths for CST-7 Run 13C beam 13

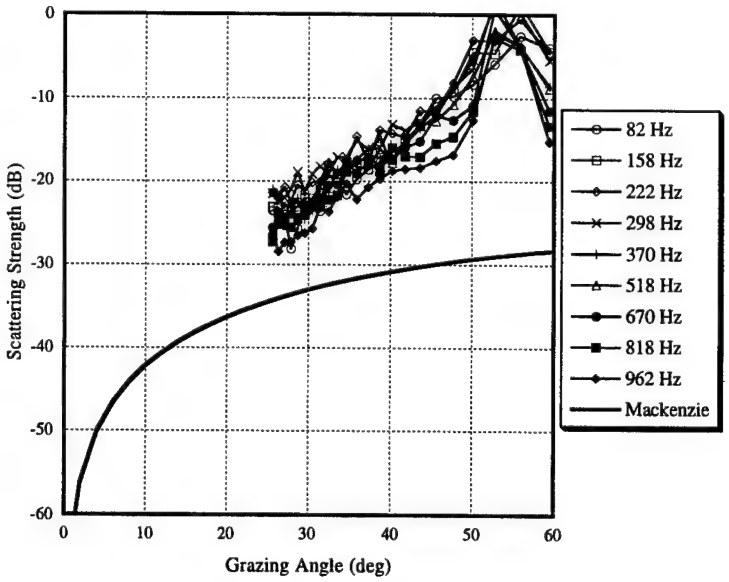

Fig. 103 — Bottom scattering strengths for CST-7 Run 16B beams 7-9

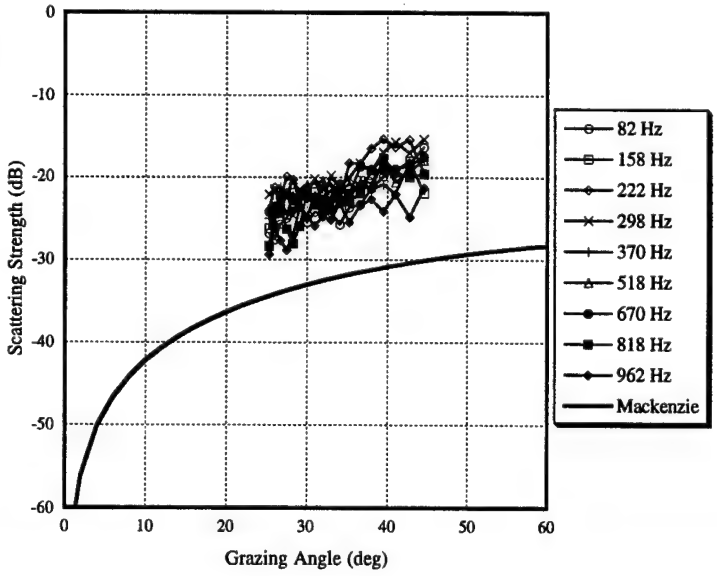

Fig. 104 — Bottom scattering strengths for CST-7 Run 16B beam 13

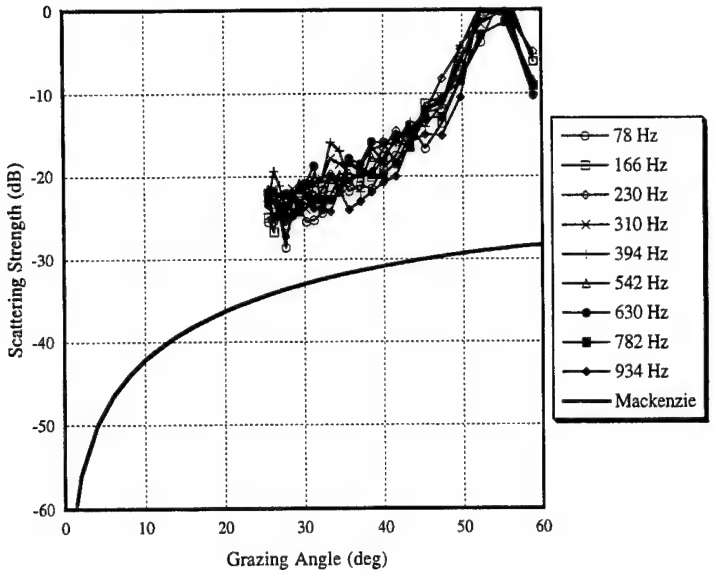

Fig. 105 — Bottom scattering strengths for CST-7 Run 16G beams 7-9

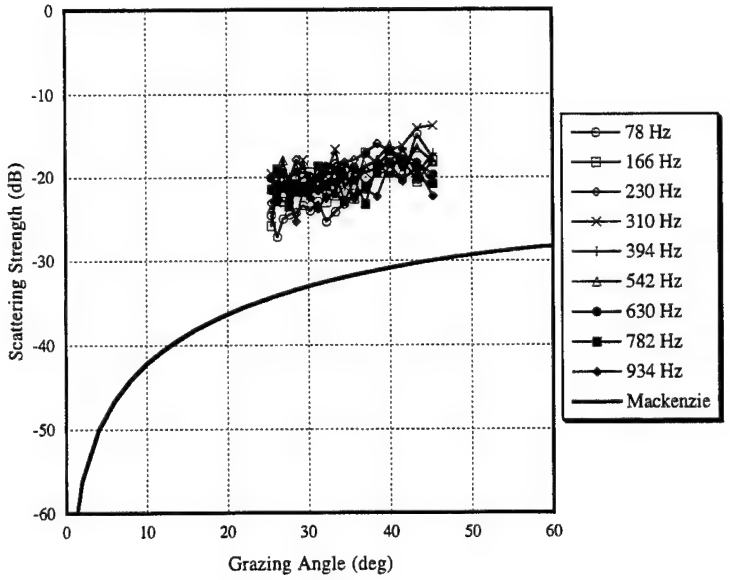

Fig. 106 — Bottom scattering strengths for CST-7 Run 16G beam 13

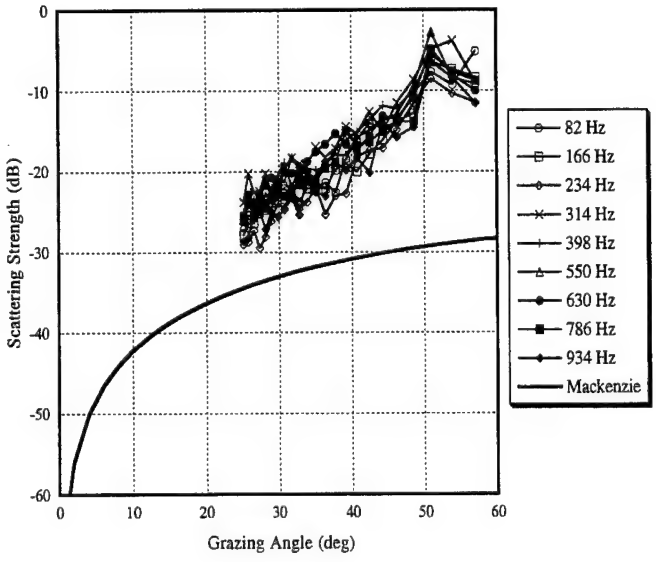

Fig. 107 — Bottom scattering strengths for CST-7 Run 18B beams 7-9

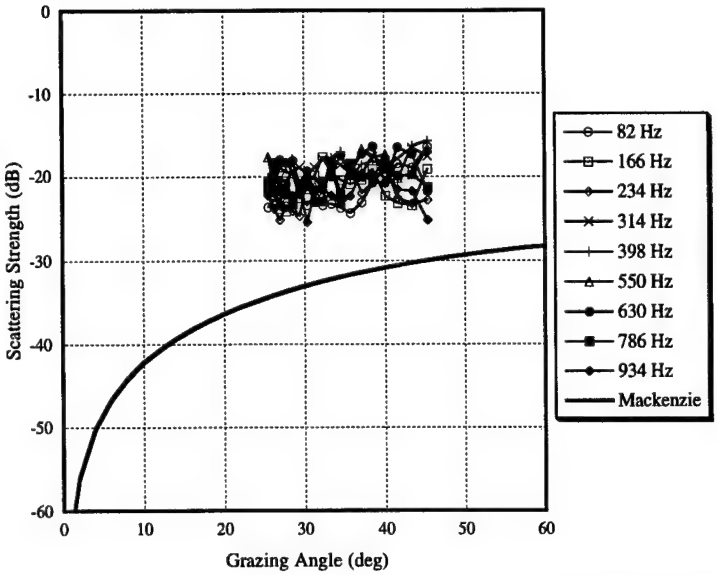

Fig. 108 — Bottom scattering strengths for CST-7 Run 18B beam 13

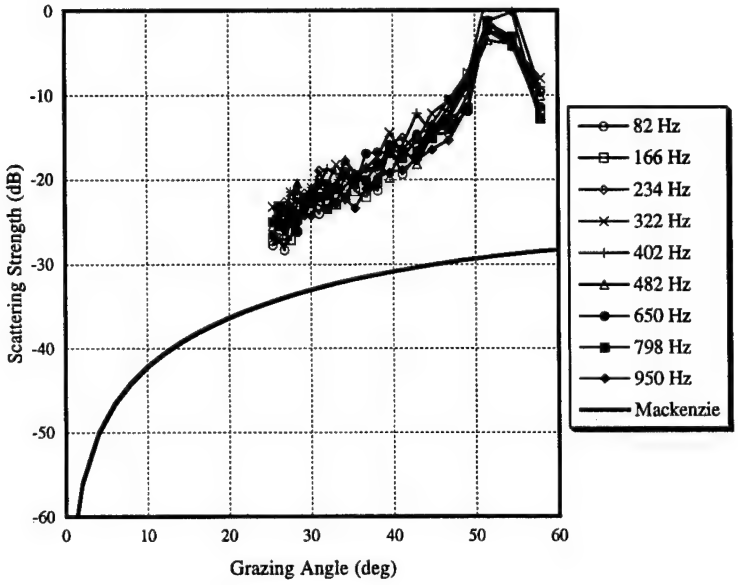

Fig. 109 — Bottom scattering strengths for CST-7 Run 19C beams 7-9

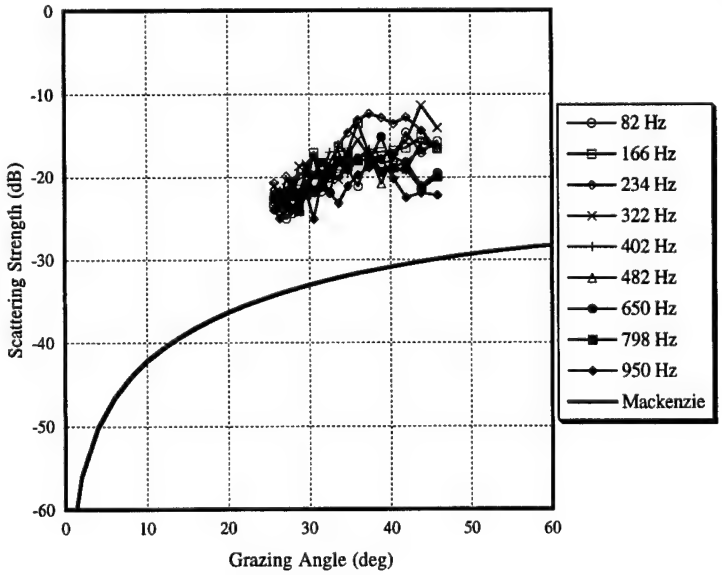

Fig. 110 — Bottom scattering strengths for CST-7 Run 19C beam 13

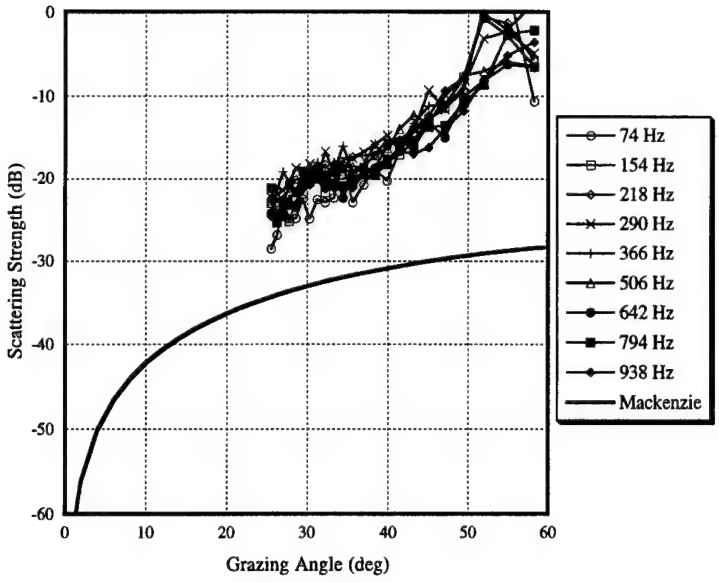

Fig. 111 — Bottom scattering strengths for CST-7 Run 20B beams 7-9

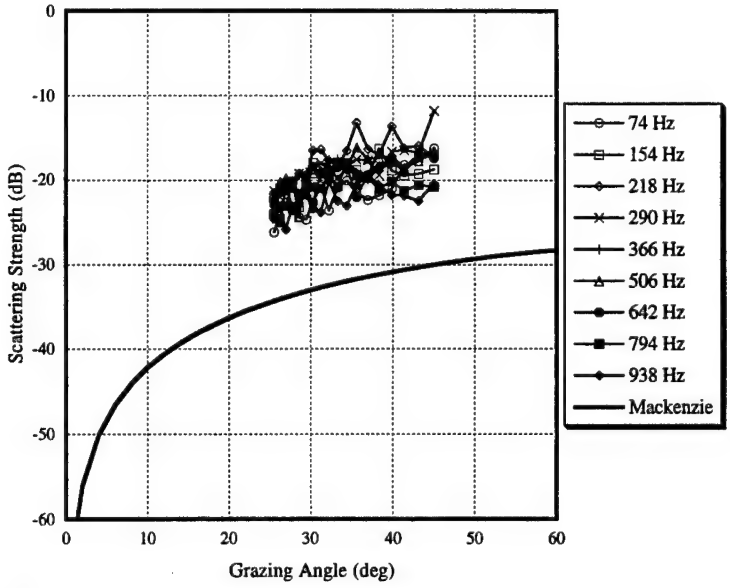

Fig. 112 — Bottom scattering strengths for CST-7 Run 20B beam 13

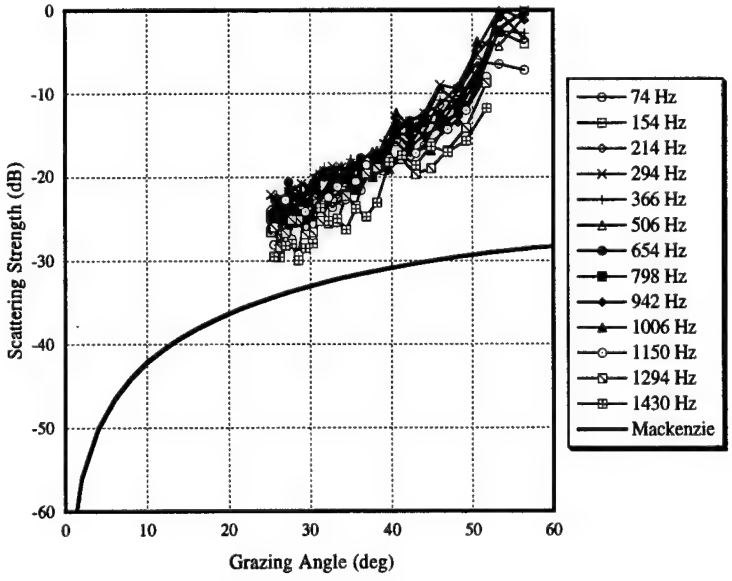

Fig. 113 — Bottom scattering strengths for CST-7 Run 21C beams 7-9

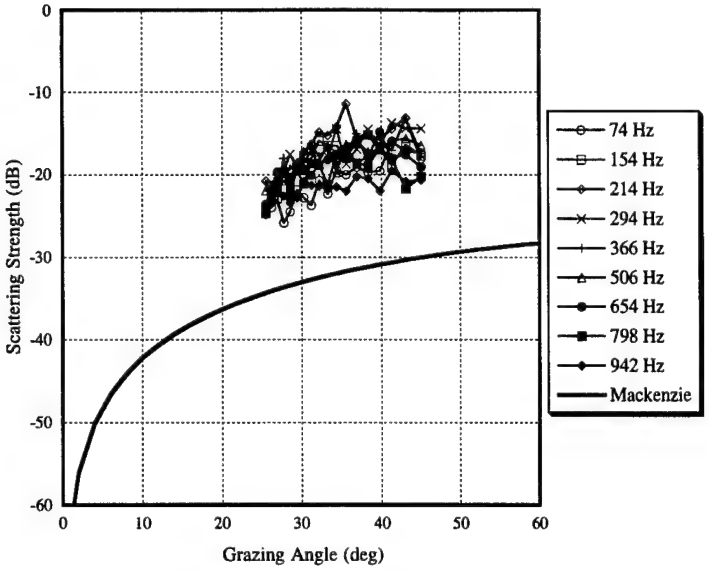

Fig. 114 — Bottom scattering strengths for CST-7 Run 21C beam 13

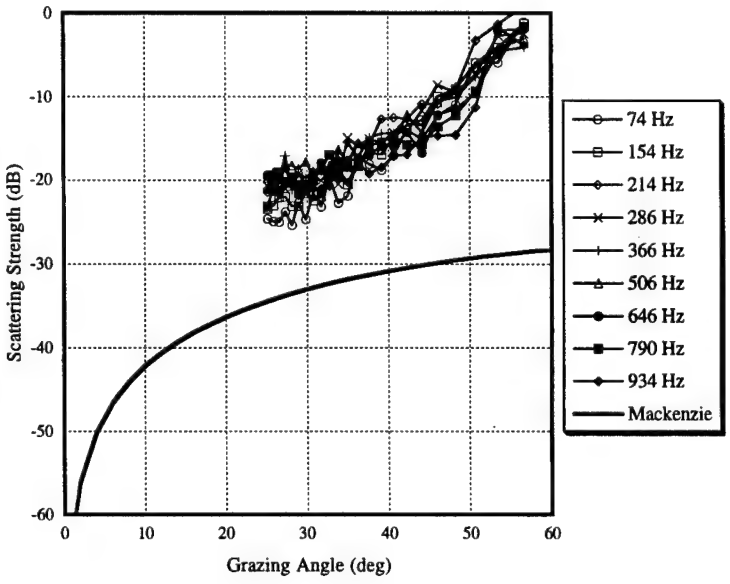

Fig. 115 — Bottom scattering strengths for CST-7 Run 23C beams 7-9

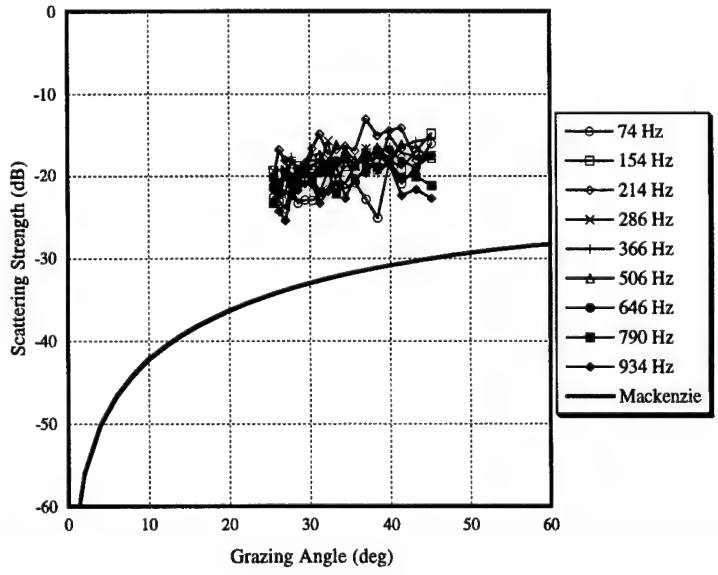

Fig. 116 — Bottom scattering strengths for CST-7 Run 23C beam 13

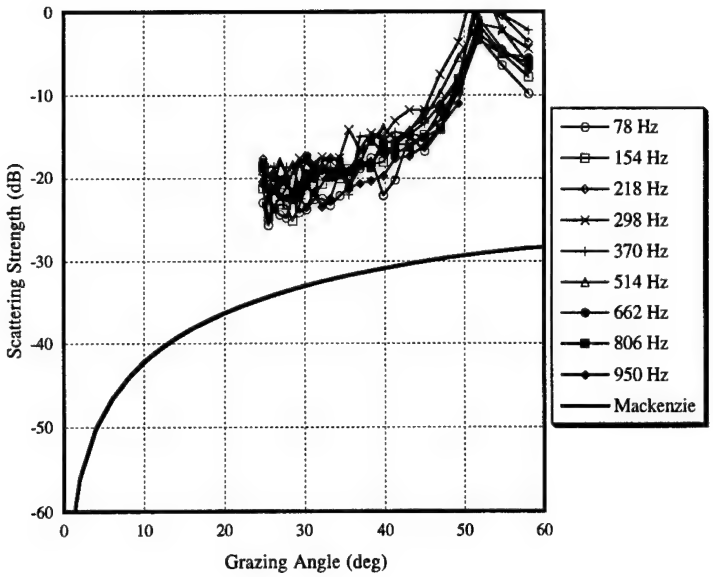

Fig. 117 — Bottom scattering strengths for CST-7 Run 24B beams 7-9

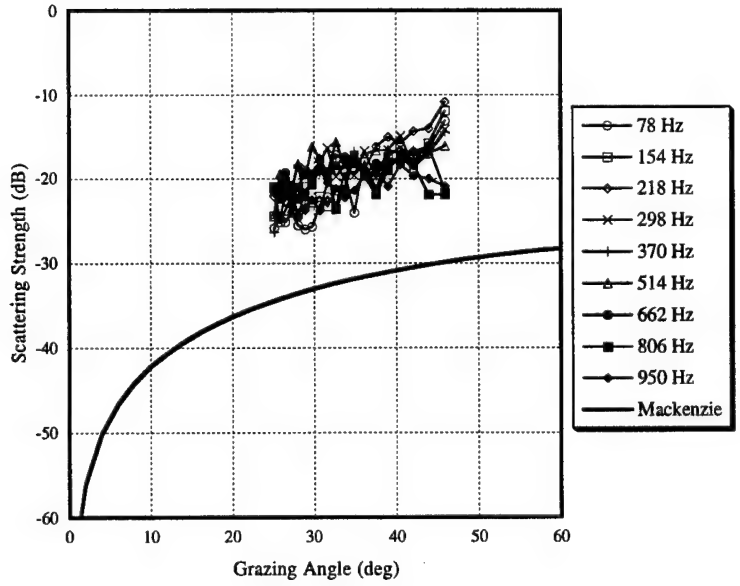

Fig. 118 — Bottom scattering strengths for CST-7 Run 24B beam 13

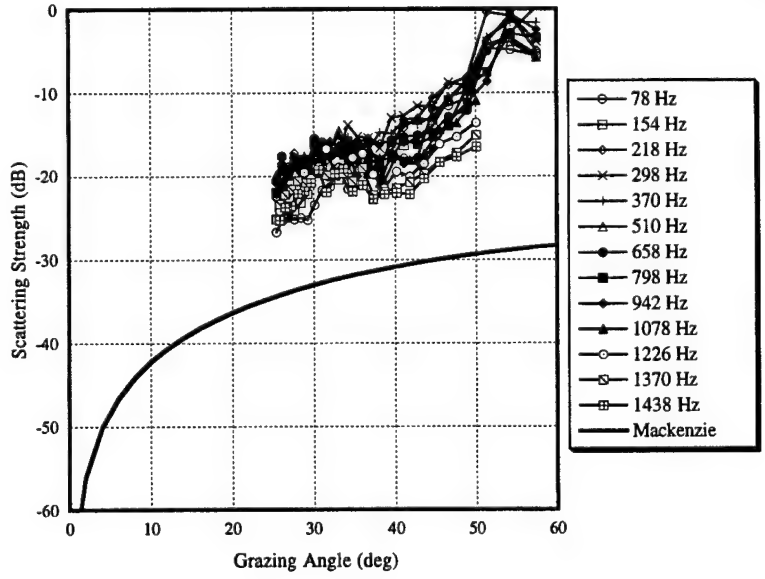

Fig. 119 — Bottom scattering strengths for CST-7 Run 25D beams 7-9

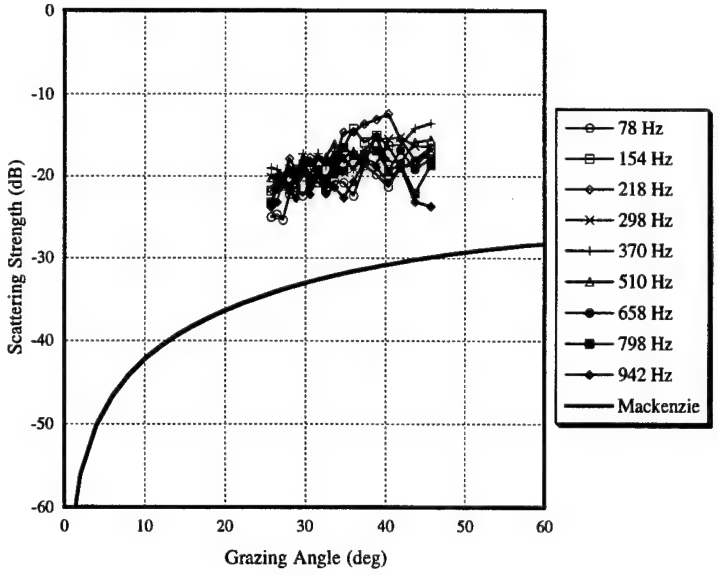

Fig. 120 — Bottom scattering strengths for CST-7 Run 25D beam 13

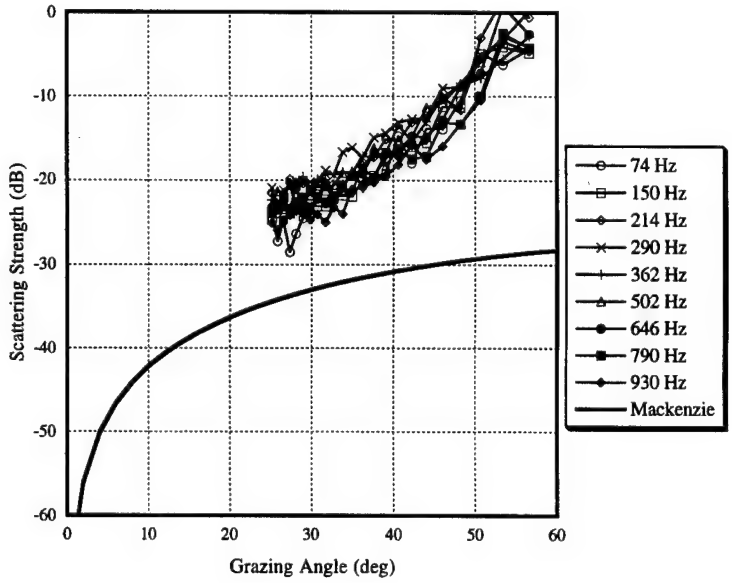

Fig. 121 — Bottom scattering strengths for CST-7 Run 26B beams 7-9

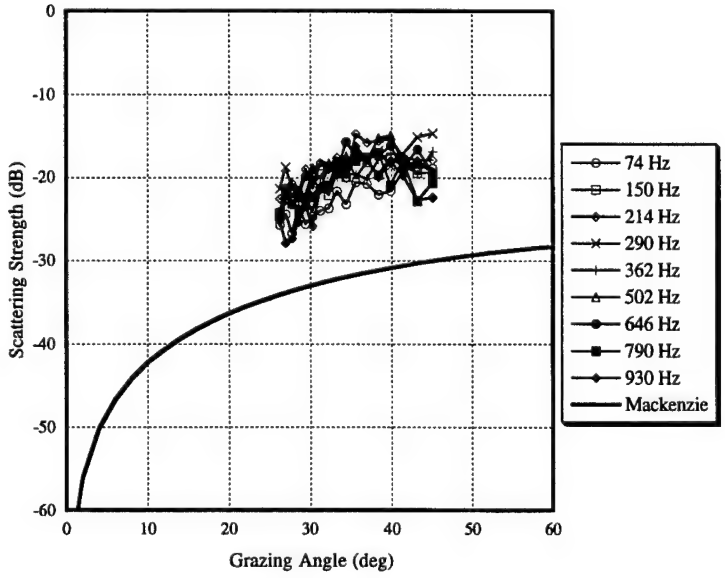

Fig. 122 — Bottom scattering strengths for CST-7 Run 26B beam 13

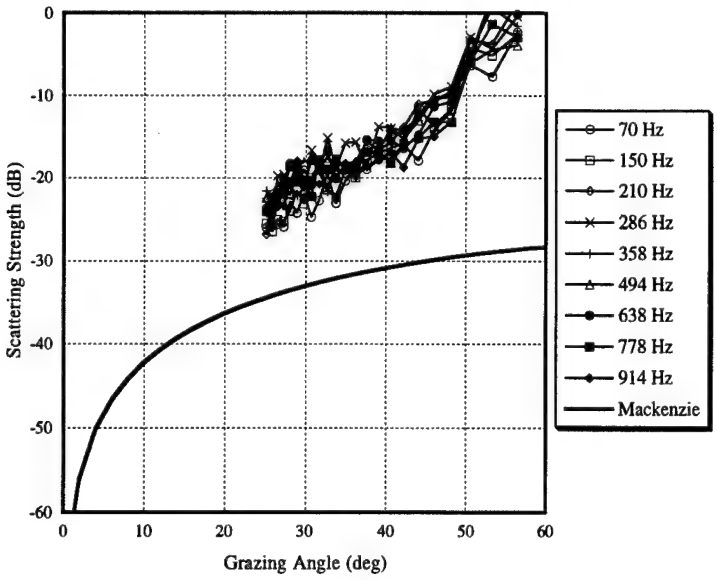

Fig. 123 — Bottom scattering strengths for CST-7 Run 29E beams 7-9

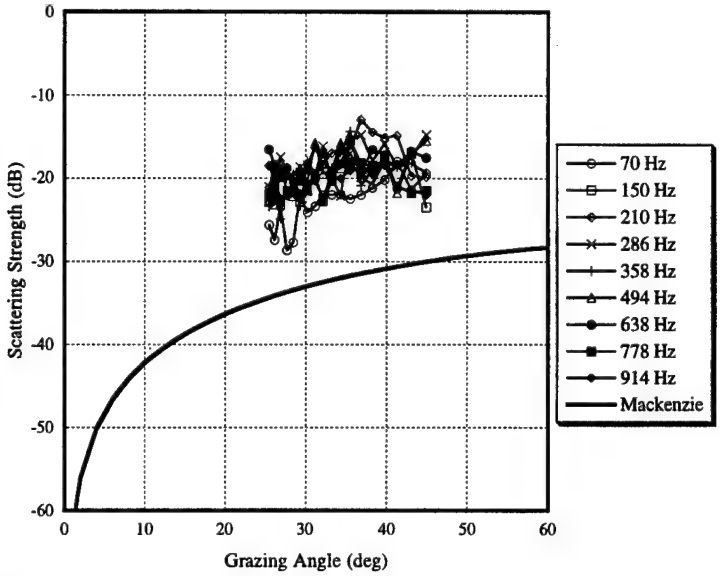

Fig. 124 — Bottom scattering strengths for CST-7 Run 29E beam 13

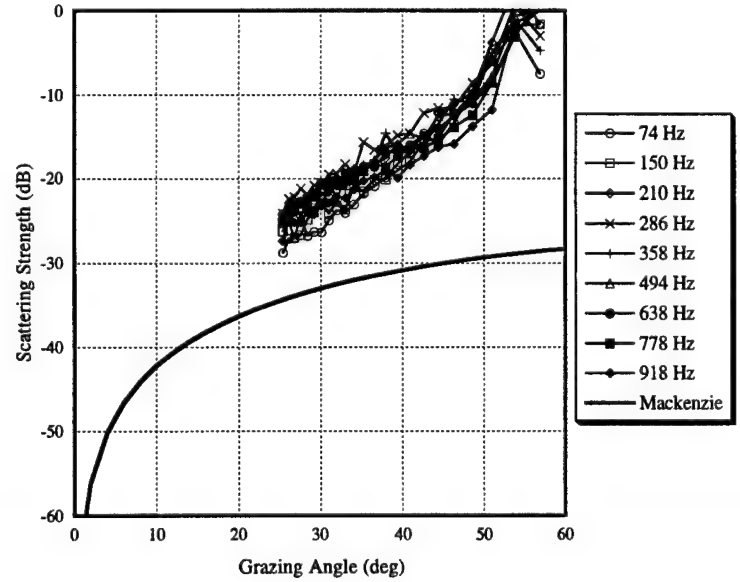

Fig. 125 — Bottom scattering strengths for CST-7 Run 34A part 1 beams 7-9

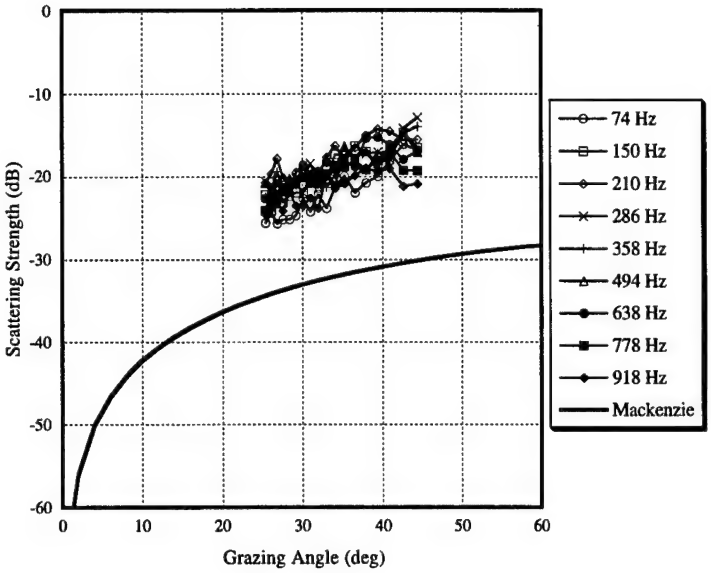

Fig. 126 — Bottom scattering strengths for CST-7 Run 34A part 1 beam 13

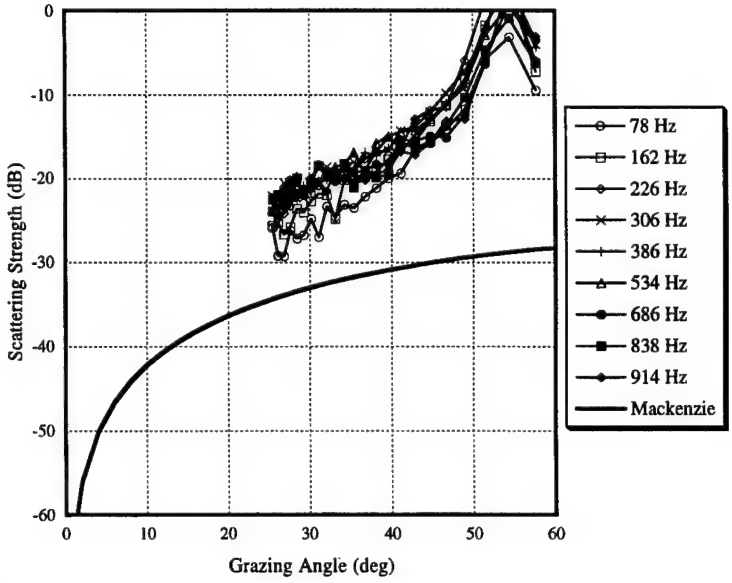

Fig. 127 — Bottom scattering strengths for CST-7 Run 34A part 2 beams 7-9

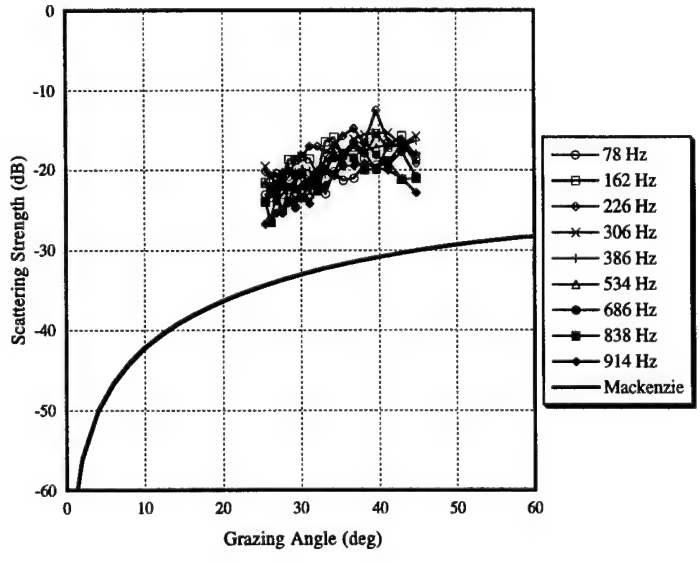

Fig. 128 — Bottom scattering strengths for CST-7 Run 34A part 2 beam 13

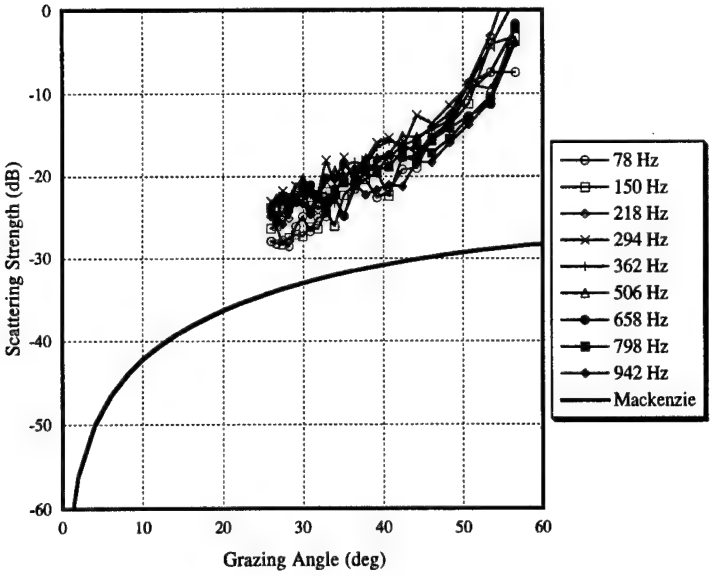

Fig. 129 — Bottom scattering strengths for CST-7 Run 34A part 3 beams 7-9

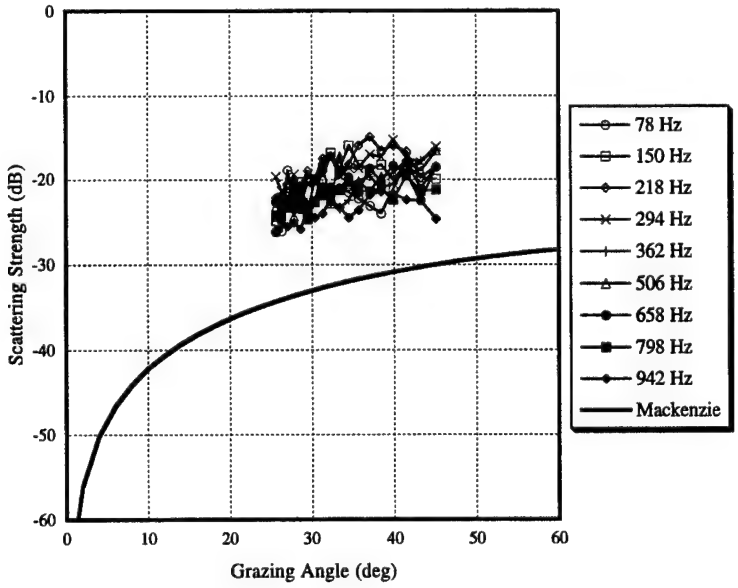

Fig. 130 — Bottom scattering strengths for CST-7 Run 34A part 3 beam 13

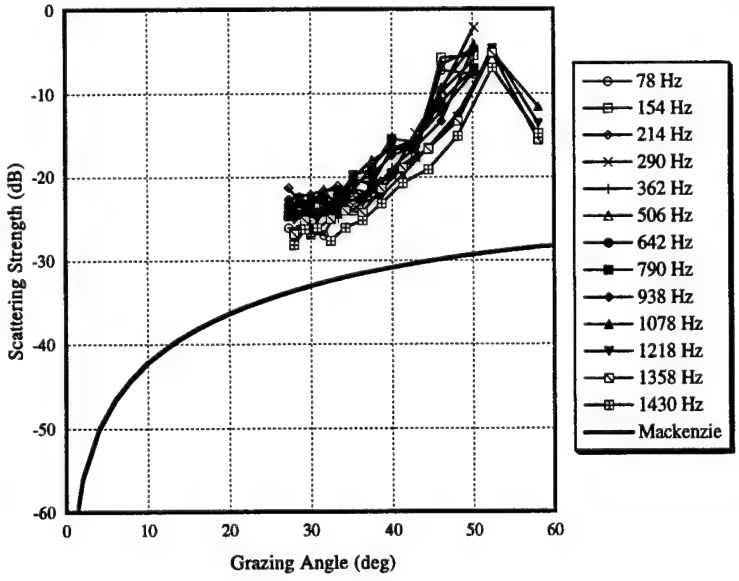

Fig. 131 — Bottom scattering strengths for CST-8 Run B1 beams 7-9

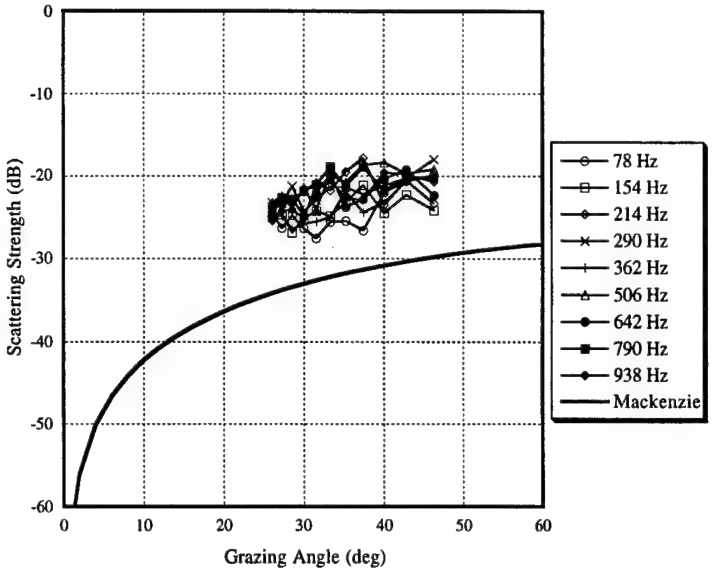

Fig. 132 — Bottom scattering strengths for CST-8 Run B1 beam 13

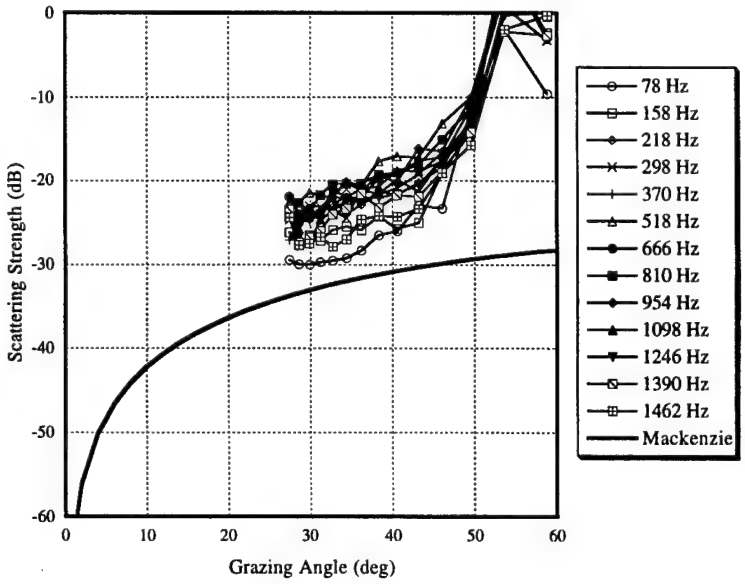

Fig. 133 — Bottom scattering strengths for CST-8 Run B3 beams 7-9

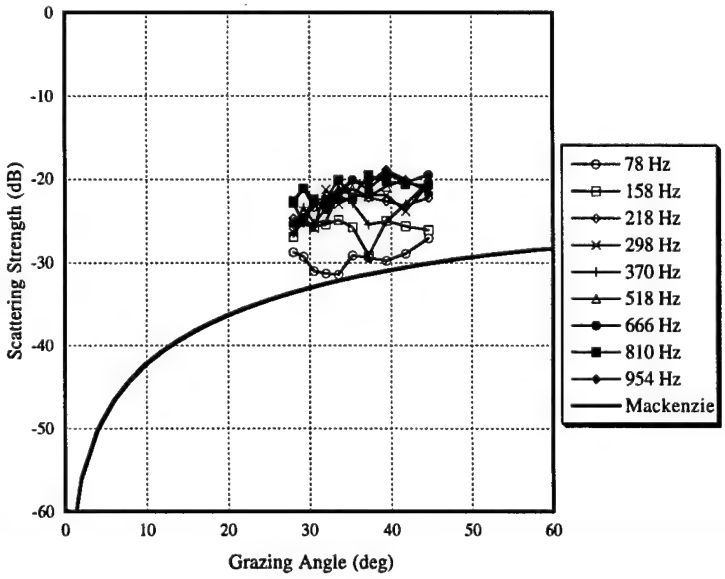

Fig. 134 — Bottom scattering strengths for CST-8 Run B3 beam 13

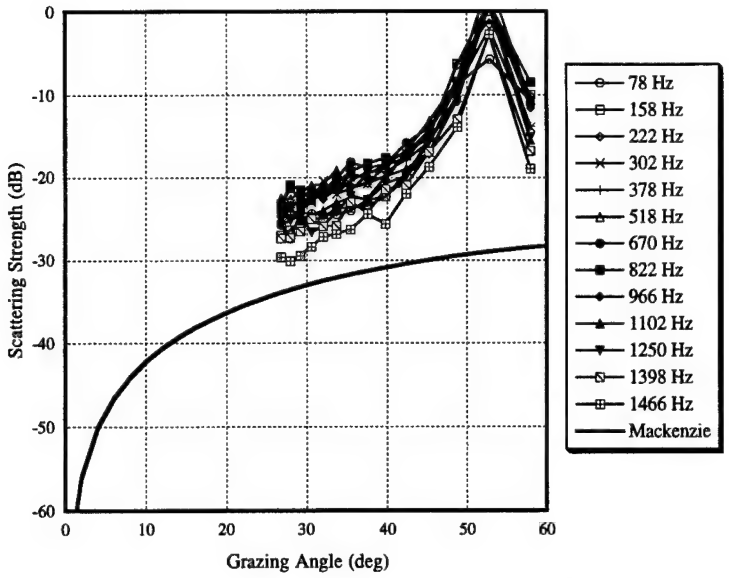

Fig. 135 — Bottom scattering strengths for CST-8 Run B7 beams 7-9

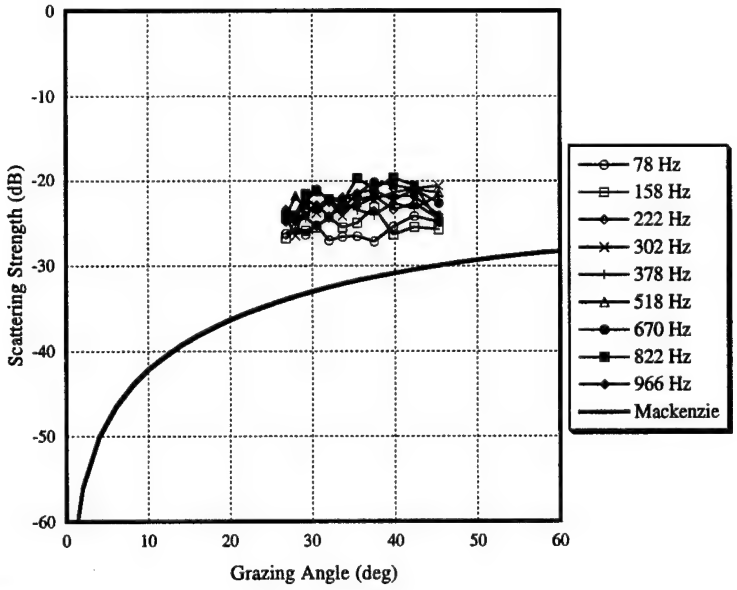

Fig. 136 — Bottom scattering strengths for CST-8 Run B7 beam 13

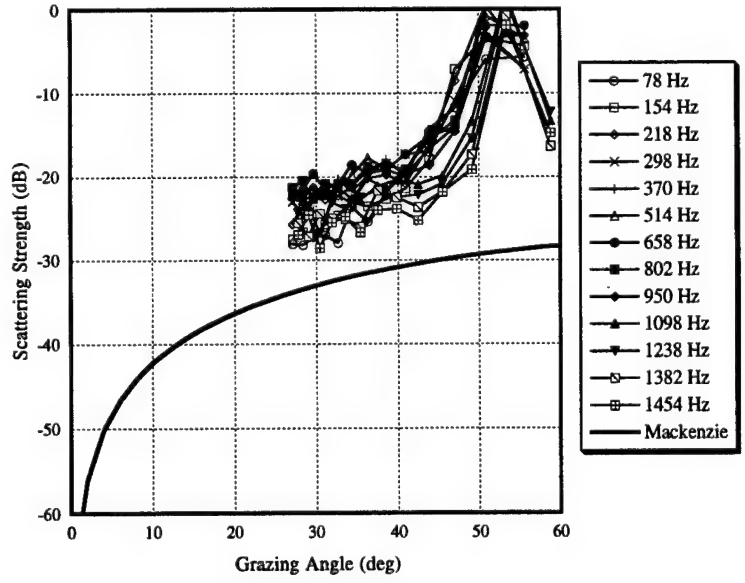

Fig. 137 — Bottom scattering strengths for CST-8 Run B9 beams 7-9

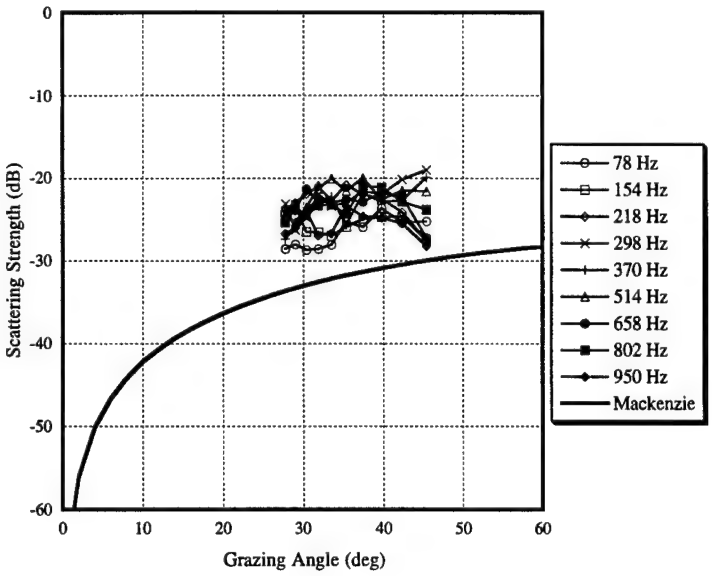

Fig. 138 — Bottom scattering strengths for CST-8 Run B9 beam 13

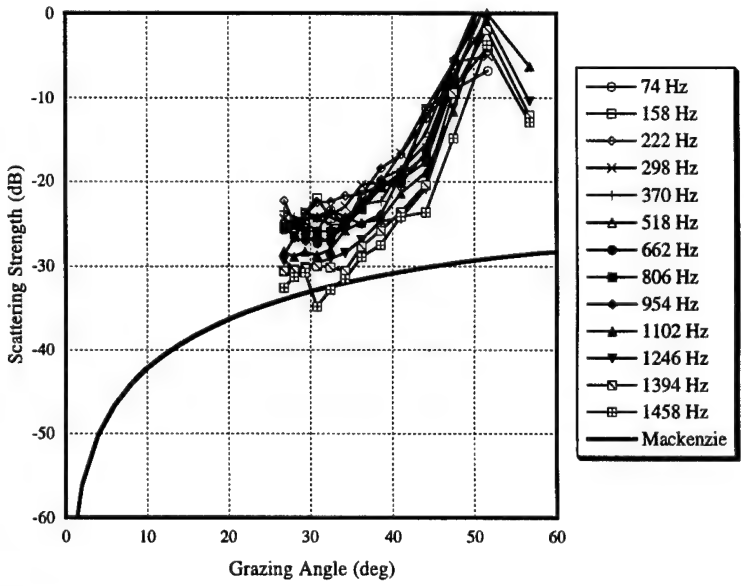

Fig. 139 — Bottom scattering strengths for CST-8 Run B11 beams 7-9

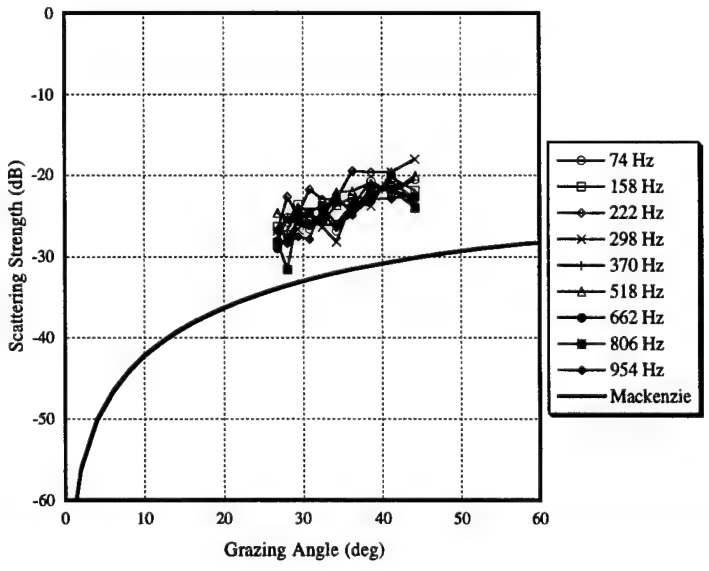

Fig. 140 — Bottom scattering strengths for CST-8 Run B11 beam 13

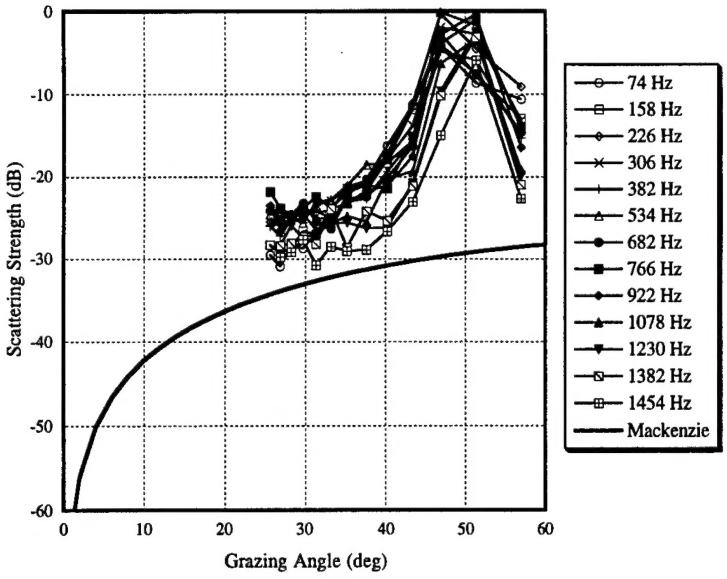

Fig. 141 — Bottom scattering strengths for CST-8 Run B13 beams 7-9

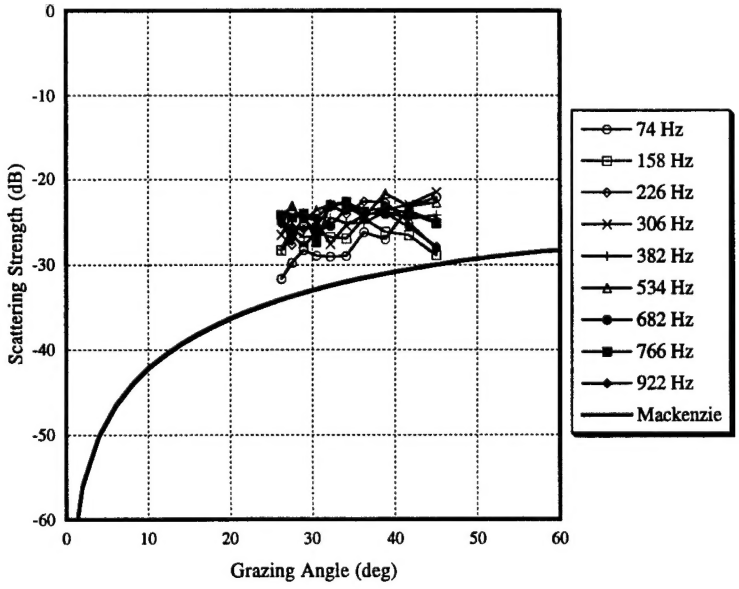

Fig. 142 — Bottom scattering strengths for CST-8 Run B13 beam 13

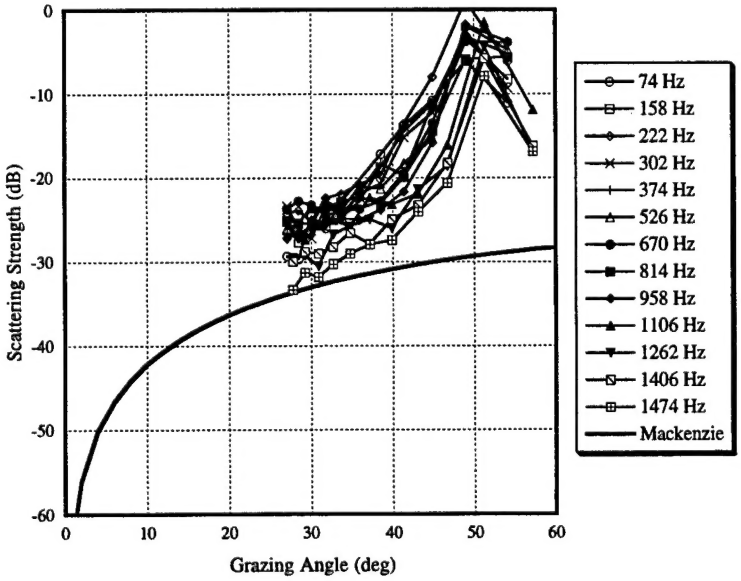

Fig. 143 — Bottom scattering strengths for CST-8 Run B14 beams 7-9

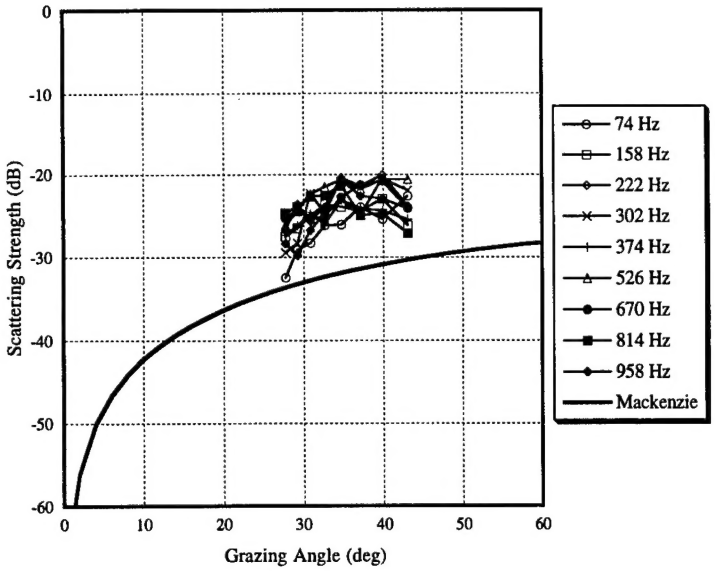

Fig. 144 — Bottom scattering strengths for CST-8 Run B14 beam 13

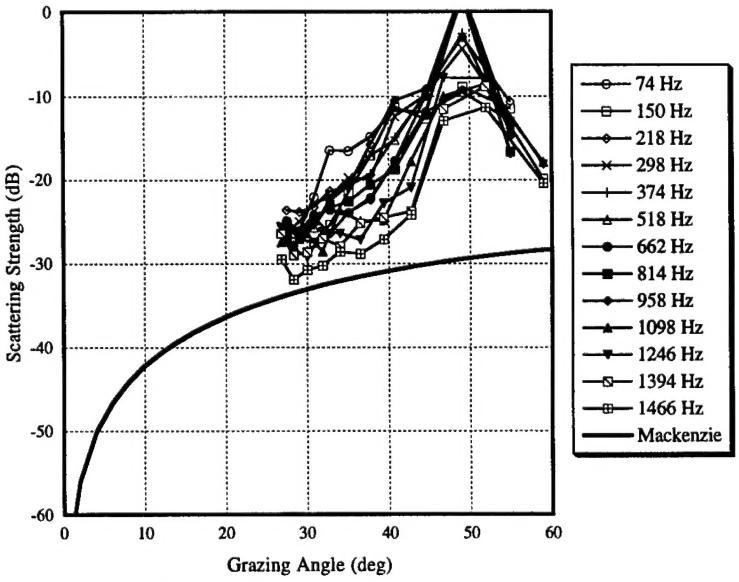

Fig. 145 — Bottom scattering strengths for CST-8 Run B15 beams 7-9

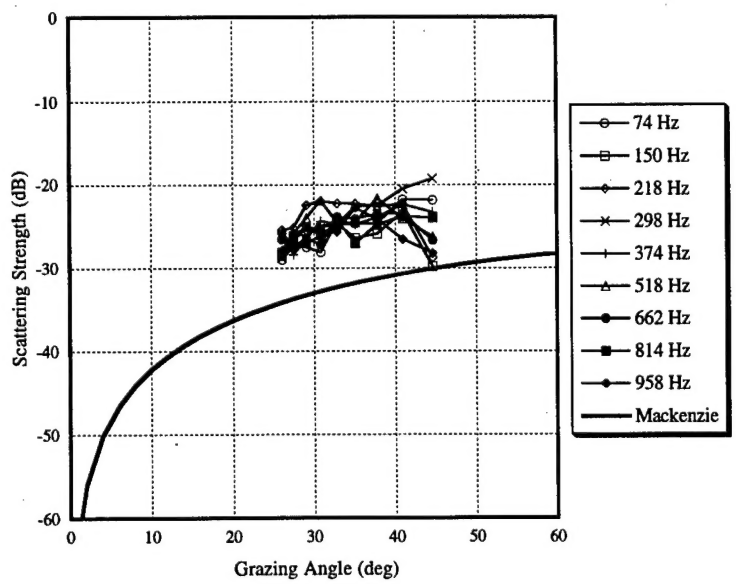

Fig. 146 — Bottom scattering strengths for CST-8 Run B15 beam 13

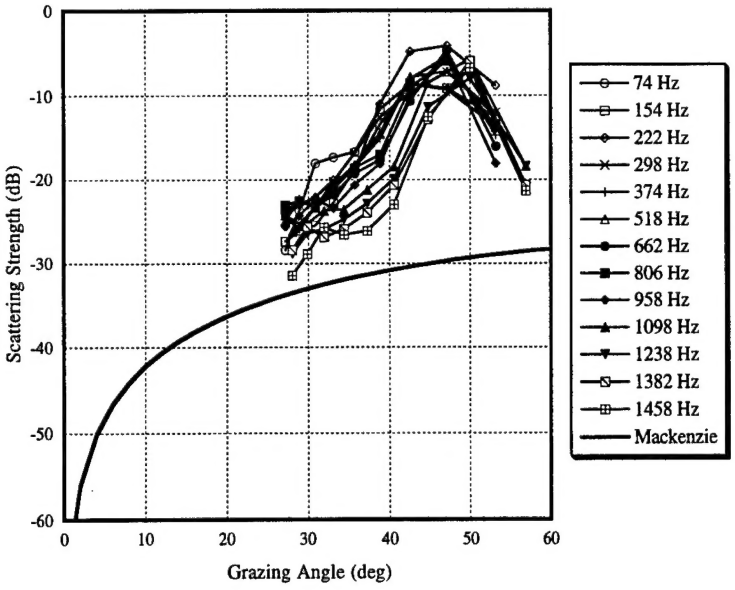

Fig. 147 — Bottom scattering strengths for CST-8 Run B16 beams 7-9

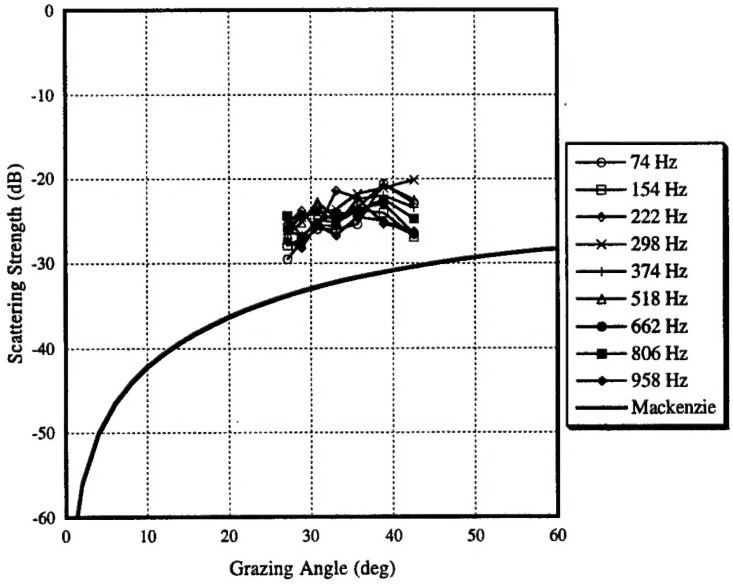

Fig. 148 — Bottom scattering strengths for CST-8 Run B16 beam 13

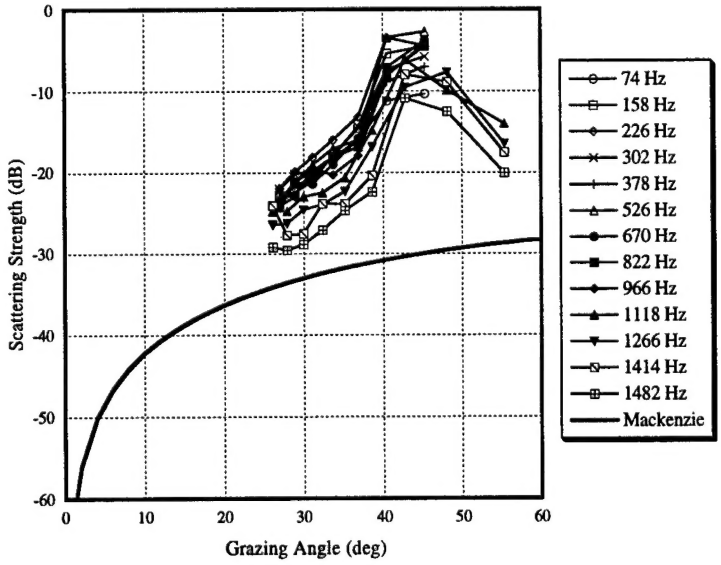

Fig. 149 — Bottom scattering strengths for CST-8 Run B17 beams 7-9

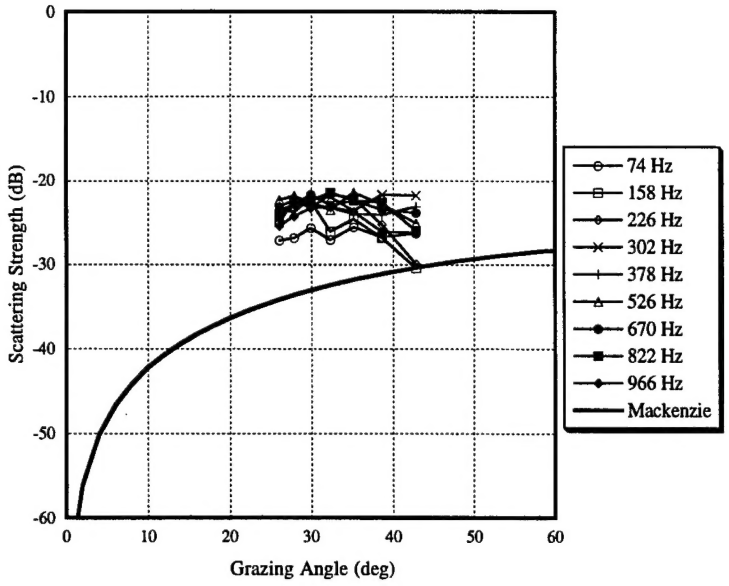

Fig. 150 — Bottom scattering strengths for CST-8 Run B17 beam 13

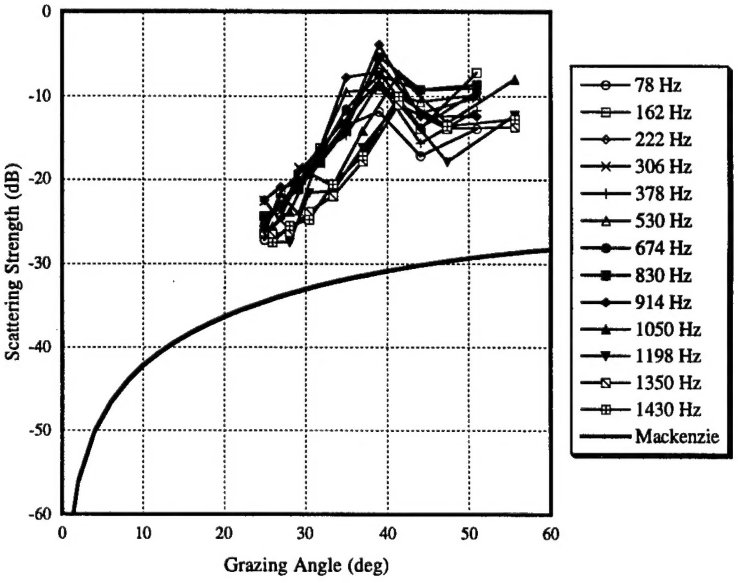

151 — Bottom scattering strengths for CST-8 Run B18 beams 7-9

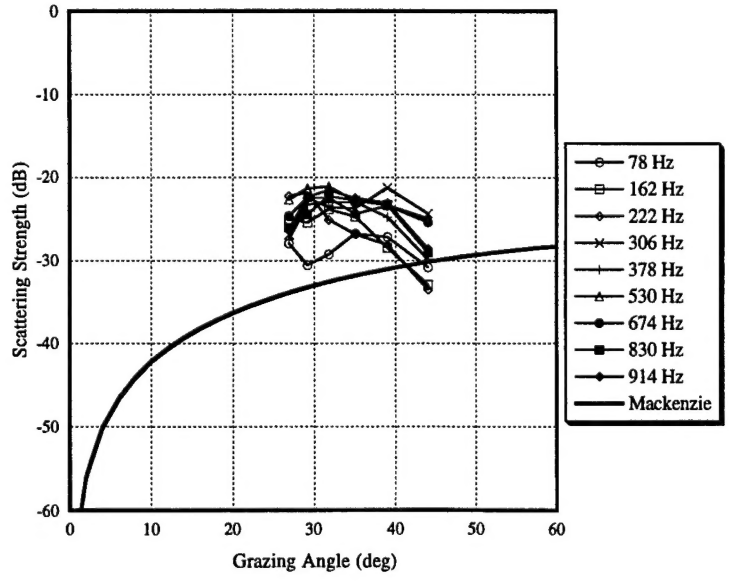

Fig. 152 — Bottom scattering strengths for CST-8 Run B18 beam 3